Thermo-Mechanical Analysis of Temporary Bonding Systems for Flexible Microelectronics Fabrication Applications

by

Jesmin Haq

A Dissertation Presented in Partial Fulfillment
of the Requirements for the Degree
Doctor of Philosophy

Approved April 2011 by the
Graduate Supervisory Committee:

Gregory B. Raupp, Co-chair
Bryan D. Vogt, Co-chair
Lenore Dai
Douglas Loy
Jian Li

ARIZONA STATE UNIVERSITY

May 2011

ABSTRACT

Temporary bonding-debonding of flexible plastic substrates to rigid carriers may facilitate effective substrate handling by automated tools for manufacture of flexible microelectronics. The primary challenges in implementing practical temporary bond-debond technology originate from the stress that is developed during high temperature processing predominately through thermal-mechanical property mismatches between carrier, adhesive and substrate. These stresses are relaxed through bowing of the bonded system (substrate-adhesive-carrier), which causes wafer handling problems, or through delamination of substrate from rigid carrier. Another challenge inherent to flexible plastic substrates and linked to stress is their dimensional instability, which may manifest itself in irreversible deformation upon heating and cooling cycles. Dimensional stability is critical to ensure precise registration of different layers during photolithography.

The global objective of this work is to determine comprehensive experimental characterization and develop underlying fundamental engineering concept that could enable widespread adoption and scale-up of temporary bonding processing protocols for flexible microelectronics manufacturing. A series of carriers with different coefficient of thermal expansion (CTE), modulus and thickness were investigated to correlate the thermo-mechanical properties of carrier with deformation behavior of bonded systems. The observed magnitude of system bow scaled with properties of carriers according to well-established Stoney's equation. In addition, rheology of adhesive impacted the deformation of

bonded system. In particular, distortion-bowing behavior correlated directly with the relative loss factor of adhesive and flexible plastic substrate. Higher loss factor of adhesive compared to that of substrate allowed the stress to be relaxed with less bow, but led to significantly greater dimensional distortion. Conversely, lower loss factor of adhesive allowed less distortion but led to larger wafer bow.

A finite element model using ANSYS was developed to predict the trend in bow-distortion of bonded systems as a function of the viscoelastic properties of adhesive. Inclusion of the viscoelasticity of flexible plastic substrate itself was critical to achieving good agreement between simulation and experiment. Simulation results showed that there is a limited range within which tuning the rheology of adhesive can control the stress-distortion. Therefore, this model can aid in design of new adhesive formulations compatible with different processing requirements of various flexible microelectronics applications.

Dedicated to my parents

Mr. Gazi Enamul Haq Rahmani and Mrs. Nazma Begum

ACKNOWLEDGMENTS

Firstly, I would like to thank my advisor, Professor Gregory Raupp, for his support and motivation during the course of my research work. I am fortunate to have my co-advisor, Professor Bryan Vogt, who gave me the guidance and helpful suggestions that carried me on through the difficult times. I want to thank my committee member Dr. Doug Loy who advised me and helped me in various aspects of my research. I am also thankful to my committee members, Professor Lenore Dai and Professor Jian Li for their valuable comments and suggestions. Specially, I like to thank Professor Lenore Dai for her suggestions in performing the DMA experiment.

My thanks go to the Flexible Display Center (FDC) team with whom I have interacted extensively during the course of my PhD research. Particularly, I would like to acknowledge Barry O'Brien, Scott Ageno, Emmett Howard, Michael Marrs, Jovan Trujillo, Dirk Bottesch, and Robert Naujokaitis for their many valuable discussions that helped me improve my knowledge in different aspects of my research area. I appreciate the help of FDC staff - Nick Munizza, Virginia Woolf, Consuelo Romero, Marilyn Kyler, Diane Carrillo, Kay Barror, Susan Allen and Steve Rednour in using the different tools of the FDC clean-room. I am also thankful to Huan Ma for her help in using DMA tool. I would like to mention the names – Parul, Xinxin, Lingyan and Jessica whose presence and fun-loving-spirits made my stay here enjoyable.

My special thanks are to my son, my husband, my brother and sister who have been a constant source of loving support and strength to me. Most

importantly, none of this would have been possible without the love and encouragement of my parents to whom this dissertation is dedicated to.

Finally I acknowledge the U.S. Army Research Laboratories for their financial support in my research project and Henkel Corp. for the supply of adhesives and for their active collaboration in the project.

TABLE OF CONTENTS

Page

CHAPTER Page

CHAPTER Page

LIST OF TABLES

Table Page

LIST OF FIGURES

Figure Page

Figure Page

Chapter 1

Introduction

1.1 Overview

A processing technology based upon temporary bond-debond approach has been developed that enables direct fabrication of high performance electronic devices on flexible substrates. This technique enables flexible plastic and metal foil substrates to be processed through automated standard semiconductor and flat-panel tool sets without tool modification. The key property for processing with these tool sets is rigidifying the flexible substrates through temporary bonding to carriers that can be handled similar to silicon wafers or glass substrates in traditional electronics manufacturing. Though 'roll-to-roll processing (R2R)' of flexible substrates will allow for continuous production, significant increase in throughput and reduction in capital cost and device cost [1], R2R will require many *ad hoc* modifications to existing tools and development of new tools. Moreover, challenges exist in innovations of new process recipes and system integration. Therefore, the entry cost into roll-to-roll electronics manufacturing through new tool set design and installation, new process development will limit the applications of flexible electronics in near future [2]. Also the processing of free standing flexible substrates has difficulties primarily in handling due to their tendency to warp and fold. Flexible substrates may become stretched, kinked, dimpled or scratched during unwind and wind. A rigid carrier can suppress this bending of the flexible structure during processing and can provide requisite

planarity, dimensional stability, and lithographic registration during thin film transistor (TFT) fabrication. The motivation behind this work is to develop temporary bond-debond technique for batch fabrication of flexible electronics which will be a viable interim manufacturing option that should allow flexible electronics to enter the market in volume much sooner than possible using true roll-to-roll processing.

In this dissertation we will investigate the technical challenges that are involved in the development of temporary bond-debond method and where there is considerable potentials to overcome these challenges by systematically control the properties of adhesive and carrier for a specified flexible substrate. The major thrust of this dissertation will be qualitative and quantitative study of the effect of thermo-mechanical properties of carrier and rheology of adhesive on deformation behavior of bonded system (Flexible Plastic Substrate-Adhesive-Carrier) under stress. The dissertation will be organized as follows:

In the introductory chapter, flexible electronics and its potential applications are discussed. The technological and processing challenges for fabrication of electronics on flexible substrates are briefly discussed. Different techniques for fabrications of flexible electronics including transfer processes and direct fabrication processes, roll-to-roll and plate-to-plate processes are introduced and compared.

In Chapter 2, we investigate the temporary bond-debond approach for fabrication of electronics on flexible plastic substrates. In this technique the substrate is temporarily adhered to a rigid carrier plate during processing; after the

fabrication is complete, the flexible substrate is separated from the carrier through a debond process. The principle challenges for this process will be discussed. Finally the impact of careful selection of flexible substrate, carrier and adhesive as a system on bonding-debonding efficiency will be investigated.

In Chapter 3, we examine the potential to control the stress of the bonded system that is developed during processing predominately through thermal-mechanical property mismatches between the carrier and flexible substrate. To investigate the role of the thermo-mechanical properties of the carrier and rheology of adhesive, the stress and subsequent bowing of bonded systems are examined systematically using different carriers and two different adhesives. In addition, the alignment of the bonded system for photolithography registration is investigated for the two adhesives. We show that an adhesive with low loss factor ($\sim 10^{-3}$) provides high precision alignment during photolithography. It will be shown for the first time that excellent registration of the flexible circuitry fabricated on the bonded system with low stress can be achieved by using a carrier with high modulus (390 GPa) and coefficient of thermal expansion (CTE) that is closely matched to the flexible substrate and a viscoelastic adhesive with low viscoelastic loss factor.

In Chapter 4, we examine the photolithography registration and bow of the bonded system as a function of viscoelastic properties of adhesive. The adhesive that relaxes stress with low bow causes more misalignment in photolithography registration. By blending two adhesives having quite different viscoelastic properties, it is expected the blend will exhibit intermediate properties which will

allow examination of intermediate deformation behavior of bonded system. The relative loss factor of adhesive to that of flexible plastic substrate is shown to correlate directly with the distortion-bowing behavior.

In Chapter 5, a finite element model using ANSYS is developed to simulate the bow-distortion of bonded system. The nonlinear properties of adhesive and flexible plastic substrate are modeled using Prony series. The finite element model is verified against the experimental bow data of bonded systems varying the viscoelastic properties of adhesives and the thermo-mechanical properties of carriers. We show that the model can be used for designing of new adhesive formulations by tuning the viscoelastic properties to control the stress-distortion of bonded system.

In Chapter 6 we represent a summary of our findings, discuss the novelty of our method to control the stress-distortion of bonded system and a brief description of future work including improvements in temporary bond-debond method for the scale-up of flexible microelectronics on plastic substrates and further investigation into rheology of flexible plastic substrate to better predict the distortion.

1.2 Flexible Electronics

Flexible electronics have attracted great attention in recent years [3-9] and have the potential to revolutionize the interaction between humans and their electronic devices. Flexible electronics is the technology where electronic circuits are assembled by mounting electronic devices on flexible substrates comprised of polymers, organic–inorganic hybrids, thin glasses, or metal foils [10]. A generic

electronic structure is composed of a substrate, backplane electronics, a frontplane and encapsulation [6]. The structure starts with a substrate and backplane electronics are fabricated on the substrate. Backplanes provide power and signal to frontplanes or collect power and signal from the frontplanes. The frontplanes might be displays like liquid crystal (LCD), electrophoretic (EPD) or organic light emitting (OLED), might be sensors or actuators. To protect the sensitive electronic components especially organic-based electronics from atmospheric moisture and oxygen, thin barrier coating or encapsulation is required [11-13]. To make the structure flexible, all these components must comply with bending without loss of function. Degree of flexibility may vary depending upon application. The device may need to flex once such as display on curved automobile dashboard or may need to bent or flex during use but not over a range that includes folding or rolling, or device may be roll able which is as flexible as fabric [14]. The rapidly increasing demand for high performance, highly compact and portable devices along with available high-throughput manufacturing have spurred the growth of interest in manufacturing flexible electronics [9]. This paradigm shifting technology provides the opportunity to create energy-efficient products that are lightweight, ultrathin, and rugged along with potential for very large area electronics with the ability to flex, curve, conform, and roll [10]. These unique properties of the flexible electronics could have enormous impacts on consumer electronics, aviation and space electronics, life sciences, lighting, power, military applications and telecommunications [15].

1.3 Applications of Flexible Electronics

Currently, flexible electronics technology is being actively developed for applications in flexible flat panel displays. The evolution of displays took place away from the bulky cathode ray tube (CRT) to the thin active matrix liquid crystal display (LCD), and in future the paper-like flexible flat panel display is anticipated [4]. There are many new compelling applications of flexible display technology that are not possible using a rigid glass based display; for example: large area, wall sized reflective screen that could be rolled away when not in use; small portable rollable display; wearable displays integrated in garments and textiles; irregular shaped display used in the steering wheel or dashboard of an automobile; and a wristband display [4]. Active matrix organic light emitting diode (AM OLED) display fabricated on a flexible plastic substrates has potential for being lower cost, lighter weight, lower power and highly rugged with superior image quality, compared to the current glass substrate based active matrix liquid crystal displays AM LCDs [16].

Many research groups have recently reported developments in flexible electronics technology, for applications ranging from photovoltaic to electronic textiles and sensory skins [17-24]. Flexible solar cells have been developed for powering satellites [20]. These cells are lightweight, can be rolled up for launch and are easily deployable; these characteristics make them a good match for the application. Antennas fabricated in a highly integrated package on large-area flexible substrates are highly desirable, since they can be rolled up into a compact package and easily deployed into space [25]. Applications like electronic bar

codes, radio frequency identification (RFID) tags and smart credit cards would be advanced by the availability of flexible circuitry that could be integrated on curved and non-rigid surfaces[26].

Flexible sensors with the potential to bend, expand and manipulate, have captured the imagination for applications in biomedicine, artificial skin and wearable electronics [6, 24]. Here are some recent examples of research carried on flexible sensors. The shear stress sensor by Xu et al. [27] integrated with micro-electromechanical system (MEMS) and integrated circuits (ICs) onto a flexible parylene skin could be affixed to human body like band aid; chemical sensing transistors were made on fibers for wearable electronics [28-29], flexible and conformable electronic skin developed by Someya and coworkers [29-30] used pressure and thermal sensors made of organic materials on plastic substrate .

NASA is currently developing a host of deployable structures like balloons, solar sails, space-borne telescopes and membrane-based synthetic aperture radar for the exploration of space [31-32]. Each of these applications is driven by the need for a thin, low mass, large area structure (e.g., polymer-based) and also need to integrate sensing and control electronics within the structure. Conventional silicon-based electronics are difficult to integrate with such large, thin structures, due to a variety of concerns including mass, reliability and manufacturing issues [31]. Flexible electronics, particularly thin film transistors (TFTs), are a potentially key enabling technology that may allow the integration of a wide range of sensors and actuators into these types of structures [31].

1.4 Technological Challenges for Fabrication of Electronics on Flexible Substrate

Despite the attractiveness of flexible electronics, this new technology has some major technological barriers that currently hinder its widespread application. Several enabling technologies must be developed for manufacturing and rapid commercialization of flexible electronics [16]. These include: a) development of the flexible substrates with the required characteristics and the associated substrate processes [3, 6, 33-34], b) development of the TFT (thin film transistor) backplane, and front plane drive electronics designs and processes, compatible with the selected flexible substrate [6-8], and c) thin film encapsulation / barrier layers for the protection of the devices, specially OLED devices from oxygen and moisture in the ambient, for enhanced device lifetime [11-13].

During fabrication of devices, the flexible substrate will be subjected to thermal and chemical processing. Thus the dimensional stability, solvent and chemical resistance of the flexible substrate must be considered in combination with commercial availability. Flexible substrate as a drop-in replacement for glass substrate must meet many requirements:

Thermal and thermo-mechanical properties: Thermal and dimensional stability of the substrate is critical to ensure precise registration of the different layers during photolithography and for the multilayer devices to be able to withstand thermal cycling during manufacture. Plastic films undergo a variable and undesirable change in dimensions above glass transition temperature (T_g), due to molecular relaxation events associated with the increased mobility of the polymer chains,

and also due to shrinkage or expansion associated with the relaxation of residual strain within the oriented parts of the film structure. Therefore T_g is a key characteristic for the selection of plastic substrate to ensure its thermal and dimensional stability at maximum process temperature. Thermal mismatch between device film and substrate may cause the film to crack or deformation of the film-on-substrate structure during the thermal cycling of fabrication. A rule of thumb for tolerable mismatch is $\left|\Delta CTE \cdot \Delta T\right| \leq 0.1-0.3\%$ where ΔCTE is the difference in coefficients of thermal expansion between substrate and device film and ΔT is the temperature excursion i.e. deviation from stress-free temperature [6].

Optical properties: Transmissive or bottom emitting displays need optically clear substrate and a total light transmission (TLT) of > 85 % over 400-800 nm wavelength coupled with a haze of less than 0.7 % are typically required [33]. In addition, substrates for LCDs must have low birefringence.

Chemical Properties: The substrate should not release contaminants for example should not outgas oligomers under thermal-vacuum process conditions. It should be inert against process chemicals and should not react with or absorb the chemicals and solvents. Polymers absorb water and water absorption can have a very detrimental effect on dimensional stability. The plastic substrate will swell and shrink as it absorbs and desorbs the moisture.

Surface roughness: The surface smoothness and cleanliness of the flexible substrates are essential to ensure integrity of subsequent layers. The thinner the device film, the more sensitive their electrical function is to surface roughness.

With polyethylene terephthalate (PET) and polyethylene napthalate (PEN) films, improvements in surface quality is achieved through control of recipe and film process [33]. Additionally application of a coating layer, typically comprised of scratch resistant material reduces the surface defects [4]. For optical grade PEN (Teonex Q65) film, surface roughness as low as less than 1 nm has been demonstrated [33]. Such levels are necessary to ensure integrity for subsequent barrier layers, conductive coatings and pixel array resolution.

Mechanical Properties: The difference in mechanical properties, particularly stiffness, between rigid glass and flexible substrates will require different method of processing when fabricating devices on flexible substrates as compared to that on rigid glass. Issues such as variable stresses and adhesion issues at the interface between the different layers under thermal processing cycles, curvature change of the work piece under stress [35-36] and ability to withstand flex testing will be critical in determining the robustness of flexible substrate in use [37]. To date there has been limited work to define the protocols to test the robustness of flexible substrate [37-38] and there is an important need to define these protocols and determine how the structures behave on testing. Device application may require intentional bending, stretching or non planar shaping after fabrication. Therefore one needs to understand behavior of thin film devices under strain, fracture strain and fracture mechanism of device layer fabricated on flexible substrate[35].

The TFT processes developed for the rigid glass substrates cannot readily be applied for use with the flexible plastic substrates, primarily because of the

low-process temperature constraint. For flexible plastic substrate, in order to maintain the thermal and mechanical integrity the maximum process flow temperature must be sufficiently low as most plastic films have low T_g above which they exhibits tendency to expand or shrink significantly as heated or cooled. For example, polyethylene terephthalate (PET) and polyethylene naphthalate (PEN) films have T_gs' of 78 ^oC and 120 ^oC. However, the dimensional stability of plastic films can be enhanced by a heat stabilization process [39], in which the internal strain in the film is relaxed by exposure to high temperature while under minimum line tension. Heat-stabilized polyethylene naphthalate (HS-PEN) film exhibits typically shrinkage of order <0.05% when exposed to temperatures of up to 180 ^oC for 30 min [33]. In addition, once heat stabilized, the T_g effects are essentially negated and the PEN film remains a dimensionally reproducible substrate up to 180 ^oC [33]. On the contrary, rigid glass substrates have a temperature tolerance of up to 600 ^oC [6]. In addition, rigid glass substrate has a low coefficient of thermal expansion (CTE) of 4 ppm/^oC [6], which matches those of inorganic device layers, whereas for most plastic film CTE is very high as an example for HS-PEN the CTE is about 25 ppm/^oC in the range from 20 ^oC to 150 ^oC [33]. The elastic modulus of polymer substrate is a factor of 10-50 lower than that of inorganic device materials, even a small thermal mismatch stress can make the free standing substrate curve and cause misalignment during the overlay registration of the device. Because of the limitations of lower process temperature capability, lack of dimensional stability, and the thermal stresses due to the CTE mismatch between the TFT thin films and

the substrate, new low temperature plastic compatible TFT processes must be developed. To obtain functional transistors on free-standing plastic substrates, the mechanical stress needs to be carefully designed where the goals of stress control are prevention of circuit fracture during fabrication; keeping the substrate flat; and accurate overlay alignment between device layers [36, 40].

Fabricating circuitry on flexible substrate presents a unique challenge for photolithography systems. The vacuum hold-down structure, which maintains the flexible panel in position during the imaging step, must be smooth and flat to ensure that the substrate remains within the depth-of-focus of the patterning system. Flexible substrate easily conforms to vacuum grooves or scratches in the hold-down structure, resulting in poor imaging [25]. During processing, distortion of the flexible substrate occurs due to dimensional instability and the high CTE. This distortion imposes difficulties in ensuring the registration of layers during multiple photolithographic steps to create an active device. Several methods have been adopted to compensate for substrate distortion such as pattern recognition-based image processing system that views alignment marks on the mask and substrate, and a fine positioning stage that moves the mask into alignment with the substrate, based on feedback from the image processing system [25, 41]. A step-and-repeat technology that incorporates active compensation architecture has been demonstrated where intrinsic and process induced distortion effects have been premeasured and are accommodated for during stitching and overlay procedure [41]. However compensation for nonlinear distortion and resolution limitations are both problematic. One novel approach for minimizing distortion is

by tuning the silicon nitride gate dielectric process to balance the stress in the gate layer [36]. However, this approach is dependent upon each material and specific processing that limits the broad actability of stress balancing as a route to limit distortion. Direct-write techniques represent an emerging class of patterning processes [42-45]. Laser direct write patterning can be used to compensate for distortion, but this technique is too slow for high volume production. Ink-jet printing is another direct-write technology that digitally modifies the resist pattern based on previous layer pattern immediately before printing. However resolution of ink-jet printing is limited by blurring of feature edges as the resist droplets spread out before drying. For the flexible electronics to gain practical, high volume applications, all these technical and processing challenges must be overcome.

1.5 Different Techniques for Fabrication of Electronics on Flexible Substrate:

One of the most fundamental challenges in fabrication of flexible electronic systems is how to process on a malleable substrate. Two basic approaches have been employed to address this challenge: 1) transfer and bonding of completed circuits to a flexible substrate and 2) fabrication of the circuits directly on the flexible substrate [6]. There are different methods for transfer-and-bond technique, but the basic approach is that the circuit is fabricated by standard method on a substrate like a Si wafer or glass plate and then it is transferred from original substrate to a flexible substrate by using laser irradiation [46] or a sacrificial release layer [47] as described below.

1.5.1 SUFTLA (Surface Free Technology by Laser Annealing/Ablation)

Seiko Epson Corporation has pioneered the laser released process termed as Surface Free Technology by Laser Annealing/Ablation (SUFTLA) and fabricated polycrystalline-silicon thin film transistor (poly-Si TFT) backplanes [5, 46, 48-49]. Figure 1.1 shows the process sequence for SUFTLA.

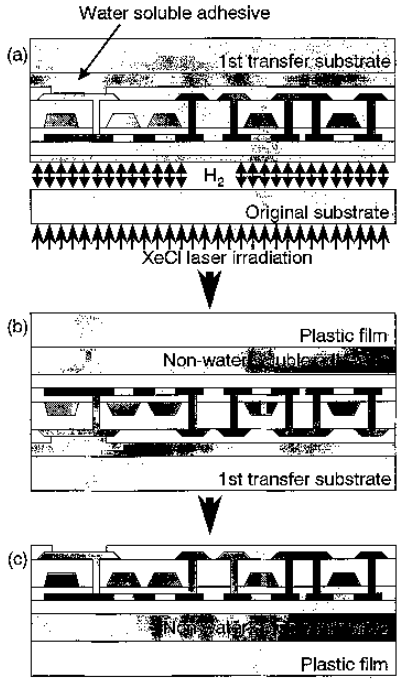

Figure 1.1: Process sequence of SUFTLA. The TFTs and TFT backplane are peeled from the original substrate and transferred onto another substrate by XeCl excimer laser irradiation [48].

First, an amorphous silicon (a-Si) film is deposited as an exfoliation layer on conventional glass or quartz substrates (original substrates). The CMOS poly-Si TFTs are fabricated on the a-Si film. The TFT substrate is then glued onto another glass substrate (1st transfer substrate) using a water soluble adhesive stiffened by UV light. Then a XeCl excimer laser is used to irradiate the back side of the TFT substrate. Upon laser irradiation, hydrogen from the exfoliation layer is evolved and causes the detachment of TFTs from the original substrate. Next, the first

transfer substrate on which the TFTs are transferred is glued onto a plastic film (PES: poly-ether-sulfone) using an adhesive. In this case, a non-water-soluble adhesive, which is also stiffened by UV light, is used. The first transfer substrate with plastic film is cut and soaked in water. When the water-soluble adhesive dissolves in water, the TFTs are transferred onto plastic substrate.

1.5.2 Nano-Structured Separation Layer Approach

Fabrication of polycrystalline-silicon thin film transistor was demonstrated by Lee et al. [47] using nano-structured separation layer approach. The schematic process flow is shown in Figure 1.2.

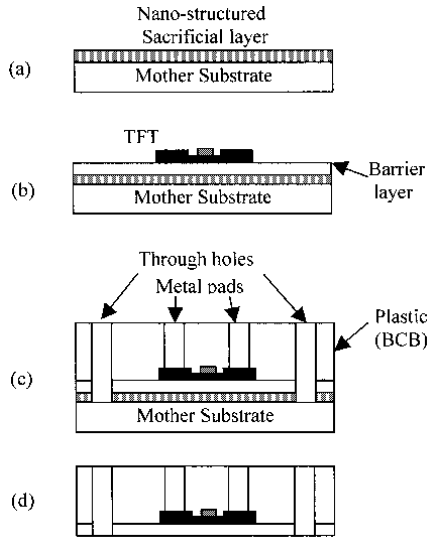

Figure 1.2: Schematic process flow of the nano-structured separation technique (a) Deposit sacrificial layer on mother substrate. (b) Fabricate TFTs on barrier layer. (c) Coat plastic and define through-holes and contact holes. (d) Release TFTs onto plastic from mother substrate [47].

The process flow starts with the deposition of a nano-structured high surface-to-volume ratio film on a “mother” substrate. This film functions as a sacrificial release layer and high surface-to-volume ratio facilitates the chemical transport. Then a barrier layer is deposited on top of the release layer and TFT fabrication is

carried out. Upon completion of the fabrication processing, the barrier layer around each TFT region is cut out using photolithography and dry etching to make TFT islands. Then a polymer film is spin-coated and through-holes are formed in the polymer film, which serves as conduits to transport chemical into the release layer. During the release process, the sacrificial column/void network film is selectively removed by the chemical solution supplied through the through-holes defined on the polymer film. The barrier layer prevents the device regions from being attacked during the separation step. After the separation, the coated polymer film becomes the final plastic substrate.

Each of these processes, SUFTLA and nano-structured separation layer, has their own inherent advantages and limitations. The layer transfer processes involve complex processing and transfer steps but circumvent the thermal, mechanical limitations during processing posed by plastic substrates. Direct fabrication of TFTs on flexible substrate is the most direct approach to the manufacturing of large area electronic surfaces without any involvement of transfer process steps [6]. It also opens up new opportunities for combining the advantages of having a flexible substrate with low cost roll-to-roll processing [3].

1.5.3 Roll-to-Roll (R2R) Manufacturing

Roll-to-roll (R2R) processing (also called “web processing”) of microelectronics would be a revolutionary advancement in process capability [1-2, 9, 25]. It offers the advantages of continuous production of fine-featured thin film devices; increasing throughput by allowing high levels of automation and by eliminating the overhead time involved in loading and unloading panels into

lithographic imaging tools and chemical processing stations as compared to batch process; these characteristics result in reduction of anticipated manufacturing cost as well as capital investment [1, 25]. Much like newspaper production, this process cost-effectively creates electronic devices on a roll of a large flexible substrate. Additionally R2R processing leads to lower contamination levels, and thus higher yields due to the minimal human handling that is needed to process the substrates [25]. However, careful attention must be given to the roll handling system in order to maintain a smooth, clean substrate surface—which is an absolute necessity for TFT processing. For example, static buildup on the substrate can lead to the collection of dust and particulates on the surface, which ultimately causes a reduction in yield [25]. A schematic of R2R manufacturing is shown in Figure 1.3.

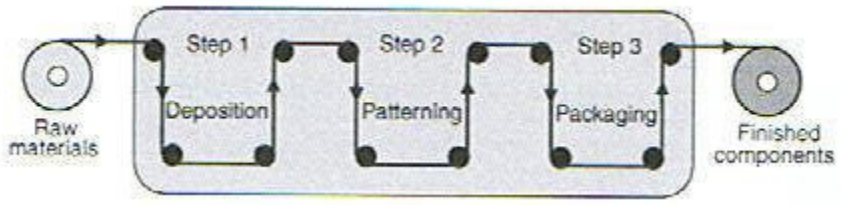

Figure 1.3: Roll-to-Roll manufacturing: Process starts with a roll of flexible substrate, the roll goes through different process steps like deposition, patterning and packaging, finally the product also come out in a roll [1]

However, initial development of flexible manufacturing with R2R will require development of new process tools and process techniques. The flexible substrates may become stretched, kinked, dimpled, or scratched during unwind and wind. Any deformation or surface roughness of the substrate will cause issues in integration of different layers and in alignment during photolithography. Microelectronics requires a number of patterning steps and the pattern can be

developed by the additive processes of directly printing the active materials like laser printing, or subtractive patterning by photolithography. All of these techniques can be adapted to web processing. But the major challenge is that backplane circuit needs high precision, alignment and yield. The roll to roll photolithography and etching tools available currently are not capable of less than 2 μm resolution and overlay registration, which is required for current TFT technology [1]. Particularly roll to roll photolithography when combined with tensioning applied for winding and with process cycles at elevated temperature, both of which cause substrate deformation, makes the overlay registration difficult [6]. Inspection tools currently exist for plastic R2R processing but they do not offer the level of defectivity inspection required for microelectronics. With feature sizes becoming increasingly smaller, in the 0.10 μm range, it is placing great demands on inspection and monitoring systems. These challenges provide a major impediment to rapid commercialization of flexible electronics with R2R manufacturing.

1.5.4 Plate-to-Plate Manufacturing

The current practice is to manufacture backplanes on glass plates or silicon wafers in batch mode. Flexible substrates, cut to sheets, can be drop-in replacement for the rigid glass plates or silicon wafers using the conventional tools. However the processing of free standing flexible substrates has difficulties primarily in handling due to their tendency to warp and fold [50]. Flexible sheet substrates can be handled in several ways during processing: attached in a frame held loosely [51], formed during processing using coat-laser process [52] or

mounted on a rigid carrier using temporary bond-debond technique [53]. However holding the substrate loosely in a frame is a technique confined to laboratory as the device film may crack or sample may curve from mismatch strain between the deposited films and the substrate. Any variation of the stress induced curvature between alignment steps results in misalignment of mask overlay during photolithography [36]. In coat laser release and in temporary bond-debond technique, the rigid carrier attached to the flexible substrate can suppress this bending of the flexible structure by providing the structural support during processing.

1.5.4.1 Coat-Laser Release Process

The coat–laser release process is based on excimer laser ablation of organic polymers. The laser separation process is schematically depicted in Figure 1.4.

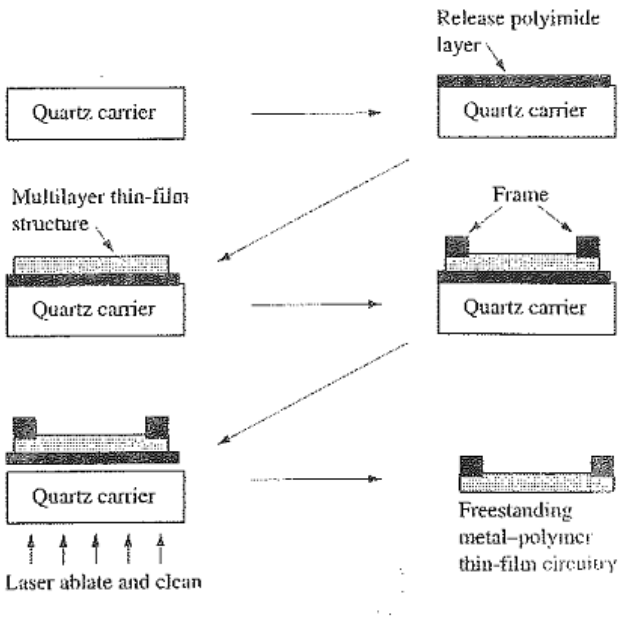

Figure 1.4: Schematic representation of the laser ablation process for fabricating freestanding multilayer thin-film structures [52]

The process starts with an optically transparent carrier which is coated with a spin coated polyimide film. The multilayer thin film device is then fabricated on the film. The polymer film acts as release layer at glass-polymer interface and as plastic substrate at device-polymer interface. Excimer laser light passed through the transparent carrier ablates the polyimide at the glass-polymer interface [52, 54]. Controlled etching of organic polymers is achieved by using pulsed ultraviolet laser radiation from excimer lasers [55]. The remaining polymer and the multilayer thin films make up the flexible device. Philips has developed a version of this process known as EPLaR™ (electronics on plastic by laser release) to produce TFT arrays for flexible OLED devices [56-57]. During the laser ablation process, the conversion of the solid release layer to the primarily gaseous by products results in a sudden volume expansion and a shock wave is transmitted through the thickness of the thin film layers in the structure. For this process to be

useful, it is critical that the force exerted by this mechanical shock wave be below the threshold value to prevent damage in the thin film structure [52].

1.5.4.2 Temporary Bond-Debond Technique

In this technique, the flexible substrate is temporarily adhered to a rigid carrier plate and processed using standard automated tools and procedures. Once the fabrication is complete, the flexible substrate is separated from the carrier through a debond process. Reversible wafer bonding technique was developed for handling thin and ultrathin substrates [58-59] and also for flexible devices [50, 53]. Handling of thin substrates is difficult because of their fragility and tendency to warp and fold. The substrates need to be supported during the thinning like backside grinding process and through subsequent processes such as photolithography, deposition etc [59]. Dragoi *et al.* demonstrated reversible wafer bonding method for handling fragile GaAs and InP wafers using wax or dry film intermediate layer [58]. Later Puligadda *et al.* demonstrated temporary wafer bonding process using thermoplastic and thermoset adhesive [59]. In this process the carrier wafer is coated with the adhesive and the device wafer (possibly after application of a protective layer) is brought into contact with adhesive coated carrier wafer under vacuum and temperature. Bonding of device wafer to the carrier wafer improves the mechanical strength and the backside lithography or back thinning could be easily performed. The temporary bonding process flow is shown in Figure 1.5.

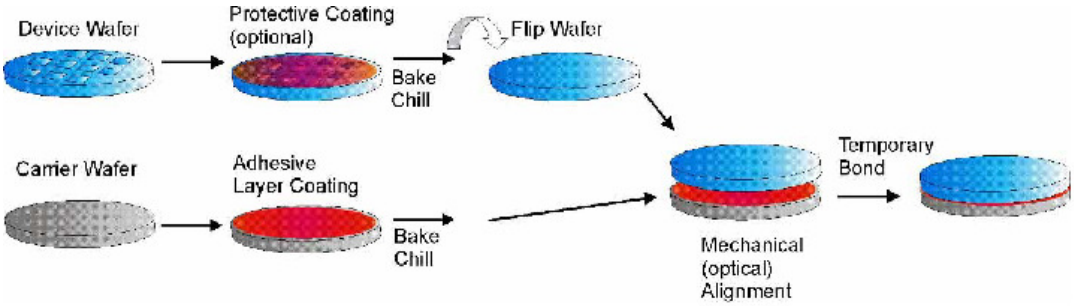

Figure 1.5: Temporary bonding process flow, device wafer temporarily bonded to adhesive coated carrier wafer [59]

For debonding two methods are employed: 1) the wafer stack is immersed in a solvent bath and the adhesive is dissolved [58] and 2) the wafer stack is placed on a heated vacuum chunk and heated at the decomposition temperature of adhesive [58-59]. Then the thinned device wafer is slid apart from the carrier wafer in a controlled manner such that the wafers stays parallel to each other until completely apart or the thinned wafer is carefully removed from the carrier using a wedge-off motion. The debonding methods are shown in Figure 1.6. These debonding techniques leave adhesive residue on both carrier and device wafer and also the debonding technique could develop stress which can lead to wafer breakage.

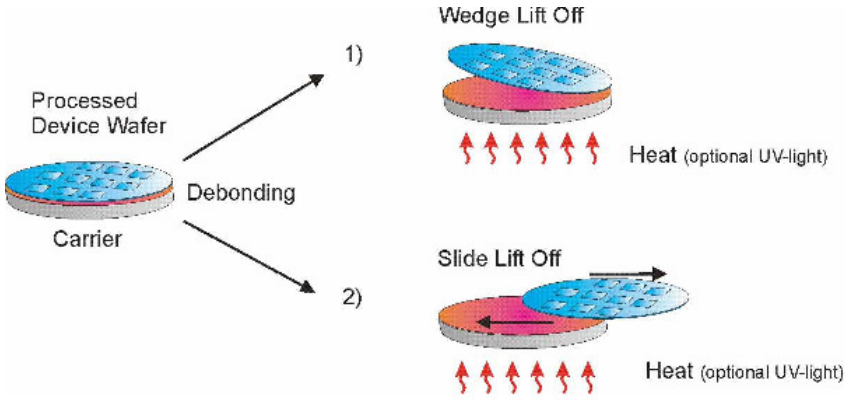

Figure 1.6: Two methods of debonding the thinned device wafer from carrier wafer 1) wedge lift off method and 2) slide lift off method [59]

The temporary bond-debond approach is also applied for fabrication of electronics on flexible substrate [53]. The advantage of temporary bond-debond approach over roll-to-roll approach is that it allows the use of conventional automated tools for manufacturing. There is no need for the development of entirely new tool systems that can handle flexible substrates. However, unlike the roll-to-roll approach, the temporary bond-debond approach utilizes batch mode fabrication and does not offer the advantages of continuous production. Therefore, temporary bond-debond technique can be considered as an interim path to break through the technological barriers for fabrication of high performance TFTs directly on flexible substrate.

Lemmi et al. [53] demonstrated fabrication of thin film transistors on polyimide substrate using temporary bond-debond technique where process temperature was below 105^{o}C limited by the stability of the adhesive and photolithography registration. Schematic of the process flow is shown in Figure 1.7.

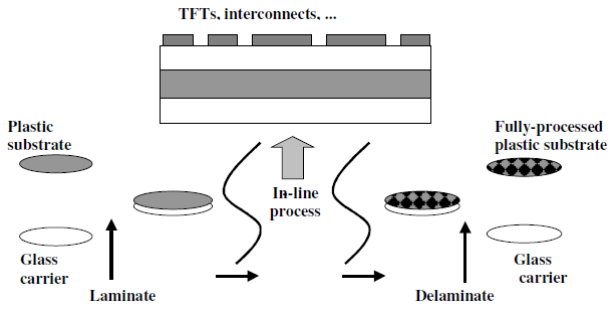

Figure 1.7: Lamination of plastic wafers on glass carriers, in-line processing and delamination of fully patterned plastic wafer from the carrier [53]

The plastic substrate is laminated on a glass carrier using an adhesive. Then the laminated wafers go through the standard fabrication process steps, where the

maximum process temperature used is 105 ^{o}C. After completion of all processes, the wafers are delaminated and annealed at 320 ^{o}C. Even utilizing 105 ^{o}C as the maximum process temperature, a deformation of 5 μm over a 150 mm wafer is observed. However, near zero deformation is required for precise photolithographic registration. The TFT performance also tends to degrade when the maximum process temperature is reduced because of the difficulty of forming high quality films for gate insulators and channel silicon layers at low temperatures [48].

Herein we discuss our development of a temporary bond-debond technique for fabricating thin film transistor backplanes on flexible plastic substrates at a maximum process temperature of 180 ^{o}C. Near zero deformation of plastic substrate (< 5 ppm) is achieved using the temporary bond-debond technique. Backplanes produced utilizing the temporary bonding method are integrated with front plane technologies to produce a flexible 320 x 240 pixel active-matrix electrophoretic displays. It is expected that using temporary bond-debond technique, it will be possible to manufacture other flexible microelectronic devices.

1.6 References

[1] Abbie Gregg*, et al.*, "Roll-to-Roll manufacturing of flexible displays," in *Flexible Flat Panel Displays*, ed, 2005, pp. 409-445.

[2] K. J. Allen, "Reel to real: prospects for flexible displays," *Proceedings of the IEEE,* vol. 93, pp. 1394-1399, 2008.

[3] W. A. MacDonald*, et al.*, "Latest advances in substrates for flexible electronics," *Journal of the Society for Information Display* vol. 15, pp. 1075-1083, 2007.

[4] G. P. Crawford, "Flexible flat panel display technology," in *Flexible Flat Panel Displays*, G. P. Crawford, Ed., ed: Wiley-SID, 2005, pp. 1-9.

[5] M. Miyasaka, "Flexible microelectronics becoming a reality with SUFTLA transfer technology,," *Journal of the Society for Information Display* vol. 15, pp. 479-484, 2007.

[6] I.-C. Cheng and S. Wagner, "Overview of flexible electronics technology," in *Flexible Electronics : Materials and Applications* W. S. Wong and A. Salleo, Eds., ed: Springer, 2009, pp. 1-20.

[7] G. B. Raupp*, et al.*, "Low-temperature amorphous-silicon backplane technology development for flexible displays in a manufacturing pilot-line environment," *Journal of the Society for Information Display,* vol. 15, pp. 445-454, 2007.

[8] Y. Sun and J. A. Rogers, "Inorganic semiconductor for flexible electronics," *Advanced Materials,* vol. 19, pp. 1897-1916, 2007.

[9] A. H. Firester, "Macroelectronics: large area flexible electronics for sensors, displays, and other applications," in *Proceedings of SPIE*, Bellingham, WA, 2004, pp. 29-37.

[10] H.-L. Chen*, et al.*, "Guest Editorial," *Journal of Display Technology,* vol. 5, pp. 169-171, 2009.

[11] A. P. Ghosh*, et al.*, "Thin-film encapsulation of organic light-emitting devices," *Applied Physics Letter,* vol. 86, p. 223503, 2005.

[12] J.-M. Han*, et al.*, "Novel encapsulation method for flexible organic light-emitting diodes using poly(dimethylsiloxane)," *Japanese Journal of Applied Physics,* vol. 47, pp. 8986-8988, 2008.

[13] A. B. Chwang*, et al.*, "Thin film encapsulated flexible organic electroluminescent displays," *Applied Physics Letter,* vol. 83, pp. 413-415, 2003.

[14] M.-C. Choia*, et al.*, "Polymers for flexible displays: From material selection to device applications," *Progress in Polymer Science* vol. 33, pp. 581-630, 2008.

[15] D. Gamota, "Near-term opportunities for large-area flexible electronics: photovoltaics, displays and sensors could lead an industry revolution," *Printed Circuit Design & Fab,* Apr 1, 2009.

[16] K. R. Sarma, "a- Si TFT OLED fabricated on low-temperature flexible plastic substrate," *Materials Research Society Symposium Proceedings,* vol. 814, pp. 1-12, 2004.

[17] J. Perrenoud*, et al.*, "Flexible CdTe solar cells and modules: challenges and prospects," in *Proceedings of SPIE* San Diego, 2009, pp. L1-L5.

[18] A. Abouraddy and Y. Fink, "Multimaterial photosensitive fiber constructs enable large-area optical sensing and imaging," in *Proceedings of SPIE*, Orlando, 2009, pp. H1-H10.

[19] B. Kelley. (2009) Flexible electronics developing for diverse applications *SPIE Newsroom*. 21 August.

[20] A. Romeo*, et al.*, "High-efficiency flexible CdTe solar cells on polymer substrates," *Solar Energy Materials & Solar Cells,* vol. 90, pp. 3407-3415, 2006.

[21] E. Bonderover and S. wagner, "A woven inverter circuit for e-textile applications," *IEEE Electron Device Letters,* vol. 25, pp. 295-297, 2004.

[22] S. P. Lacour*, et al.*, "Mechatronic system of dielectric elastomer actuators addressed by thin film photoconductors on plastic," *Sensors and Actuators A: Physical,* vol. 111, pp. 288-292, 2004.

[23] F. Lorussi*, et al.*, "Strain sensing fabric for hand posture and gesture monitoring," *IEEE Transactions on Information Technology in Biomedicine,* vol. 9, pp. 372-381, 2005.

[24] S. Carson, "Flexible electronic structures show potential for artificial muscles or biological tissues," *Argonne,* vol. I11, pp. 28-30, 2007.

[25] Kanti Jain*, et al.*, "Flexible electronics and displays," *Proceedings of the IEEE,* vol. 93, pp. 1500-1510, 2005.

[26] T. Wang*, et al.*, "RFICs on polydimethylsiloxane for flexible electronics applications," *Electronic Letters,* vol. 43, 2007.

[27] Y. Xu*, et al.*, "IC-integrated flexible shear stress sensor skin," *Journal of Microelectromechanical Systems,* vol. 12, pp. 740-747, 2002.

[28] G. P. Collins, "Next strech for plastic electronics," *Scientific American,* vol. 291, pp. 76-81, 2004.

[29] T. Someya, *et al.*, " A large area flexible pressure sensor matrix with organic field effect transistors for artificial skin applications," *Proceedings of the National Academy of Sciences* vol. 101, pp. 9966-9970, 2004.

[30] T. Someya and T. Sakurai, "Integration of organic field effect transistors and rubbery pressure sensors for artificial skin applications," *IEEE International Electron Devices Meeting,* vol. 8.4, pp. 203-206, 2003.

[31] E. Brandon, *et al.*, "Flexible electronics for space applications," *Materials Research Society Symposia Proceedings,* vol. 814, pp. I9.7.1-I9.7.12, 2004.

[32] J. Huang, "The development of inflatable array antennas," *IEEE Antennas and Propagation Magazine,* vol. 43, pp. 44-50, 2001.

[33] W. A. MacDonald, *et al.*, "Enginnered films for display technologies," in *Flexible Flat Panel Displays*, G. P. Crawford, Ed., ed, 2005, pp. 11-33.

[34] V. Zardetto, *et al.*, "Substrates for flexible electronics: A practical investigation on the electrical, film flexibility, optical, temperature, and solvent resistance properties," *Journal of Polymer Science Part B: Polymer Physics,* vol. 49, pp. 638-648, 2011.

[35] H. Gleskova, *et al.*, "Mechanics of thin-film transistors and solar cells on flexible substrates," *Solar Energy,* vol. 80, pp. 687-693, 2006.

[36] I-Chun Cheng, *et al.*, "Stress control for overlay registration in a-Si : H TFTs on flexible organic-polymer-foil substrates " *Journal of the Society for Information Display,* vol. 13, pp. 563-568, 2005.

[37] S. D. R. Gorkhali, *et al.*, "Reliability of transparent conducting substrates for rollable displays: a cyclic loading inverstigation.," *Society for Information Display, Digest of Technical Papers,* pp. 1332–1335, 2003.

[38] P. C. T. Bouten, "Failure test for brittle conductive layers on flexible display substrates," *22nd International Display Research Conference, Conference Proceedings,* pp. 313–316, 2002.

[39] W. A. MacDonald, *et al.*, "New developments in polyester films for flexible electronics.," *Materials Research Society Symposium Proceedings* vol. 769, pp. 283–290, 2003.

[40] K. H. Cherenack, *et al.*, "Amorphous-silicon thin-film transistors fabricated at 300 °C on a free-standing foil substrate of clear plastic," *IEEE Electron Device Letters* vol. 28, pp. 1004-1006, 2007.

[41] S. Gardner, "Precision photolithography on flexible substrates," ed: Azores, 2006, pp. 1-5.

[42] W. S. Wong, *et al.*, "Digital lithography for large-area electronics on flexible substrates," *Journal of Non-Crystalline Solids* vol. 352, pp. 1981–1985, 2006.

[43] H. Sirringhaus and S. Burns, "Alignment Tolerant Patterning on Flexible Substrates," WO/2006/059162, 2006.

[44] W. S. Wong, *et al.*, " Digital lithographic processing for large-area electronics," *Journal of the Society for Information Display,* vol. 15, pp. 463-470, 2007.

[45] K. R. Kim and K. Y. Baek, "A laser selective etching process for next-generation flexible display," in *Proceedings of the Laser Microfabrication Conference*, Phoenix, USA, 2006, pp. 198-202.

[46] T. Shimoda and S. lnoue, "Surface Free Technology by Laser Annealing (SUFTLA)," *IEDM Technical Digest. International,* vol. 99, pp. 289-292, 1999.

[47] Y. Lee, *et al.*, "High-Performance Poly-Si TFTs on Plastic Substrates Using a Nano-Structured Separation Layer Approach," *IEEE Electron Device Letters,* vol. 24, pp. 19-21, 2003.

[48] S. Inoue, *et al.*, "Surface-Free Technology by Laser Annealing (SUFTLA) and its application to poly-Si TFT-LCDs on plastic film with integrated drivers," *IEEE Transactions on Electron Devices,* vol. 49, pp. 1353-1360, 2002.

[49] T. Hashimoto;, *et al.*, "Device manufacturing method " *US Patent,* vol. 7029960, 2006.

[50] G. Nisato, "Flexible Devices," WO/2005/048669.

[51] H. Gleskova, *et al.*, "a-Si:H TFTs made on polyimide foil by PECVD at 150^{o}C," *Proceedings of the Materials Research Society,* vol. 508, pp. 73-78, 1998.

[52] F. E. Doany and C. Narayan, "Laser release process to obtain freestanding multilayer metal polyimide circuits," *IBM Journal of Research and Development* vol. 41, pp. 151-155, 1997.

[53] F. Lemmi, *et al.*, "High-performance TFTs fabricated on plastic substrates," *IEEE Electron Device Letters,* vol. 25, pp. 486-488, 2004.

[54] G. Arjavalingam;, *et al.*, "Multi-layer thin film structure and parallel processing method for fabricating same ", US Patent 5258236, 1993.

[55] R. Srinivasan and V. Mayne-Banton, "Self-developing photoetching of Polyethylene terephthalate films by far-ultraviolet excimer laser radiation," *Applied Physics Letter,* vol. 41, pp. 575-578, 1982.

[56] I. French and D. McCulloch, "Active matrix displays and other electronic devices having plastic substrates," *International Patent* vol. WO2005/050754 A1, 2005.

[57] H. Lifka*, et al.*, "Ultra-thin flexible OLED device," *Society of Information Display Symposium, Digest Technical Papers,* vol. 38, pp. 1599-1602, 2007.

[58] V. Dragoi*, et al.*, "Reversible wafer bonding for reliable compound semiconductor processing," *IEEE,* pp. 331-334, 2002.

[59] R.Puligadda*, et al.*, "High performance temporary adhesives for wafer bonding applications," *Matererials Research Society Symposium Proceedings.,* vol. 970, pp. 239-249, 2007.

Chapter 2

Temporary Bond-Debond Technology for Flexible Electronics

2.1 Introduction

Temporary bond-debond technology for applications in wafer thinning process as mechanical support to device wafer was introduced in Chapter 1. In this case, processed device wafer was mounted on carrier wafer for wafer thinning process [1-2]. Similarly, this process has been used to fabricate thin film transistors (TFTs) on flexible plastic substrates at temperatures below 105 ^{o}C, limited by the stability of the adhesive and photolithography registration. A deformation of the plastic substrate of 5 μm over a 6 inch wafer surface was demonstrated [3]. In this case, the flexible substrate was bonded temporarily to a rigid carrier and then processed using standard microelectronics tools. In addition to the advantage of enabling the use of existing equipment, the rigid carrier can also suppress the bending of the flexible structure during processing to provide requisite planarity, dimensional stability, and lithographic registration during device fabrication. Following device fabrication, debonding the carrier from the flexible substrate yields a flexible electronic device. Thin film transistors (TFT) are generally selected for flexible electronics for flexibility and low cost. However, TFT performance tends to degrade when the process temperature is reduced because of the difficulty of forming high quality films for gate insulators and channel silicon layers at low temperatures [4]. The concentration of defects (dangling Si bonds) increases, the mass density decreases, and the doping

efficiency drops in silicon layers [5]. The films with low mass density and high charge trapping generally exhibit poor electronic properties. This change is usually attributed to reduced surface mobility of the film-building radicals due to lower thermal energy on the growth surface [6]. The gate dielectric material must have good insulating properties and low charge-trapping rate at lower electric fields, and should form a high-quality interface with the semiconductor layer. The reduction of deposition temperature often leads to a material with high hydrogen concentration and poor dielectric performance [7]. Therefore it is beneficial to fabricate transistors at high temperature. However the maximum tolerable process temperature is limited by the type of substrate used: <300, <600 and <1000 ^{o}C for plastic, glass and steel substrates respectively [8]. Therefore it is desired to develop the temporary bond debond method to retain bond integrity at the maximum possible process temperature compatible with the substrate used in addition to maintaining precise photolithographic registration during TFT fabrication process steps.

Successful implementation of the temporary bond-debond method requires simultaneous development of new adhesive formulations, selection of compatible carrier plate-flexible substrate pairs and optimization of the associated process steps. The principal challenges are as follows: First, the adhesive must form a sufficiently strong bond between the flexible substrate and rigid carrier to withstand the full range of thin-film transistor (TFT) fabrication conditions experienced in processing. These include photolithography, thermal vacuum, reactive plasma, wet acid/base and solvent processes. In addition to these

stringent adhesion requirements, the adhesive also must allow easy separation of carrier and flexible substrate once fabrication is completed. These two requirements are generally incompatible with most adhesive formations, since strong adhesion of the flexible substrate to the carrier plate will typically result in difficulties in removing the fabricated flexible device. Second for high quality, defect-free displays and other high performance electronic devices, the debonding process must not damage or degrade the performance of the TFT arrays on the flexible substrate and also not leave any adhesive residue on the substrate. Third, the stress that is developed during processing predominately through thermal-mechanical property mismatches between the polymer-based flexible substrates and rigid carriers like glass or silicon leads to the bowing of the bonded system or delamination of the flexible substrate from the rigid carrier. Bowing leads to wafer handling problems in processing equipments. The coefficient of thermal expansion (CTE) of most commonly available polymers that are considered for flexible substrates like polyimide (PI), polyethylene terephthalate (PET), polyethylene naphthalate (PEN) etc. are significantly greater than readily available, rigid inorganic materials that are considered for carriers like glass and silicon. In addition to considerations related to the technical difficulties associated with the flexible substrate-carrier system, the materials utilized for the bond-debond technology must be considered globally in the process. Therefore the temporary bonding adhesive must also be "semiconductor grade" to avoid particle formation in the cleanroom environment, impurities that might contaminate the TFTs, and outgasing in vacuum processing tools. Finally the bonding and

debonding processes must be manufacturable (fully automatic, reproducibly yielding defect-free, high integrity bonded layers). To meet all these requirements, the selection of the carrier plate, flexible substrate and adhesive are all critical to the success of the bond-debond method.

2.2 Selection of Bonded Assembly

2.2.1 Choice of Flexible Substrate

In order for flexible substrates to serve as drop-in replacement for glass substrate, they need to be able to mimic the properties of glass, like dimensional stability, thermal stability, optical clarity, solvent resistance, low permeability of oxygen and moisture, low coefficient of thermal expansion (CTE), smooth surface, no contaminants extracted during processing, and inert against process chemicals [8]. For example thermal and dimensional stability of the substrate is critical to ensure precise registration of the different layers during photolithography and for the multilayer devices to be able to withstand thermal cycling during manufacture [9-12]. The surface smoothness and cleanliness of the flexible substrates are essential to ensure integrity of subsequent layers [13]. In addition, TFT performance degrades due to interaction with moisture and oxygen [12]. Metal foil substrates offer an advantage of high process temperature capability with acceptable dimensional stability; they are inherently impermeable, thereby no barrier layer is required to protect the substrate from ambient moisture and oxygen. However, metal foils do require planarization due to poor surface smoothness characteristics and electrical insulation prior to use as a substrate in device fabrication. Another significant liability for metal foil is its intrinsic

limited flexibility because of high modulus. Conversely, plastic substrates are easily bendable and flexible; they are typically optically transparent and thus are compatible with both the bottom emitting and the top emitting OLED device architectures. Additionally, plastic substrates are commonly believed to have a lower cost potential compared to the metal foil substrate [12]. However, there are a number of major limitations for available plastic substrates including limited process temperature capability, lack of dimensional stability and greater difference in the coefficient of thermal expansion (CTE) between the plastic substrate and the materials in the TFT thin films. In the long term, fabrication on plastic substrates is desired over metal foils. Here we will illustrate the bond-debond process applied to plastic substrates. Choice of a plastic substrate is more challenging as thermal and dimensional stability (T_g compatible with device process temperature [8]), low moisture uptake, moderate CTE (<20 ppm/^oC [13]), good surface properties (roughness in several nanometer scale [13]), compatibility with TFT process chemistry and high optical transmission in the visible range (>85% [13]) are critical. Based upon these considerations, polyethylene naphthalate (PEN) substrates (Teonex® brand) are utilized as the plastic substrate in the bond-debond process for fabricating the backplane on flexible substrates.

2.2.2 Choice of Carrier

The carrier wafer provides structural support to flexible substrate during handling and processing. The carrier should be sufficiently thick to be rigid, but thickness should be minimized, less than 1.1 mm, for easy handling due to weight and decreasing the carrier cost. Additionally, the surface roughness should be

low, within hundred nanometer range. Carrier material must have high purity to prevent ion leaching from the carrier that could potentially degrade the ultimate TFT performance. Above all, the carrier should be designed to minimize the stress development during processing that would lead to bow and wafer handling issues. Therefore the carrier should have low initial internal stress and its CTE should closely match the CTE of flexible substrate. In the carrier selection, the radius of curvature of the bonded wafer being as large as possible, preferably infinite, is the first key screening parameter, since device fabrication with automated wafer handling requires planar substrates, the bow value needs to be within 60-70 μm for 6 inch wafer. Additionally, vacuum is a common method for holding the wafers in place during process, but vacuum failure can occur for highly bowed wafers. The radius of curvature of the carrier-substrate system depends on material properties such as elastic modulus (E) and Poisson ratio (ν), thickness, and mismatch in strain (ε) between the materials [14]. This mismatch strain, ε, has two dominant components; one is the thermal mismatch strain caused by the difference between the coefficients of thermal expansion (α) of the materials, the other one is the built-in strain (ε_{bi}) [15]. Therefore, $\varepsilon = (\alpha_1 - \alpha_2)\Delta T + \varepsilon_{bi}$, where ΔT is the difference between the room temperature and the process temperature. The built-in strain (ε_{bi}) of the carrier can be minimized through pre- screening of carriers from bow measurement of as received carriers. Carriers with high bow values, greater than 50-60 μm, are rejected during pre-screening. Then if ΔT is fixed, mismatch strain can be minimized by minimizing the difference between coefficients of thermal expansion between carrier and flexible substrate. The

types of glass carriers, such as D263T, AF45 and Corning Eagle 2000 have different CTE, thickness and modulus. Additionally a silicon carrier and a specialty carrier Alumina having high modulus and CTE are investigated for minimization of bow.

2.2.3 Adhesive Considerations

Adhesion between two surfaces is complex and depends upon chemistry, mechanics, and surface science of the adhesive, carrier and substrate [16]. For the adhesive, liquid-like properties are desired to ensure good contact with the surface, but solid properties are desired to sustain stress of the joint and to provide sufficient shear strength between the substrate and carrier. The thermal stress developed between the carrier and flexible substrate based upon CTE mismatch can be released by the flow of the adhesive or by bowing of the carrier-substrate system. Thus the adhesive behavior has a strong impact on the thermo-mechanical reliability of the assembly. Besides bonding the carrier and substrate, the adhesive must also keep the flexible substrate fixed in position to reduce the distortion during processing. Also the viscoelastic behavior of bonding adhesive is dependent on the processing temperatures of TFT fabrication. Therefore in addition to a host of chemical, physical and thermal property requirements that must be met by the adhesive, mechanical properties of adhesive also need to be carefully considered to prevent significant distortion of the substrate and/or bow of the carrier. Two different type of adhesives, one is thermoplastic elastomer and the other is UV curable thermoset, supplied by Henkel Corp., are investigated to understand the relation of bow and distortion of the bonded system with

viscoelastic property of adhesive. For elastomer polymer, energy storage is always accompanied by some energy dissipation during deformation. The entanglements of the long elastomer chains act as obstructions to the movement of the polymer chains. These obstructions enable the elastomer to store energy—an elastic property. Thermosets are cured irreversibly through heat, through a chemical reaction or through irradiation such as UV irradiation. As a result of curing, covalent cross-linkages form, which ensures that the thermoset will return to its original configuration when the stress is removed showing the elastic property.

2.3 Experimental

The temporary bonding-debonding method for manufacturing of flexible electronics consists of (1) initial bonding of substrate to rigid carrier using adhesive, (2) lithographic and vacuum deposition processes to fabricate TFTs and (3) clean de-bonding of the flexible electronic backplane from the carrier plate.

2.3.1 Bonding and Processing

In the bonding process, the adhesive is first deposited on carrier by standard solution deposition technique (i.e., spin, spray, screen, roll-coat). For adhesive formulations containing solvent (used for stainless-steel substrates), a post-apply-bake (PAB) is used to remove residual solvent. This bake is done on hotplates in two steps. During the first step, the adhesive coated wafer is heated at 80°C for 30 min, and during the second step it is heated at 130°C for 15 min to ensure all residual solvent is removed. The flexible plastic substrate is then

laminated to the adhesive coated carrier using a hot roll laminator (Western Magnum). Prior lamination, the plastic sheet is baked through a heat-stabilization cycle at180 ºC which helped relieve the internal stress of the plastic sheet. For UV curable adhesive, the curing is done through plastic sheet using UV radiation after lamination. Dymax UV curing unit is used at UVA wavelength (400-315 nm) for irradiation. Finally, the bonded system is baked under vacuum at 180 ºC for 1 hr. This post-lamination bake is used to test if the bonded system can withstand the high temperature and high vacuum conditions encountered during TFT fabrication. Also this baking cycle helps the bonded substrate to relieve internal stresses and reduce plastic deformation in all the following processes. The laminated system is subsequently cleaned using detergent followed by QDR (quick-dump-rinse) and SRD (spin-rinse-dry). Figure 2.1 schematically illustrates this wafer bonding process.

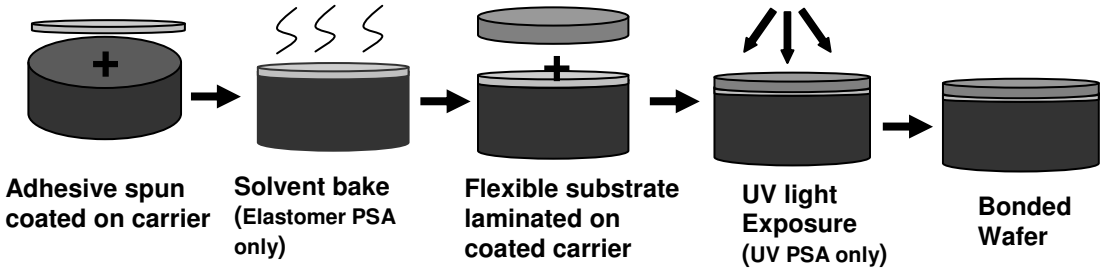

Figure 2.1: Schematic of adhesive bonding process

The bonded wafers were then processed to fabricate TFT arrays. The processing steps included all the standard microelectronics processing steps, for example plasma enhanced chemical vapor deposition (PECVD), wet and dry etching, sputtering and photolithography.

2.3.2 Debonding Issues and Solutions

Different techniques can be employed to release the device wafer from the carrier substrate at the end of fabrication process. For example, the wafer can be immersed in a solvent bath to dissolve the adhesive [1], but this requires long debonding time due to solvent diffusion limitations based upon the limited area of the adhesive between the carrier and flexible substrate exposed to solvent. Alternatively, the wafer can be heated to induce decomposition of the adhesive or at minimum a requisite reduction in adhesion force [1-2]. The decomposition temperature must be high enough so that the adhesive is thermally stable during processing, but still low enough so that the plastic substrate does not degrade at that temperature. The debonding methods by exposure to solvent and heating are shown schematically in Figure 2.2 (a) and 2.2(b) respectively.

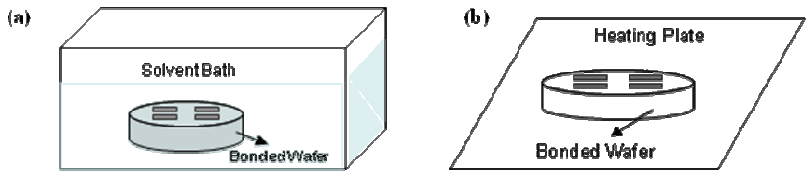

Figure 2.2: Different debonding methods (a) bonded wafer immersed in solvent bath to dissolve adhesive, (b) bonded wafer heated on heating plate to decompose or reduce adhesion force of adhesive

A third alternative is to expose the system to a laser for ablation of the adhesive. In this mechanism, the laser energy is converted to heat to cause thermal decomposition of the polymer [17]. Alternately in laser release process, a thin polymer layer is cast from solution on glass, followed by TFT fabrication and backside excimer laser-induced release by melting/ablation of the polymer at the glass polymer interface [18]. Debonding by laser exposure is shown in Figure 1.5. Fourthly, the flexible substrate can be mechanically debonded from the

carrier. A thin wire or blade can pass through and mechanically separate the flexible substrate from the carrier. However, the wire needs to be thin enough and/or adhesive thick enough so that the wire can pass in between carrier and flexible substrate and additionally, adhesive residue remains both on carrier and flexible substrate after separation. Alternately, ultra-violet (UV) curing can be utilized to obtain very low adhesion strength to cause adhesive failure, preferably from flexible substrate. Debonding by thin wire and UV curing are shown schematically in Figure 2.3 (a) and 2.3 (b) respectively.

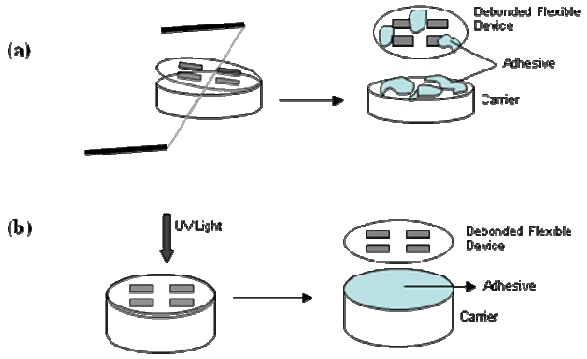

Figure 2.3: Debonding (a) by passing through thin wire between carrier and flexible substrate, adhesive residue remains on both carrier and flexible substrate (b) by UV curing causes adhesive failure preferably from flexible substrate

Crosslinking of the polymer adhesive reduces the intimate contact with the adherend by limiting elastic deformation and viscous flow, while enhancing its cohesive strength to promote adhesive failure [19-20]. Above the gel point, additional crosslinking causes significant strain hardening in extension leading to early detachment of fibrils from the adhesive film and hence lower peel strength [21]. Due to the neat delamination offered by this last method, we utilized crosslinking of the adhesive to debond the plastic substrate, which enabled the substrate to be easily peeled from the carrier.

2.4 Results

2.4.1 Bonded-Debonded Wafer

The final bonded system consisting of a 150 mm HS-PEN (heat stabilized polyethylene napthalate) substrate (supplied by DTF) bonded to a rigid carrier is shown in Figure 2.4(a). Laminated plastic substrates using the temporary bonding technique have been subsequently processed to fabricate TFT arrays. These bonded systems can be processed using standard automated toolsets for the fabrication such as shown in Figure 2.4(b) where a bonded plastic wafer is processed using an automated photoresist coater tool. The ability to utilize automated tools leads to improved yield and less device to device variability. After full processing to fabricate an array of TFTs for display backplane, the flexible substrate is debonded by peeling-off and the debonded flexible device retained its original flexibility as shown in Figure 2.4 (c).

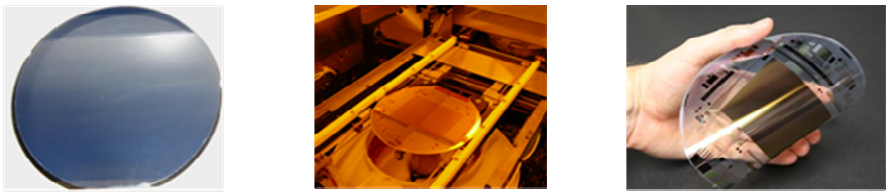

Figure 2.4: HS-PEN substrate at different stages of processing: (a) bonded to carrier prior to TFT fabrication, (b) automated photoresist coater tool handling the bonded plastic wafer, and (c) flexible plastic wafer after process completion and debonding

2.4.2 Impact of Processing Conditions on Bonding Efficacy

During TFT fabrication process steps, the wafers experience high temperature and high vacuum conditions. Additionally, a wide variety of solvents and chemicals are used for depositing and etching different layers in the TFT

arrays fabricated on the flexible substrates. The maximum process temperature, 180 ^{o}C, is constrained by the thermal stability of the plastic substrate. Heat-stabilised polyethylene-naphthalate film exhibits typically shrinkage of order <0.05 % when exposed to temperatures of up to 180 ^{o}C for 30 min [13]. During sputtering, a high vacuum level of 10^{-7} Torr is encountered, so the bonding must withstand these conditions with minimal degassing from the adhesive. Though dry etching is utilized when possible, some wet chemistry is involved in device fabrication. For example, buffered oxide etch (BOE) is used to etch some layers during processing. Additionally to strip photoresist, metal-ion-free (MIF) developer is used and the process utilizes a number of solvents like hexane, acetone, propylene glycol methyl ether acetate (PGMEA) and isopropyl alcohol (IPA). Detergent 8 is used for cleaning the bonded substrates. For adhesives examined herein, substrate-carrier systems sustain their bonding integrity for all these conditions.

2.4.3 Failure Modes

If the materials and/or the processes do not meet the inherent demanding requirements of the temporary bond-debond method, the bonded wafer will fail typically through two major failure modes as illustrated in Figure 2.5. Figure 2.5 (a) illustrates blistering of the adhesive between HS-PEN substrate and a glass carrier following plasma enhanced chemical vapor deposition (PECVD) of a-Si:H semiconductor channel layer. The blistering tends to occur preferentially at particle-defect and bubble-defect sites already present or created during bonding process, and is exacerbated by outgassing of the adhesive including volatilization

of residual solvent or low-molecular-weight components, during thermal or/and vacuum process steps. To prevent particle defects, the adhesives are filtered through a 1-μm fillter prior to use. Stress developed during annealing due to CTE mismatch between the carrier and flexible substrate leads to bowing of the bonded system as illustrated in Figure 2.5(b). Issues associated with these defects and stresses cause difficulties with automated processing (for bowed wafers), TFT performance degradation and yield loss. The developed temporary bond-debond method successfully addresses these issues from careful selection of substrate-adhesive-carrier system.

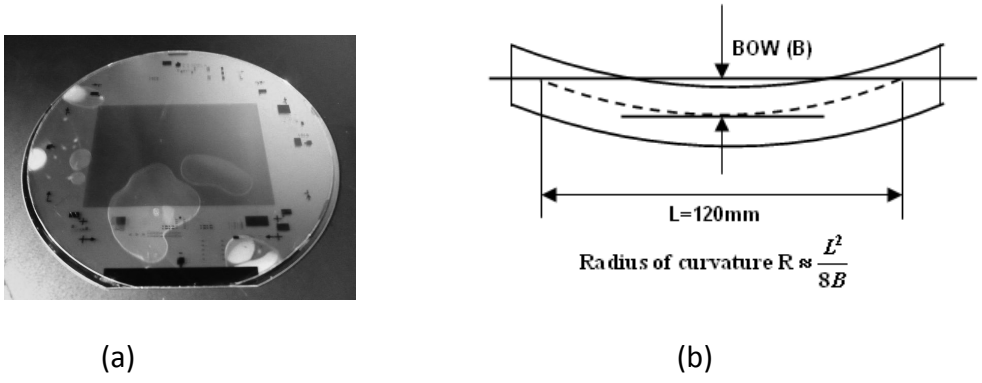

(a) (b)

Figure 2.5: Failure modes in temporary bonding/debonding: (a) an HS-PEN substrate bonded to a glass wafer with catastrophic blistering and (b) schematic representation of bow

2.5 Conclusions

A novel technology based upon temporary bond-debond has been developed to enable fabrication of thin film devices directly on flexible substrates. This process allows for traditional microelectronics and display fabrication tools to be utilized without modification in the manufacture of flexible electronics. The flexible substrate temporarily laminated to a rigid carrier can be processed using conventional automated TFT fabrication tools. After full TFT fabrication, the

flexible substrates are delaminated and retain their flexibility. We believe that temporary bond-debond manufacturing scheme is a viable interim manufacturing option prior to implementation of roll-to-roll processing that should enable rapid market entry of flexible electronics and displays with minimum requirements in capital investment.

2.6 References:

[1] V. Dragoi, *et al.*, "Reversible wafer bonding for reliable compound semiconductor processing," *IEEE,* pp. 331-334, 2002.

[2] R.Puligadda, *et al.*, "High performance temporary adhesives for wafer bonding applications," *Matererials Research Society Symposium Proceedings.,* vol. 970, pp. 239-249, 2007.

[3] F. Lemmi, *et al.*, "High-performance TFTs fabricated on plastic substrates," *IEEE Electron Device Letters,* vol. 25, pp. 486-488, 2004.

[4] S. Inoue, *et al.*, "Surface-Free Technology by Laser Annealing (SUFTLA) and its application to poly-Si TFT-LCDs on plastic film with integrated drivers," *IEEE Transactions on Electron Devices,* vol. 49, pp. 1353-1360, 2002.

[5] J. Robertson, "Deposition mechanism of hydrogenated amorphous silicon," *Journal of Applied Physics,* vol. 87, pp. 2608-2617, 2000.

[6] J. Perrin, "Reactor design for a-Si:H deposition," in *Plasma Deposition of Amorphous-Based Materials*, C. P. Bruno G, Madan A, Ed., ed San Diego, CA,: Academic Press, 1995, pp. 177-241.

[7] A. Sazonov, *et al.*, "Low-temperature amorphous and nanocrystalline silicon materials and thin-film transistors," in *Flexible Electronics: Materials and Applications*, W. S. Wong and A. Salleo, Eds., ed: Springer, 2009.

[8] I.-C. Cheng and S. Wagner, "Overview of flexible electronics technology," in *Flexible Electronics : Materials and Applications* W. S. Wong and A. Salleo, Eds., ed: Springer, 2009, pp. 1-20.

[9] J. H. Souk and W. Lee, "A practical approach to processing flexible displays," *Journal of the Society for Information Display,* vol. 18, pp. 258-265, 2010.

[10] Kanti Jain*, et al.*, "Flexible electronics and displays," *Proceedings of the IEEE,* vol. 93, pp. 1500-1510, 2005.

[11] F. Lemmi*, et al.*, "Poly-Si TFTs from glass to plastic substrates: process and manufacturing challanges," *Materials Research Society Symposium Proceedings,* vol. 814, pp. I1.6.1-I1.6.11, 2004.

[12] K. R. Sarma, "a- Si TFT OLED fabricated on low-temperature flexible plastic substrate," *Materials Research Society Symposium Proceedings,* vol. 814, pp. 1-12, 2004.

[13] W. A. MacDonald*, et al.*, "Enginnered films for display technologies," in *Flexible Flat Panel Displays*, G. P. Crawford, Ed., ed, 2005, pp. 11-33.

[14] G. G. Stoney, "The tension of metallic films deposited by electrolysis," *Proceedings of the Royal Society of London. Series A,* vol. 82, pp. 172-175, 1909.

[15] H. Gleskova*, et al.*, "Mechanics of thin-film transistors and solar cells on flexible substrates," *Solar Energy,* vol. 80, pp. 687-693, 2006.

[16] G.Fourche, "An overview of the basic aspects of polymer adhesion," *Polymer Engineering and Science,* vol. 35, pp. 957-967, 1995

[17] V. Loryuenyong*, et al.*, "Photo-polymer wafer bonding for double layer transfer," *Materials Research Society Symposium Proceedings,* vol. 768, pp. G5.6.1-G5.6.6, 2003.

[18] F. E. Doany and C. Narayan, "Laser release process to obtain freestanding multilayer metal polyimide circuits," *IBM Journal of Research and Development* vol. 41, pp. 151-155, 1997.

[19] A. Zosel, "Effect of crosslinking on tack and peel strength of polymers," *Journal of Adhesion,* vol. 34, pp. 201-209, 1991.

[20] T. P. Russell and H. C. Kim, "Tack--a sticky subject," *Science,* vol. 285, pp. 1219-1220, 1999.

[21] C.Creton and P.Fabre, "Tack," *Comprehesive Adhesion Science,* vol. 2, pp. 1-24, 2001.

Chapter 3

Temporary Bond-Debond Process: Impact of Adhesive and Carrier Properties on Performance of Flexible Electronics

3.1 Introduction

Manufacturing of electronics on flexible substrates is challenged by the difficulties in alignment and conformity of the substrate through deposition, patterning and etch processes [1-5]. Flexible plastic substrates are not dimensionally and thermally stable like traditional glass or silicon substrates. During high temperature processing, deformation or distortion of the substrate occurs due to the coefficient of thermal expansion (CTE) mismatch between the device layers and the flexible substrate. This distortion imposes difficulties in ensuring the registration of layers during multiple photolithographic steps to create an active device. Several methods have been adopted to compensate for substrate distortion such as pattern recognition-based image processing system, step-and-repeat technology that incorporates active compensation architecture, direct-write techniques etc. These methods and their limitations were introduced in Chapter 1. It is highly desirable that the plastic substrate does not deform at all. The temporary bond-debond process can be used as an alternative technique to minimize flexible substrate distortion. In this process, the flexible substrate is temporarily adhered to rigid carrier using a specialty adhesive. The rigid carrier should act to fix the flexible substrate in its position by the adhesive and prevent distortion at elevated temperatures. Another fundamental challenge is to control

the stress developed during the bonding-debonding process and the fabrication process steps; these stresses evolve predominately through thermal-mechanical property mismatches between the carrier and flexible substrate. The stress is relaxed through bowing of the bonded system (flexible substrate-adhesive-carrier), which can lead to wafer handling issues or delamination of the flexible substrate from the rigid carrier. In particular, we examine heat-stabilized polyethylene-napthalate (HS-PEN) as the flexible substrate. HS-PEN has been developed as a plastic substrate for flexible electronics applications and exhibits good thermal and dimensional stability, low moisture uptake (typically absorb approximately 1400 ppm of moisture at equilibrium; the exact figure depends on temperature and relative humidity [6]), and moderate CTE (26 ppm/^{o}C in 20-180^{o}C temperature range [6-7]). To investigate the impact of thermal-mechanical mismatches on wafer bow and photolithographic alignment, a series of different carriers and adhesives are examined with varying properties of carriers and adhesives. CTE, modulus and thickness of carriers have been shown to control the deformation of fully elastic multilayer systems [8-10]. Additionally, the viscoelastic properties of the adhesives used to bond the flexible substrate to the rigid carrier may also impact stress and deformation of the bonded system [11-13]. Generally viscoelastic properties of adhesives are not considered when modeling the residual stress in bonded systems [14-18]. However the viscous flow of adhesive may relax some stress developed between the two adherend. Finally, debonding from the carrier substrate is required to yield the flexible electronic device. Depending on viscoelastic property of adhesive, the peel force can be

reduced [19] and should allow the easy separation of flexible substrate from carrier without damaging or degrading the performance of the active device.

3.2 Experimental

3.2.1 Materials and processing

HS-PEN (125 μm thickness) was obtained from DuPont Teijin Films (tradename Teonex Q65A) and utilized as the flexible substrate for fabrication of thin film transistor (TFT) arrays for display backplanes. Two types of adhesive were used in this study for bonding the substrate: a solution-based Elastomer pressure sensitive adhesive (PSA) and solvent-less ultraviolet (UV) photo-curable PSA, both supplied by Henkel Corporation. Silicon wafers and D263T, AF45 and Corning Eagle 2000 glass wafers (150 mm) were utilized as carriers. The bonding process was followed as described in Chapter 2.

3.2.2 Characterization

The bow of bonded wafers was measured at ambient conditions using Optical Stylus Sensor (Tamar Technology). It measures the bow from the physical deviation of center point of the median surface of the wafer from a best fit plane through the points on the specified diameter where the median surface is the locus of the points equidistant between the front and back surfaces. Figure 3.1 shows schematically the measurement of bow. The bow was determined at the 120 mm periphery of the 150 mm bonded wafer.

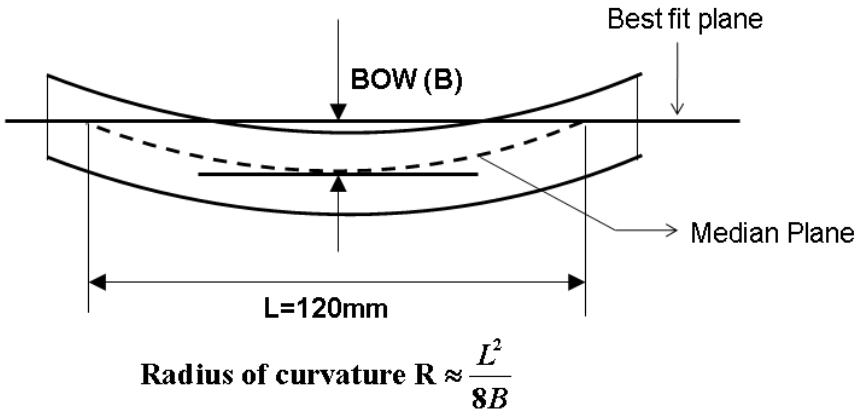

Figure 3.1: Bow by measuring the location of the median surface at the center of the wafer and determining its distance from the best fit plane

To assess the misalignment of the layers, verniers that are orthogonal pairs located at 120 mm periphery of a 150 mm wafer are utilized as shown in Figure 3.2. The first photolithographic layer prints single large square box verniers, while the second photolithographic layer prints verniers that consist of four small square boxes. In the case of a perfectly aligned substrate, the boxes from the two levels should be centered upon one another as shown in Figure 3.2. To align the second lithographic layer, the fiduciary alignment mark used is near the top of the wafer (the bottom of the wafer is defined by the flat). The misalignment between layers is quantified by monitoring the distance between the boxes of the verniers using optical microscopy (Olympus Microscope). The images of aligned or misaligned verniers are captured using the image capturing tool of the microscope. The shifting of edges of second layer verniers with respect to the similar edges of first layer verniers is calculated from the captured images using nanoscope measuring tool of the microscope.

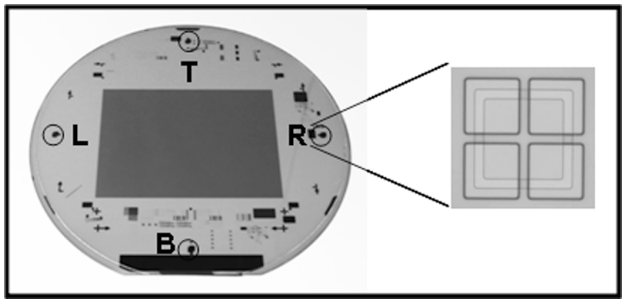

Figure 3.2: Location of four verniers, lie on 120 mm periphery of a 150 mm wafer, HS- PEN bonded to 0.9 mm thick D263T glass carrier

The rheological properties of adhesives were investigated in the temperature range -70 ^{o}C to 200 ^{o}C using Rheometric Solid Analyzer III from Texas Instrument. The rheology data was provided by Henkel Corporation.

3.2.3 Thin Film Deposition

Following the post bond bake for select bonded systems, metal film and silicon stack were deposited and patterned to measure photolithographic registration misalignment. A maximum process temperature of 180 °C was utilized to prevent thermal degradation of the flexible plastic substrate. A PECVD SiN_x film was deposited at 180^{o}C on the HS-PEN as the passivation layer. The metal bottom contact layer was deposited by sputtering at room temperature. Following photolithographic steps, the metal film was dry etched to form the first patterned layer. Subsequently, a silicon stack composed of a-SiN*x*:H dielectric and a-Si:H semiconductor was deposited by PECVD at 180^{o}C. Patterning via photolithography followed by etching the silicon stack was used to form the second patterned layer. The misalignment between the two levels, metal and silicon stack, was monitored using optical microscopy.

3.3 Results and Discussions

3.3.1 Effect of Adhesive Properties on Stress and Distortion

Since the role of an adhesive layer on distortion of flexible substrate is generally not considered, it is informative to first determine if the properties of the adhesive impact the ability to reliably align layers using photolithographic patterning. Figure 3.3 illustrates the difference in mask overlay of the two photolithographic levels for the two different adhesives. The misalignment of the lithographic layers on HS-PEN bonded to a glass carrier (0.9 mm thick D263T) using Elastomer PSA is shown in Figure 3.3(a). It is clear from the micrographs that the sample is highly misaligned for this bonded system. Examining the features more carefully illustrates that the second layer is misaligned towards the center of the wafer. This misalignment indicates that the HS-PEN substrate stretched to larger dimensions during deposition of the second layer. In particular, the bottom (B) feature has no overlap of the two printed layers, which are misaligned by 59 μm. The bottom vernier is misaligned more than the top verniers which are misaligned by 4.7 μm as the mask for printing the second layer is aligned using the fiduciary alignment mark located at upper part of the substrate. Using the same processing and materials except switching the adhesive to UV PSA yields near perfect alignment as illustrated in Figure 3.3 (b). The two mask levels nearly perfectly overlay on each other. The properties of the adhesive thus must be considered for controlling the distortion of bonded flexible substrates.

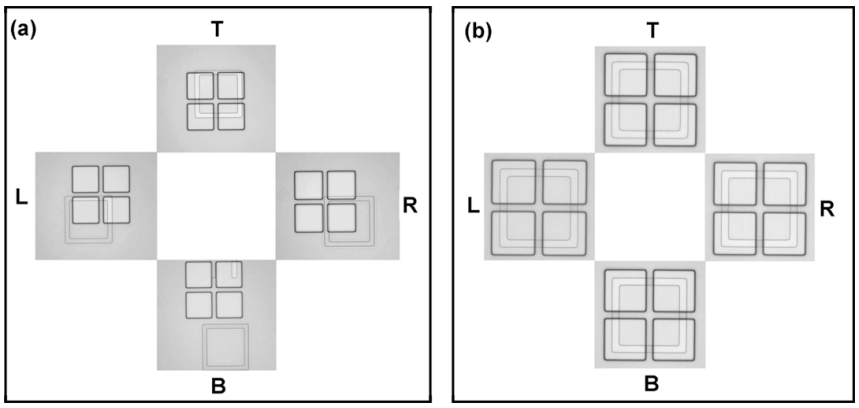

FIG 3.3 Overlay misalignment between two photolithography levels (a) misalignment using Elastomer PSA and (b) misalignment using UV PSA. PEN is seen to expand substantially with Elastomer PSA but not with UV PSA.

As mechanical deformation of the flexible substrate is responsible for the misalignment, the viscoelastic properties of the adhesives are suspected to be critical to the performance. The rheology data for the two adhesives are shown in Figure 3.4. As the UV PSA is cured initially with UV radiation in the bonded specimens, this adhesive is UV cured prior to rheological characterization. The UV curing is done under N_2 to prevent the inhibition of curing in the presence of oxygen. The first thing to note between the adhesives is that the storage modulus (G') of UV PSA is consistently greater than that of Elastomer PSA irrespective of temperature as shown in Figure 3.4(a).

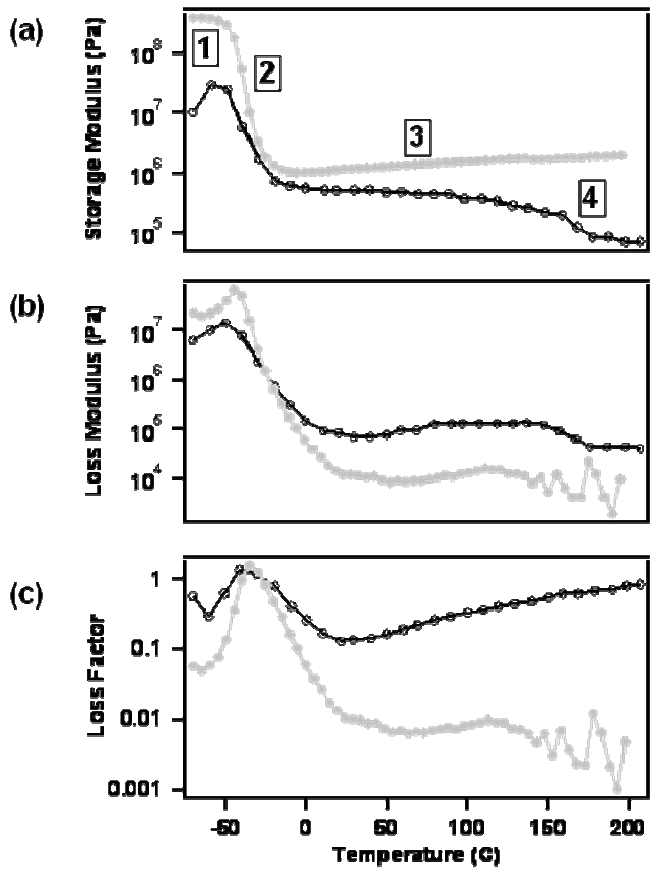

Figure 3.4. Temperature dependence of the viscoelastic properties of elastomer adhesive (O) and UV PSA (●) for (a) storage modulus (G'), (b) loss modulus (G'') and (c) loss factor (tan δ).

The viscoelastic behavior shown can be divided into four regions. In region 1 the polymer is glassy. Region 2 is the glass transition region. Typically the modulus decreases by 10^3 Pa in a 20 to 30 ^oC range in this region [20]. Region 3 is the rubbery plateau region. After the sharp drop of modulus in the glass transition region, the modulus becomes almost constant in the rubbery plateau region but the linear polymer and cross-linked polymer behaves differently. In case of linear polymer the modulus drops off slowly but for cross-linked polymer improved rubber elasticity is observed which follows the equation : $E=3nRT$, where n is the number of active chain segments in the network and RT represents the gas

constant times the temperature. The difference to note between the adhesives is that the storage modulus of UV PSA increases as it is heated to 200 ℃, while the storage modulus of Elastomer PSA decreases with temperature in the rubbery plateau region which is consistent with the fact that UV PSA is cross-linked polymer, whereas Elastomer PSA is not. Region 4 is the rubbery flow region, which is not observed for cross-linked polymer. In this region the increased molecular motion imparted by increased temperature permits assemblies of chains to move in a coordinated manner and hence to flow [20]. For cross-linked polymer, region 3 remains in effect up to decomposition temperature of the polymer. UV PSA does not exhibit region 4 whereas Elastomer PSA shows the rubbery flow region. As illustrated in Figure 3.4 (b), the loss modulus (G") of UV-PSA is significantly less than that of Elastomer PSA. Examining the two moduli simultaneously as the loss factor (tan δ), which is ratio of loss modulus to storage modulus, provides information on the viscoelastic flow properties of the adhesives. The low tan δ value indicates that most of the energy required to deform the sample is elastically recoverable. Conversely, the high tan δ value indicates that most of the deformation energy required is viscously dissipated as heat. The loss factor for Elastomer PSA is two orders of magnitude larger than for UV-PSA. This large tan δ indicates that the Elastomer PSA is more susceptible to viscous flow. The glass transition temperature is less than 0 ^{o}C for both adhesives and hence viscous flow is important at both bonding and processing condition. In addition to the quantitative difference in tan δ between the adhesives, the temperature dependence is also different. For elastomer PSA, the loss factor

increases substantially as temperature is increased over the processing window (20 to 180 ^{o}C), while tan δ of UV PSA is nearly invariant over these conditions. Therefore the difference in registration of lithographic features between the two adhesives can be explained by simply considering the viscous flow of the adhesive and its impact on the spatial control of the HS-PEN dimensions. During thermal deposition cycles, the adhesive will flow as it will be above T_g, but the extent of flow is dependent upon the loss factor and the stresses in the HS-PEN that can be released by the flow of the adhesive. Thus, the low tan δ for UV PSA does not allow the HS-PEN to significantly deform during processing through flow of the adhesive.

The difference in the viscoelastic properties of the adhesive also impacts the deformation of the substrate from stress relaxation through bow. Stress likely develops in the bonded system due to substantial CTE mismatch between the PEN substrate and glass carrier; however, the properties of the adhesive determine how (if) this stress is transferred. The difference in bow between the two adhesives is substantial as illustrated in Figure 3.5.

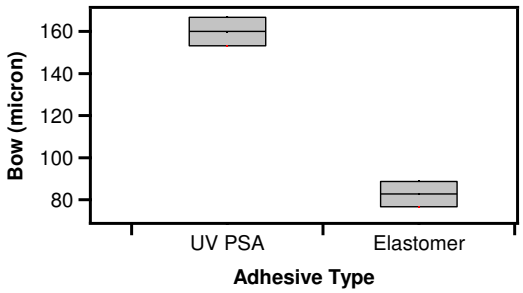

Figure 3.5 Impact of adhesive, Elastomer PSA and UV-SA, on the bow of a bonded system of HS-PEN bonded with adhesive to 0.9mm D263T glass carrier.

Interestingly, the bonded wafer using UV PSA adhesive is significantly deformed as determined by the bow measurement despite the excellent alignment of the lithographic features shown in Figure 3.3. A much smaller bow is observed for the elastomer adhesive, which performs worse for lithographic registration. The difference in bow is attributed to viscous flow of elastomer adhesive that relaxes some stresses in the bonded system. The higher temperature facilitates polymer chain mobility of adhesive that relaxes the induced thermal stress in PEN. As the system is cooled, relaxation at the hot temperature is reflected in an increased tensile stress at the cold temperature [12]. As the temperature is decreased, the viscous flow is decreased, so the tensile stress relaxes only very slowly. The initial stress state cannot be recovered fully and there is a net residual stress gain after complete thermal cycle. Therefore the bonded system bows to relax the residual stress. The bow is higher for UV PSA than that for Elastomer PSA since UV PSA has less viscous flow. In Table 3.1, comparison of distortion and bow for the two adhesives are shown.

Table 3.1 Effect of adhesive type on distortion and bow: Bonding PEN to Glass

Adhesive Type	X Distortion (ppm)	Y Distortion (ppm)	Bow (micron
Elastomer PSA	377 ± 137	510 ± 76	66 ± 9
UV PSA	1.2 ± 2	0.2 ± 1	144 ± 2

3.3.2 Effect of Carrier Properties on Stress

Despite the good registration of lithographic features using UV PSA, the large bow is undesirable in plate-to-plate (P2P) fabrication processes due to wafer handling issues. The bonded system is held in place with a vacuum chunk for

many processes, but vacuum failure can occur for highly bowed wafers. Additionally bow can lead to issues with robot arms being able to sense and transport the bonded system. These difficulties with bow mean that it is difficult to run the overall fabrication as an automated process if the bonded system exhibits significant bow. Thus, it is critical to control the bow in addition to the mechanical deformation of the plastic substrate in order to use P2P for the fabrication of flexible electronics. The bow of bonded systems has been studied extensively in the past for films directly adhered to a substrate [8-10] or bonded using an adhesive [14-18]. However, it is unclear if the models developed can be applied to the more complex bonded system examined here where viscous flow may be important. One of the most commonly invoked models for bow in elastic system is Stoney's equation [8] as shown in eq. (3.1):

$$\sigma_f = \frac{E_s t_s^2}{6 t_f R} \tag{3.1}$$

where radius of curvature R can be defined as:

$$R \approx \frac{L^2}{8B} \tag{3.2}$$

and L is the scan diameter and B is the wafer bow as illustrated in Fig 2.3.

Again stress in the film can be expressed as [21]:

$$\sigma_f = E_f \left(\alpha_f - \alpha_s \right) \Delta T \tag{3.3}$$

Here ΔT is temperature excursion experienced by the wafer and E_i, t_i and α_i are Young's modulus, thickness and thermal expansion coefficient of the i^{th} component respectively. *f* and *s* refer to the film and substrate, respectively.

From equation (3.1), (3.2) and (3.3), the wafer bow can be defined as:

$$B = \frac{3L^2}{4}\left(\frac{E_f t_f (\alpha_f - \alpha_s)\Delta T}{E_s t_s^2}\right) \tag{3.4}$$

Stoney's equation has been modified to account for the biaxial modulus of film and substrate, thicker film and multilayered structures [9, 22-23]. As additional parameters are considered, the model complexity increases rapidly. As a first approximation, the bonded system is considered solely as a film on rigid carrier, qualitatively based on Stoney's formula. In this case, the properties of carrier like biaxial modulus (E_c), thickness (t_c) and CTE (α_c) should impact the bow with a well defined dependency but this dependency could deviate from that of Stoney's equation in the case of a multilayered viscoelastic system examined here. To assess these dependencies, a series of different carriers with properties shown in Table 3.2 are utilized.

Table 3.2: Physical properties of carriers and bow of bonded system with HS-PEN using UV-SA

Carrier Type	Thickness t_c(μm)	Biaxial Modulus E_c (GPa)	CTE, α_c (ppm/^{o}C)	Avg Bow B (μm)
Silicon	680	180	2.6	192 ±8
Eagle 2000	700	92	3.2	334 ± 27
AF 45 Glass	700	86	4.5	292 ± 11
D263 T Glass	550	92	7.2	327 ± 10
D263 T Glass	700	92	7.2	235 ± 9
D263 T Glass	900	92	7.2	144 ± 2
D263 T Glass	1100	92	7.2	96 ± 1
Alumina	640	500	8.1	56 ± 3

The bow of the HS-PEN / UV-PSA / Carrier system is strongly dependent upon the choice of the carrier as illustrated in Figure 3.6.

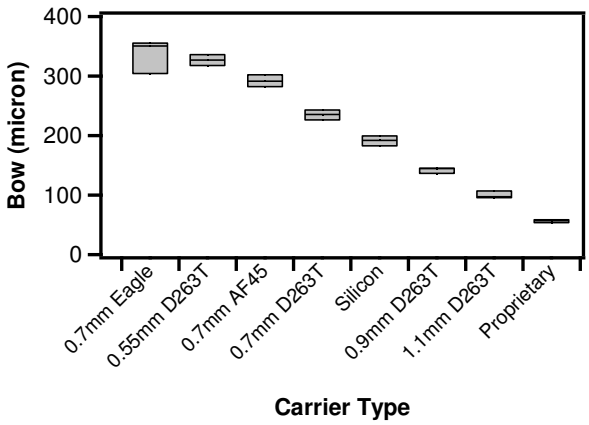

Figure 3.6. Comparison of bow for different carrier types bonded to HS-PEN using UV-PSA. Bow data are obtained after post-bond bake.

The carriers utilized enable the impact of carrier thickness (series of D263 T Glass) and carrier CTE (constant thickness of 700 μm) to be isolated without significant variation of the other two variables. By examination of the Eagle 2000, AF45 Glass and D263 T Glass (700 μm thick), the impact of carrier CTE on bow of the bonded system can be directly assessed as shown in Figure 3.7 (a). According to Stoney's equation, the bow should depend upon the difference in CTE between the carrier and adhered film. However for the polymeric adhesive and substrates utilized in this study, the CTE is temperature dependent over the range of temperatures of interest (ambient to 180 ºC). One additional difficulty with directly determining the dependency of bow on the CTE of the carrier is the limited availability of materials with similar modulus and thickness. Nonetheless, the decrease in bow with increasing CTE is expected as both HS-PEN and UV-PSA exhibit high CTEs (greater than 10 ppm/ºC). However, it is unclear how to address the difference in CTE as there are three components (carrier, HS-PEN and

UV-PSA). Thus an empirical model is assumed to have a power law dependence of bow on the carrier properties as follows:

$$B \propto (t_c)^p (\alpha_c)^q (E_c)^r \tag{3.5}$$

where p, q, and r are the exponents of the power law for the carrier thickness, CTE and biaxial modulus, respectively A system following Stoney's equation would have exponents of p = -2 and r = -1. From a regressive fit of the data in Figure 3.7 (a), the bow depends upon the CTE of the carrier to the -0.4 power (q = -0.4).

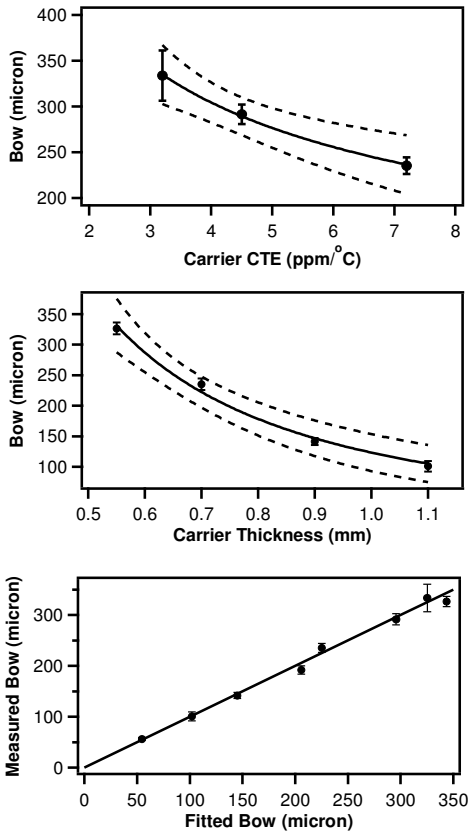

Figure 3.7 Empirical correlation between bow of bonded wafer and properties of carrier. (a) Bow vs. Carrier CTE (α_c) with 95% confidence band, Bow α $(\alpha_c)^{-0.4}$, (b) Bow vs. Carrier Thickness (T_c) with 95% confidence band, Bow α $(T_c)^{-1.7}$ and (c) Regression plot of measured vs. fitted bow, shows the data fit well to the regression model, Bow α $(T_c)^{-1.7}$ $(\alpha_c)^{-0.4}$ $(E_c)^{-0.9}$, where E_c is carrier biaxial modulus.

The impact of thickness on bow can be directly assessed using D263T glass. As thickness increases, the bow of the bonded system systematically decreases. A wider selection of thickness for the same carrier material is available and thus the dependence on the carrier thickness can be determined with less uncertainty. Figure 3.7 (b) illustrates that the bow of the bonded system is inversely proportional to carrier thickness to the power 1.70 from the best fit of the data to a power law. This dependency is close to the prediction from Stoney's equation (p = -2). This difference is within the uncertainty of the power law dependence determined from the fit of the data in Figure 3.7 (b).

Determining the impact of carrier modulus on the bow of the bonded system is more difficult to assess due to the availability of carriers. For this physical property, a multivariable regression analysis of the eight carrier types is utilized. The function as shown in eq. (3.5) is intrinsically linear as it can be transformed to a straight line by logarithmic transformation,

$$\text{Log}(B) \propto \{p\text{Log}(t_c) + q\text{Log}(\alpha_c) + r\text{Log}(E_c)\} \tag{3.6}$$

Now fitting this linearized model to the data using the Minitab software [24], an empirical relationship for the bow of the bonded systems examined is determined by fitting the exponents of the carrier thickness, CTE and biaxial modulus, which is found to be:

$$B \propto (t_c)^{-1.7} (\alpha_c)^{-0.4} (E_c)^{-0.9} \tag{3.7}$$

The regression plot is shown in Figure 3.7 (c) which shows the data fits well to the regression model. The adjusted R^2 statistics [25] for the model gives a value of 98.7%. The *t*-test was performed to determine the potential value of individual

regression coefficients in the model [25]. The *t*-test statistics for thickness (t_o=-12.74), CTE (t_o=-6.98), and biaxial modulus (t_o=-19.04) were found to be not significant (the p value is <0.001). We may conclude that each regressor contributed significantly to the model. From lack-of-fit *f*-test [25], the *f*-test statistics (f_o=181) is not significant (the p value is <0.0001) which indicates the model described the systematic variation in data adequately. Thus qualitatively, the impact of the carrier properties on bow of a bonded system consisting of a rigid carrier, viscoelastic adhesive and elastic substrate can be defined within the framework of simple power law. Interestingly, the coefficients for the dependence on thickness and modulus of the carrier are very similar to those for Stoney's equation. However, accounting for the non-linearities arising from the viscoelastic nature of the adhesive to quantitatively describe the deformation in the system will require substantial modifications.

3.3.3 Stress and Distortion using Alumina Carrier and UV curable adhesive

From analysis of bow data, the thick glass substrate appears promising. However, wafer handling of > 1.1 mm thick carriers is difficult with standard tools and also these glasses are not commercially available. Thus, an alternative material with improved mechanical properties and CTE that more closely matches the CTE of HS-PEN is desired to enable thinner carriers to be used in an automated process. By proper choice of materials, the bow can be reduced when using a thinner carrier of high CTE Alumina. To demonstrate the general applicability of considering the viscoelasticity of the adhesive for distortion of the HS-PEN substrate, both Elastomer PSA and UV PSA are examined as adhesives

for the alumina carrier bonded to HS-PEN. Similar to the results reported earlier for the glass carrier, the bow using the Elastomer PSA, 12±1 μm, is significantly less than that for the UV-PSA, 56±3 μm.

However as shown in Figure 3.8, the misalignment of the two lithographic layers is still problematic for the elastomeric PSA. Similar to the case of glass carrier, the near perfect registration is obtained on HS-PEN using UV-PSA. Though the bow is larger for the UV-PSA, this value is within tolerance limit (70-80 μm), for the vacuum chunks and robot arm handling.

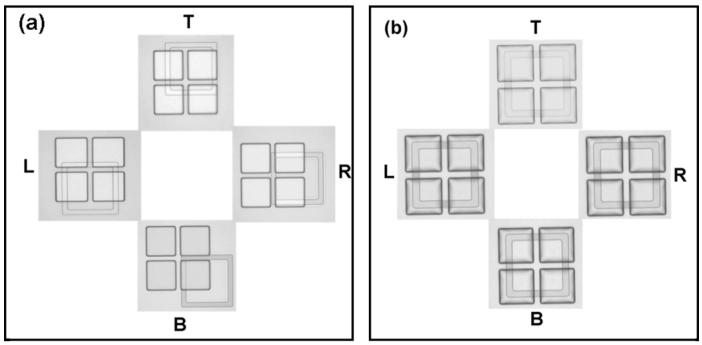

Figure 3.8. Overlay misalignment between the two photolithography levels, HS-PEN is bonded to the proprietary carrier (a) using Elastomer adhesive and (b) using UV PSA. HS-PEN expands substantially with elastomer adhesive but not when utilizing UV PSA.

This alumina carrier and UV PSA combination enables automatic handling of 150 mm bonded wafers for the fabrication of flexible micro-electronics.

3.3.4 Debonding of Flexible Electronics

The final step in the manufacture of flexible electronics using P2P is debonding the flexible substrate from the carrier. Two potential problems are damage of the active electronics as the substrate is peeled off and residual adhesive sticking to the flexible substrate. To address these potential issues, the

ease of debonding for the two adhesives is also investigated. The debonding mechanism for these two adhesives is extremely different. Using the elastomer PSA, HS-PEN is difficult to directly debond from the carrier; the HS-PEN can be peeled from the adhesive but this tends to lead to significant damage. Alternatively, the HS-PEN can be mechanically debonded from the carrier using a thin wire that passes between carrier and flexible substrate. However, adhesive residue will remain on both the carrier and flexible substrate after separation. Conversely, the HS-PEN from the UV-PSA can also be debonded in a more controllable process due to the UV curing process. This crosslinking of the polymer adhesive beyond the gel point promotes adhesive failure through significant strain hardening, so the substrate peels cleanly from the adhesive with minimal force. This force requirement is greater than experienced during TFT processing, so the bonded system can be processed. To understand the differences in the debonding between the UV-PSA and elastomer PSA, we can consider the adhesive failure energy model [26-27]. There are two primary energy components considered in the model: the intrinsic surface energy and the dissipated energy The intrinsic surface energy arises from the thermodynamic interactions between the adhesive and adherend at the interface. The dissipated energy is the energy lost during deformation due to the viscoelastic nature of adhesive material. A third factor considering bond formation process related to wetting behavior of adhesive governed by the viscoelastic nature of adhesive is also important [28].

The energy balance equation is as follows:

$$P=(I+D)\times\left(A/A_o\right) \cong D\times\left(A/A_o\right) \left[\because\ D \gg I\right] \tag{3.8}$$

where P is the peel failure energy, I is the intrinsic surface energy, D is the dissipated energy, A is the contact area between adhesive and adherend and A_o is the total area available for contact. The energy dissipated during a peel test is proportional to the intrinsic surface energy and to the loss modulus in the linear viscoelastic measurement of the adhesive [29] as shown in the following equation:

$$D \propto I \bullet G''(\omega) \text{ where } G'' \text{ is the loss modulus at peel frequency} \tag{3.9}$$

The kinetic term A/A_o is related to the creep compliance J(t), of the adhesive through the following equation [28]:

$$A/A_o = 1 - e^{-J(t)} \cong J(t) \tag{3.10}$$

J(t) is related to storage modulus through the following equation [30]:

$$J(t) = \frac{1}{G'(\omega)} \times \frac{1}{\left[1+\tan\delta^2(\omega)\right]} \cong \frac{1}{G'(\omega)} \ \left[\text{in case when } \tan\delta \ll 1\right] \tag{3.11}$$

Now combining equations (3.8) to (3.11), the simplified correlation for the adhesive peel strength, P has been proposed [19]:

$$P \propto I \times \frac{G''(\omega_1)}{G'(\omega_2)} \tag{3.12}$$

here G'' is the loss modulus at peel frequency ω_1 and G' is the storage modulus at the bonding frequency ω_2.

As illustrated in Figure 3.3, Elastomer PSA has a much larger loss factor (G''/G') in comparison to UV PSA. This difference in viscoelastic properties would suggest that higher peel energy is required for the Elastomer PSA according to eq. (3.12). This difference in viscoelasticity is likely responsible for differences in debonding difficulty between the adhesives. After debonding of the flexible TFT backplane from the rigid carrier, this backplane can be integrated with flexible frontplane electronics to create a functional device. For example, combining the TFT array with an electrophoretic ink yields a bendable, flexible display as illustrated in Figure 3.9. This display is 3.2x2.4 $in.^2$ in dimension with a pixel size of 260x260 μm^2 Further details regarding the display performance and fabrication are reported elsewhere [31].

Figure 3.9 Example of an electrophoretic display that is built on flexible substrate HS-PEN using the temporary bond-debond process. The TFT array fabrication for the backplane utilized a bonded system consisting of HS-PEN, UV-PSA and the specialty carrier.

Therefore by proper tuning of the viscoelastic properties of the adhesive and thermo-mechanical properties of the carrier, it is possible to mitigate wafer handling issues and photolithography misalignment issues that are common to

backplane processing on flexible substrate. To avoid registration problems between lithographically defined layers, it is important that the adhesive have low tanδ over the temperature range of the processing. Fortuitously, a low tanδ for the adhesive also leads to facile debonding of the flexible substrate from the carrier after TFT fabrication.

3.4 Conclusion

A temporary bond-debond technique that provides easy, cost effective handling of flexible substrate has been demonstrated. Careful selection of adhesive as well as carrier is required for proper alignment of lithographic layers and low bow to enable automated handling. The bow of the bonded system is found to not correlate with the degree of misalignment between photolithographic steps; instead the viscoelastic loss factor of adhesive is found to correlate strongly with the registration of layers. A low viscoelastic loss factor leads to less distortion of the flexible substrate and also enables facile debonding of the substrate after device fabrication. The bow of the bonded system is problematic for automated wafer handling that is required for manufacture. For a fixed adhesive / flexible substrate system, the physical properties of the carrier on bow of the bonded system scale according to the well established Stoney's equation. Minimization of the bow requires maximizing the modulus and thickness of the carrier and minimizing the mismatch in CTE. By careful choice of adhesive and carrier, TFT arrays for display backplanes can be successfully produced in high yield on flexible substrates.

3.5 References

[1] W. S. Wong, *et al.*, "Digital lithography for large-area electronics on flexible substrates," *Journal of Non-Crystalline Solids* vol. 352, pp. 1981–1985, 2006.

[2] J. H. Souk and W. Lee, "A practical approach to processing flexible displays," *Journal of the Society for Information Display,* vol. 18, pp. 258-265, 2010.

[3] Kanti Jain, *et al.*, "Flexible electronics and displays," *Proceedings of the IEEE,* vol. 93, pp. 1500-1510, 2005.

[4] H. Gleskova, *et al.*, "Mechanics of thin-film transistors and solar cells on flexible substrates," *Solar Energy,* vol. 80, pp. 687-693, 2006.

[5] F. Lemmi, *et al.*, "Poly-Si TFTs from glass to plastic substrates: process and manufacturing challanges," *Materials Research Society Symposium Proceedings,* vol. 814, pp. I1.6.1-I1.6.11, 2004.

[6] B. A. MacDonald, *et al.*, "Enginnered films for display technologies," in *Flexible Flat Panel Displays*, G. P. Crawford, Ed., ed, 2005, pp. 11-33.

[7] B. A. MacDonald, *et al.*, "New developments in polyester films for flexible electronics.," *Materials Research Society Symposium Proceedings* vol. 769, pp. 283–290, 2003.

[8] G. G. Stoney, "The tension of metallic films deposited by electrolysis," *Proceedings of the Royal Society of London. Series A,* vol. 82, pp. 172-175, 1909.

[9] P. Townsend, *et al.*, "Elastic relationships in layered composite media with approximation for the ease of thin films on a thick substrate," *Journal of Applied Physics,* vol. 62, pp. 4438-4444, 1987.

[10] M. Benabdi and A.A.Roche, "Mechanical properties of thin and thick coatings applied to various substrates," *Journal of Adhesion Science and Technology,* vol. 11, pp. 281-299, 1997.

[11] S. Radhakrishnan, *et al.*, "Material behavior uncertainty in the design of bonded systems – Part I: Shear displacement and stress prediction," *Materials and Design* vol. 28, pp. 2706-2711, 2007.

[12] G. R. Humfeld and D. A. Dillard, "Residual stress development in adhesive joints subjected to thermal cycling," *Journal of Adhesion* vol. 65, pp. 277-3.6, 1998.

[13] I. Sadaba*, et al.*, "A study of residual stress effects due to adhesive bonding of MEMS components," *Applied Mechanics and Materials,* vol. 5-6, pp. 493-500, 2006.

[14] Z. Q. Jiang*, et al.*, "Thermal stresses in layered electronic assemblies," *Journal of Electronic Packaging,* vol. 119, pp. 127-132, 1997.

[15] I. Sadaba*, et al.*, "A study of residual stress effcts due to adhesive bonding of MEMS components," *Applied Mechanics and Materials,* vol. 5-6, pp. 493-500, 2006.

[16] J.-H. Lim*, et al.*, "Warpage modeling and characterization to simulate the fabrication process of wafer-level adhesive bonding," *IEEE Int'l Electronics Manufacturing Technology Symposium,* 2007.

[17] J. Wanga and S. Zeng, "Thermal stresses analysis in adhesive/solder bonded bimaterial assemblies," *Journal of Applied Physics,* vol. 104, pp. 113508(1-8), 2008.

[18] E. Suhir, "Stresses in adhesively bonded bi-material assemblies used in electronic packaging," *Materials Research Society Symposium Proceedings,* vol. 72, pp. 133-138, 1986.

[19] H. W. H. Yang, "Water based polymers as pressure-sensitive adhesives-viscoelastic guidelines," *Journal of Applied Polymer Science,* vol. 55, pp. 645-652, 1995.

[20] L.H.Sperling, "Glass-Rubber transition behavior," in *Physical Polymer Science*, ed, 3rd Ed, pp. 300-306.

[21] E. Suhir, "An approximate analysis of stresses in multilayered elastic thin films," *Journal of Applied Mechanics* vol. 55, pp. 143-148, 1988.

[22] J. S. Kim and K. W. Palik, "The multilayer-modified Stoney's formula for laminated polymer composites on a silicon substrate," *Journal of Applied Physics,* vol. 86, pp. 5474-5479, 1999.

[23] A. Atkinson, "Residual stress and fracture of laminated ceramic membranes," *British Ceramic Proceedings,* vol. 54, 1995.

[24] B. F. Ryan*, et al.*, "MINITAB Handbook: Updated for Release 14," ed. Belmont, CA: Brooks/Cole Thomson Learning, 2005.

[25] D. C. Montgomery and G. C. Runger, "Multiple Linear Regression," in *Applied Statistics and Probability for Engineers*, 3rd ed: John Wiley & Sons, pp. 410-467.

[26] A. N. Gent and A.J.Kinloch, "Adhesion of viscoelastic materials to rigid substrates. III. Energy criterion for failure," *Journal of Polymer Sciience PartA-2,* vol. 9, pp. 659-668, 1971.

[27] E. H. Andrews and A. J. Kinloch, "Mechanics of adhesive failure," *Proceedings of the Royal Society London A,* vol. 322, pp. 385-399, 1973.

[28] H. W. H. Yang, "Water-based polymers as pressure sensititive adhesives-viscoelastic guidelines," *Journal of Applied Polymer Science,* vol. 55, pp. 645-652, 1995.

[29] M. F. Tse, "Studies of triblock copolymer-tackifying resin interactions by viscoelasticity and adhesive performance " *Journal of Adhesion Science and Technology,* vol. 3, pp. 551-570, 1989.

[30] S.G.Chu, in *Handbook Of Pressure Sensitive Adhesive Technology, 2nd Ed*, D. Satas, Ed., ed New York: Springer, 1989, p. 179.

[31] G. B. Raupp*, et al.*, "Low-temperature amorphous-silicon backplane technology development for flexible displays in a manufacturing pilot-line environment," *Journal of the Society for Information Display,* vol. 15, pp. 445-454, 2007.

Chapter 4

Rheology Study of Adhesive Blends and Impact on Stress-Distortion of Bonded Wafers

4.1 Introduction

Two different adhesives with quite different mechanical properties were examined in the context of temporary bond-debond for flexible electronics in Chapter 3. It was shown that rheology of adhesive play a crucial role to control the stress developed between two adherend having different thermo-mechanical properties. Also deformation of a temporarily bonded flexible plastic film to a rigid carrier using adhesive was found to strongly depend on viscoelastic properties of adhesive. Because the manner in which the adhesive responds to the thermal stresses induced during device fabrications critically determines the bow-distortion of bonded wafer, understanding the stress response (rheology) of the adhesive is important for further improvements in the bond-debond processes, and in particular to obtain bonded wafers with minimum bow and distortion. For fabrication of large-scale flexible electronic devices for example Gen II size displays (470 mm x 370 mm) may need further improvements in temporary bond-debond technology developed for 150 mm size wafers. According to Stoney's equation [1], same set of flexible substrate-adhesive and carrier system will show higher bow for larger substrates. Therefore there will be more stringent requirement for stress control as the automated handling tools have limited tolerance for wafer bow. With the advancements in photolithography, layer

alignment allows some distortion compensation The current available photolithography tool, Azores 5200gT Panel Printer^{TM}, incorporates active compensation architecture (ACA) through which intrinsic substrate and process-induced dimensional distortion effects are automatically pre-measured and accommodated during step-and-repeat stitching and layer-alignment ("registration") process steps [2-3]. There is some room for PEN distortion (around 300-400 ppm) which can be compensated during photolithography registration. Therefore there exists a trade-off between distortion and bonded system bow.

In Chapter 3, it was shown Elastomer PSA and UV PSA have differing stress response (i.e., low bow and high distortion versus high bow and low distortion), and their viscoelastic properties are also quite different. The more compliant adhesive Elastomer PSA was shown to relax stress of the bonded system with less bow but allowed distortion of PEN. This resulted in high misalignment during photolithography registration. On the contrary, the more rigid adhesive UV PSA prevented PEN distortion, which resulted in precise alignment during photolithography registration, but led to large wafer bow. It is therefore suspected that adhesives with intermediate storage and loss moduli might provide improvements in the balance between bow and distortion of the bonded system. One facile route to modulate the viscoelastic behavior of a polymer is through blending [4-6]. Miscible blending of a low MW resin tackifier into a pressure sensitive adhesive polymer increased loss modulus while simultaneously decreased storage modulus [4]. The ductility and impact resistance

of polystyrene was shown to improve by incorporating dispersed rubber phase [6]. The rheological behavior of incompatible polymer blends were shown to depend on various factors, such as the rheological characteristics of each component, the composition, the interfacial tension, the domain structure, and the particle size and distribution [7].

In this Chapter, we will systematically investigate the influence of viscoelastic properties of the adhesive on the stress-distortion of HS-PEN bonded to carrier. A blend of an elastomer pressure sensitive adhesive (PSA), which leads to limited bow with high distortion, and an ultraviolet light-curable adhesive (UV PSA), which limits distortion of PEN with modest bow, is utilized to provide variation in the viscoelastic properties of the adhesive. The blend is expected to exhibit intermediate viscoelastic properties, which will allow examination of intermediate PEN distortion and stress relaxation

4.2 Experimental

4.2.1 Materials and processing

Two types of adhesive supplied by Henkel Corporation were used in this study: a solution-based elastomer pressure sensitive adhesive (elastomer PSA) and a solvent-less ultraviolet photo-curable pressure sensitive adhesive (UV-PSA, product no: WFP20141-94B). The blends were prepared by adding UV-PSA to Elastomer PSA and then magnetically stirred overnight at room temperature for thorough mixing. For the blends, the percentage by mass of UV-PSA in the adhesive formulation is utilized to specify the composition. The bonded materials

used are D263T glass (150 mm diameter, 0.9 mm thick) obtained from Stemmerich Inc. as the carrier and HS-PEN (125 µm thick) obtained from DuPont Teijin Films (trade name Teonex Q65A) as the substrate.

In the bonding process, the adhesive was first spun coat on the glass carrier and a post-apply bake (PAB) was applied to remove the solvents in two steps: 80^{o}C for 30 min and 130 ^{o}C for 15 min to ensure that all residual solvent was removed. Subsequently, the flexible HS-PEN substrate was laminated on the adhesive coated carrier using a hot roll laminator (Western Magnum). After lamination, the adhesive was cured using a Dymax UV curing unit at UVA wavelength (400-315 nm) for 20 s through the transparent plastic. Finally, the bonded wafer was baked under vacuum at 180 ^{o}C for 60 min. The laminated system was subsequently cleaned using detergent followed by QDR (quick-dump-rinse) and SRD (spin-rinse-dry).

4.2.2 Characterization

Rheological properties of adhesives were characterized using Dynamic Mechanical Analyzer (DMA Q800, Texas Instrument).

Theory of Dynamic Mechanical Analysis (DMA):

In DMA, a sinusoidal strain [$\varepsilon(t)$] (or stress [$\sigma(t)$]) is applied to a sample at specified frequency/ies (ω) and the corresponding stress (or strain) is measured. If a sinusoidal strain is applied to an ideal elastic solid, at any point in time the stress will be proportional to the strain in accordance to Hooke's law:

$$\varepsilon(t) = \varepsilon_o \cdot \sin(\omega t)$$
$$\sigma(t) = E \cdot \varepsilon(t) = E \cdot \varepsilon_o \cdot \sin(\omega t) = \sigma_o \cdot \sin(\omega t) \tag{4.1}$$

where E is elastic modulus, ε_o is strain amplitude and σ_o is stress amplitude. Thus for an ideal solid, the stress will be a sinusoidal function in phase with the strain as shown in Figure 4.1. Now if a sinusoidal shear strain [$\gamma(t)$] is applied to an ideal liquid, at any point in time the stress [$\tau(t)$] will be proportional to the strain rate [$\dot{\gamma}(t)$] in accordance to Newton's law of viscosity:

$$\gamma(t) = \gamma_o \cdot \sin(\omega t)$$
$$\tau(t) = \eta \cdot \dot{\gamma}(t) = \eta \cdot \frac{d\gamma(t)}{dt} = \eta \cdot \gamma_o \cdot \omega \cdot \cos(\omega t) = \tau_o \cdot \sin\left(\omega t + \frac{\pi}{2}\right) \tag{4.2}$$

where η is the viscosity of liquid. Thus for an ideal liquid the stress will be a sinusoidal function 90^o out of phase with the strain as shown in Figure 4.1.

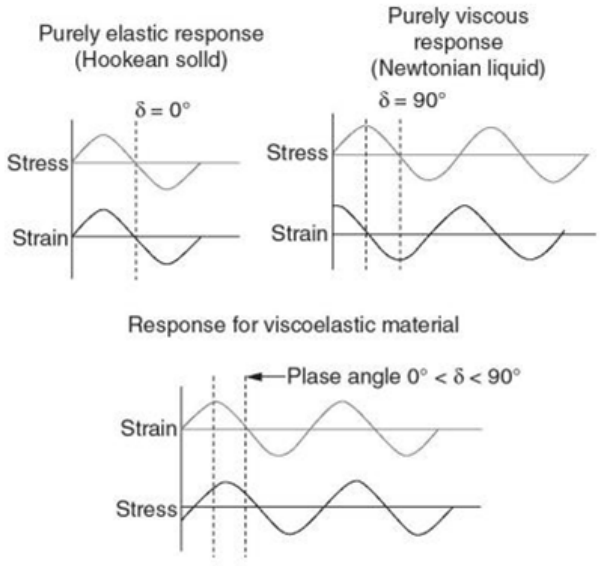

Figure 4.1: DMA sinusoidal stress-strain response curves for ideal elastic, ideal viscous and viscoelastic materials. The phase shift between stress and strain for a viscoelastic material lies between those for the ideal materials [8].

A viscoelastic material has properties intermediate between those of an ideal solid and an ideal liquid and exhibits a phase lag somewhere between 0^o (ideal solid) and 90^o (ideal liquid) also shown in Figure 4.1. DMA applies a given strain and measures the resulting stress as well as the relative amplitudes of stress (σ_o) and strain (ε_o) and the phase lag (δ), which is a measure of the relative degree of viscous character to elastic character.

Dynamic mechanical analysis data are most commonly reported using a quantity known as the complex modulus that evolves from a complex variable treatment of the sinusoidal deformation [9-10]. The complex modulus may be defined as the ratio of the sinusoidal stress to strain:

$$G^* = \frac{\sigma(t)}{\varepsilon(t)} = \frac{\sigma_o \cdot e^{i(\omega t+\delta)}}{\varepsilon_o \cdot e^{i(\omega t)}} = \left(\frac{\sigma_o}{\varepsilon_o}\right) e^{i\delta} = \left(\frac{\sigma_o}{\varepsilon_o}\right)\left(\cos(\delta) + i\sin(\delta)\right) \tag{4.3}$$

The complex modulus may be divided into real and imaginary components:

$$G^* = G' + iG''$$

where

$$G' = \frac{\sigma_o}{\varepsilon_o}\cos(\delta) \tag{4.4}$$

$$G'' = \frac{\sigma_o}{\varepsilon_o}\sin(\delta)$$

G' is referred to as the storage modulus and is a measure of the elastic character or solid-like nature of the material; G'' is referred to as the loss modulus and is a measure of the viscous character or liquid-like nature of the material. A third quantity is defined by taking ratio of the loss modulus to the storage modulus:

$$\frac{G''}{G'} = \frac{\sin(\delta)}{\cos(\delta)} = \tan(\delta) \tag{4.5}$$

This quantity is known as the material loss factor or loss tangent or more commonly, "tanδ" (pronounced tan delta). Tan δ ranges from zero for an ideal elastic solid to infinity for an ideal liquid. It represents the ratio of energy dissipated to energy stored per cycle of deformation.

Sample Preparation:

For DMA measurement, the adhesive formulations were poured into a mold and the solvent was evaporated at ambient condition for several days to prevent bubble formation during bake. Then the adhesive was baked to remove the residual solvent. Finally, the adhesive was UV cured under N_2 and was cut into rectangular strips approximately 7.5 mm x 4 mm x 1.2 mm (height x width x thickness)

Determination of Linear Viscoelastic Region:

To accurately evaluate the relationships between molecular structure of polymers and viscoelastic behavior requires that DMA experiments be conducted in regions where the viscoelastic properties observed are independent of imposed stress or strain levels. That is, experiments must be conducted in the linear viscoelastic region (LVR) [8]. The linear region can be measured for a material using a strain sweep test. In a strain sweep test, the frequency of the test is fixed and the amplitude is incrementally increased. A good rule to find the end of the linear region, is to find the amplitude at which the initial value of the storage modulus changes by $\approx 5\%$ [11].

The strain sweep experiment was performed to determine the LVR of different blend adhesives. Figure 4.2 shows the dependence of the normalized

storage modulus on amplitude for three different adhesive formulations: neat Elastomer PSA, 5 wt-% UV-PSA blend, and neat UV-PSA. The linear regime behavior is strongly dependent upon the formulation. Subsequent measurements were conducted at amplitudes exclusively within this experimentally-determined linear viscoelastic region.

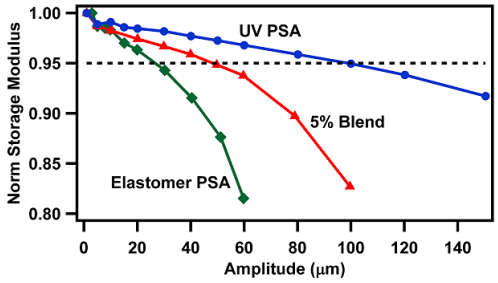

Figure 4.2: Strain Sweep Test to determine linear viscoelastic region (LVR) of different adhesives.

Operation Mode:

For all samples, the experiment was carried out in thermal scan mode at a constant frequency of 10 Hz. All relevant mechanical data were obtained from a single thermal scan completed within a few hours. The temperature was scanned at a constant rate of 3 ^{o}C/min from room temperature to 200 ^{o}C. Tension clamp was used where the sample was strained in tension between a fixed clamp and a moving clamp. In tensile oscillation, a static (preload) force of 0.002 N was applied to keep the sample taut. A force track of 110%, that make the static force dependent on dynamic force to maintain the specified amplitude during measurements, was applied.

Static Force = Force track x Dynamic Force

where Dynamic Force = Stiffness x Amplitude

Bow and Photolithographic Misalignment Measurement:

The bow of the bonded wafers was measured similarly as described in Chapter 3. Also the photolithographic misalignment between layers was monitored following the same procedure as described in Chapter 3.

4.3 Results and Discussions

4.3.1 Effect of Adhesive Blend Rheology on Stress and Distortion

Figure 4.3 illustrates the difference in overlay of the two photolithographic levels for three different adhesive formulations consisting of blends of the UV-PSA and Elastomer PSA.

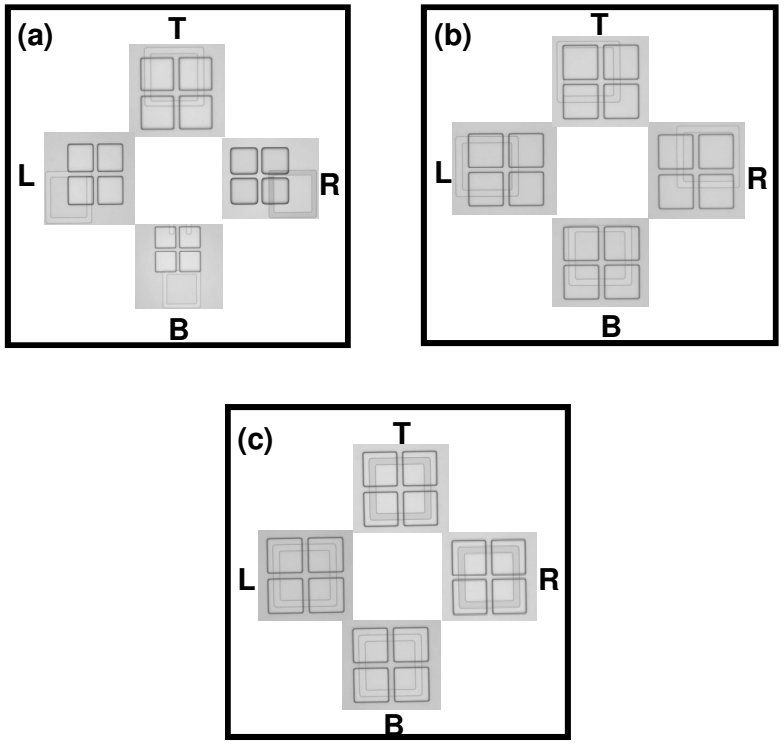

Figure 4.3 Overlay misalignment between two photolithography levels using different adhesive formulations containing (a) 2 wt% (b) 5 wt% and (c) 10 wt% UV PSA blends. The HS-PEN expanded substantially with 2% blend, to some extent at 5% and negligibly with 10% blend.

For the 2 wt % blend of UV curable PSA bonded system, as shown in Figure 4.3(a), a high level of misalignment is evident. The observed extent of misalignment is similar to that observed for pure Elastomer PSA. Close examination of the features illustrates that the first layer is misaligned towards the edge of the wafer. This misalignment indicates that the HS-PEN substrate stretched to larger dimensions during deposition of the second layer. In particular, the bottom verniers are misaligned more than the top verniers, which is consistent with the fact that the mask for printing the second layer is aligned using the fiduciary alignment mark located at upper part of the substrate. Using the same processing and materials except switching the adhesive to 10 wt % blend results in significant improvement in layer alignment as illustrated in Figure 4.3(c) where the two mask levels almost perfectly overlay. This excellent alignment is comparable to that obtained for the pure UV-PSA. An intermediate extent of misalignment is observed when using 5 wt % of UV–PSA in the adhesive blend formulation as shown in Figure 4.3(b). Quantification of the misalignment-distortion for a wider range of adhesive formulations is given in Table 4.1. Interestingly, there is only a narrow composition range in the blend where the distortion is impacted. Figure 4.4 illustrates the difference in bow of the HS-PEN substrate-adhesive-glass carrier system for the different adhesive blends.

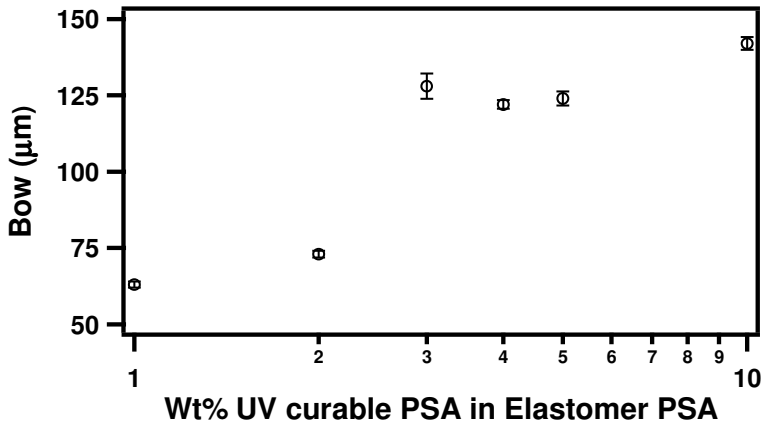

Figure 4.4. Impact of Elastomer PSA and UV curable PSA blend ratio on the bow of a bonded system. HS-PEN bonded with adhesive to 0.9mm D263T glass carrier.

Bow values similar to that for pure Elastomer PSA were found for the 1 % and 2 % blend. A modest increase in bow was observed for the 3 %, 4 %, and 5 % blend adhesives with a similar bow observed for each. Increasing the UV-PSA content to 10 % further increased the bow to a level comparable to the pure UV curable PSA.

In Table 4.1, the distortion and bow for the different blend adhesives and pure adhesives are summarized.

Table 4.1 Effect of blending UV curable adhesive in Elastomer PSA on distortion and bow: Bonding HS-PEN to 0.9mm D263T glass carrier

Blend Ratio (wt% of UV PSA)	X Distortion (ppm)	Y Distortion (ppm)	Bow (µm)
0	377 ± 137	510 ± 76	66 ± 9
1	361 ± 41	436 ± 46	63 ± 1
2	445 ± 8	556 ± 14	73 ± 1
4	37 ± 12	106 ± 14	122 ± 2
5	199 ± 43	12 ± 5	124 ± 3
10	2 ± 3	10 ± 1	142 ± 2
100	1.2 ± 2	0.2 ± 1	145 ± 1

X distortion is calculated from distance between the left (L) and right (R) boxes of the verniers on different layers whereas Y distortion is calculated from distance

between the top (T) and bottom (B) boxes of the verniers on different layers. In examining the misalignment and bow of these adhesive formulations (Table 4.1), they can be categorized in three groups with similar distortion and bow: (1) Elastomer PSA, 1 % and 2 % blend adhesive, (2) 4 %, and 5 % blend adhesive, and (3) 10 % blend and UV curable adhesive.

Because the stress and distortion of bonded system should be directly related to the flow properties of the adhesive, it is instructive to examine the viscoelastic properties of the formulations. The rheological data comparing the storage modulus, loss modulus and loss factor for different adhesive blends in each category are shown in Figure 4.5.

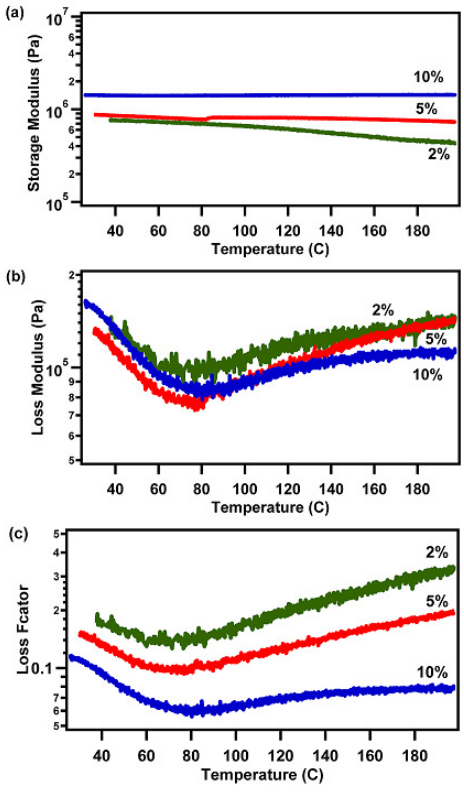

Figure 4.5 Comparison of temperature dependence of the viscoelastic properties (a) storage modulus (E'), (b) loss modulus (E'') and (c) loss factor (tan δ) for different adhesive formulations consisting of UV-PSA/Elastomer PSA blends.

As the UV–PSA fraction is increased, the storage modulus increases. This observation is not surprising considering that the storage modulus for UV-PSA is an order of magnitude larger than that for elastomer PSA. Additionally, the temperature dependence of the storage modulus is composition dependent with a decrease for the 2% blend as temperature increases, while the storage modulus of the 5% blend and 10% blend remain almost constant with temperature. Interestingly, the loss moduli for different adhesive blends do not show any significant difference (Figure 4.5b). This finding is especially surprising as the loss modulus should be related to the relaxation of the adhesive and logically the distortion of the substrate. However for the HS-PEN to slip and the distortion to occur, the adhesive must flow as the system (substrate-adhesive-carrier) remains well bonded during processing. To assess the flow properties of the adhesive, the aggregate of the two moduli represented as the loss factor (tan δ) is the appropriate parameter. Figure 4.5c illustrates the compositional dependence of the loss factor with a decrease in tan δ as the UV-PSA fraction is increased in the blend. This behavior is consistent with the observed compositional dependence for the distortion.

However, the loss factor for the 10% blend adhesive is closer to that of pure Elastomer PSA than that of pure UV-PSA. Despite this difference, the bow and distortion using a 10% blend adhesive or pure UV-PSA are statistically similar. This result indicates that control of distortion of the bonded plastic substrate would not be improved by blindly decreasing the loss factor (flow properties of the adhesive). A small range of loss factor appears to dramatically

impact the distortion and bow. However, what controls the cut-off value of tan δ for minimizing the distortion is not clear at this juncture.

4.3.2 Comparison of HS-PEN and Blend Adhesives Rheology

To better understand why there is such a narrow range of loss factor that controls the bow and distortion, the viscoelasticity of the semi-crystalline HS-PEN is examined. The rheological data for HS-PEN as a function of temperature is shown in Figure 4.6.

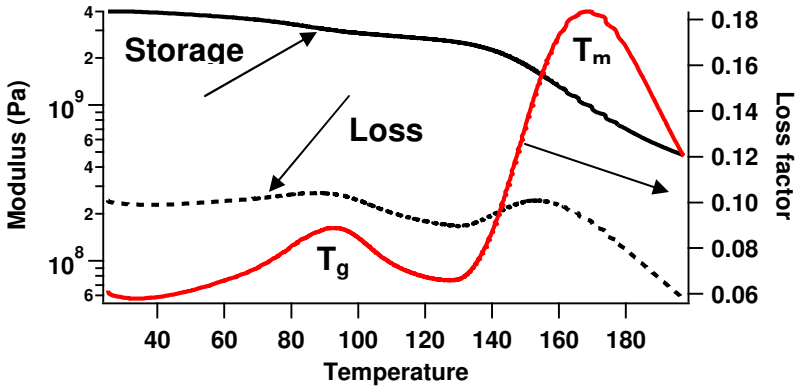

Figure 4.6: Temperature dependence of the storage and loss modulus as well as loss factor for heat stabilized polyethylene naphthalate (HS-PEN)

HS-PEN is a semi-crystalline thermoplastic material. Semi-crystalline thermoplastics have both amorphous and crystalline regions. As the temperature rises above T_g, only the amorphous component of the structure initially makes the transition to the entropy-elastic state while the ordered crystalline region retains their energy-elastic nature [12]. The softening of amorphous phase manifests itself as a drop in storage modulus, which is more pronounced when the degree of crystallinity of polymeric material is low. The softening temperature range of the amorphous phase of a semi-crystalline polymer is fairly broad. The crystallite

melting point of the crystalline region (T_m) occurs at higher temperature and is relatively sharp as the ordered molecular domains break-up at well defined activation energy. Semi-crystalline polymeric materials are widely used in the temperature range between their T_g and T_m. In this temperature range, they still have adequate rigidity (as a result of the intact crystalline structure) and exhibit good impact resistance and toughness [12]. Both transitions are clearly observed in the loss factor for the HS-PEN.

For measurement of photolithographic registration misalignment, the metal film and silicon stack were deposited and patterned on the bonded HS-PEN using a maximum process temperature of 180 °C. At this maximum temperature, the flow of the adhesive should also be at a maximum and hence the viscoelastic properties at this temperature should provide insight into the differences in distortion of the photolithographically defined verniers. Figure 4.7 illustrates the viscoelastic properties of HS-PEN and different adhesive blends at 180 ^{o}C.

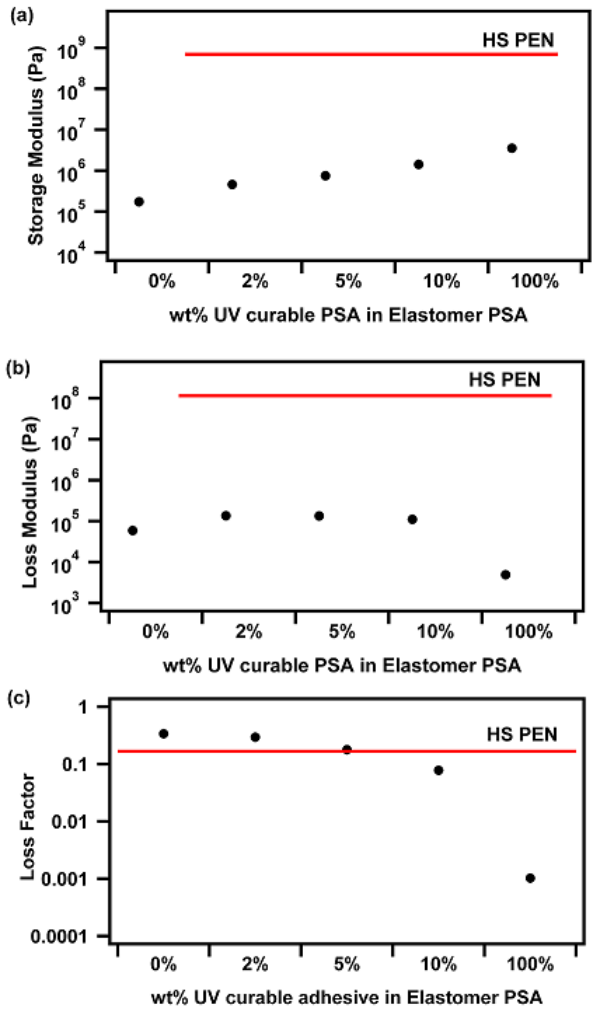

Figure 4.7: Comparison of the viscoelastic properties of HS-PEN with those of different adhesive blends (a) storage modulus (E'), (b) loss modulus (E'') and (c) loss factor (tan δ)

The storage modulus of HS-PEN is three orders of magnitude higher than that of any adhesive formulations as shown in Figure 4.7(a). The loss modulus is also three orders of magnitude higher for HS-PEN as shown in Figure 4.7(b). The loss factor, the ratio of loss modulus to storage modulus, shows a different trend as shown in Figure 4.7(c). The loss factor of pure Elastomer PSA and 2% blend is significantly higher than that of HS-PEN; in this case, the adhesive flows more than the HS-PEN leading to large distortion. Increasing the UV-PSA content to

5 % yields an adhesive with a loss factor similar to the loss factor of HS-PEN and intermediate distortion behavior. Interestingly, the loss factors of both the 10% blend and pure UV-PSA are less than that of HS-PEN. When the loss factor of adhesive is higher than that of HS-PEN, the adhesive allows the HS-PEN to expand or shrink freely during thermal processing and significant distortion of HS-PEN occurs. Conversely when the loss factor of adhesive is lower than that of HS-PEN, the flow of the HS-PEN is greater than that of the adhesive. Thus, the properties of the HS-PEN will control the distortion. The stress/bow can also be explained using the same logical arguments. These results explain the three groups of stress-distortion adhesives discussed earlier. This result implies that loss factor of adhesive as compared to HS-PEN is the critical parameter to be considered during adhesive formulation to control stress-distortion of bonded wafer. Additional improvements in the distortion-bow when the adhesive exhibits a lower loss factor than the substrate appear to require alteration of the carrier or substrate.

4.4 Conclusion

The viscoelastic flow property of adhesives is readily manipulated by blending two adhesives having significantly different viscoelastic properties. The storage modulus of adhesive was increased by blending the high modulus adhesive at increasing ratios into the low modulus adhesive without significant changes in the loss modulus, and thus loss factor was decreased as the high modulus adhesive content is increased. A small window in loss factor is found to

control distortion and bow of the bonded wafer. The difference in the viscoelastic flow property of the adhesive and HS-PEN is the critical parameter for precise registration of layers during photolithography and to control the stress developed during processing. Depending on the stress and distortion limitations of manufacturing tools, the viscoelastic properties of adhesive can be used as guiding parameters to design adhesive formulations suitable for using in temporary bond-debond method to manufacture flexible electronics.

4.5 References

[1] G. G. Stoney, "The tension of metallic films deposited by electrolysis," *Proceedings of the Royal Society of London. Series A,* vol. 82, pp. 172-175, 1909.

[2] S. Gardner, "Precision photolithography on flexible substrates," ed: Azores, June 2006, pp. 1-5.

[3] G. B. Raupp*, et al.*, "Low-temperature amorphous-silicon backplane technology development for flexible displays in a manufacturing pilot-line environment," *Journal of the Society for Information Display,* vol. 15, pp. 445-454, 2007.

[4] H. W. H. Yang, "Water-based polymers as pressure sensititive adhesives-viscoelastic guidelines," *Journal of Applied Polymer Science,* vol. 55, pp. 645-652, 1995.

[5] Y. C. Leong*, et al.*, "The viscoelastic properties of natural rubber pressure-sensitive adhesive using acrylic resin as a tackifier," *Journal of Applied Polymer Science,* vol. 88, pp. 2118-2123, 2003.

[6] I. K. Partridge, in *Multicomponent Polymer Systems*, I. S. Miles and S. Rostami, Eds., ed London: Longman Scientific and Technical, 1992, pp. 149-186.

[7] J. H. Choi*, et al.*, "A linear viscoelastic model of matrix/core–shell modifier polymer blends," *Journal of Polymer Science: Part B: Polymer Physics,* vol. 38, pp. 942-953, 2000.

[8] R. P. Chartoff*, et al.*, "Dynamic Mechanical Analysis (DMA)," in *Thermal Analysis of Polymers, Fundamentals and Applications*, J. D. Menczel and R. B. Prime, Eds., ed: John Wiley & Sons, Inc., 2008.

[9] J. D. Ferry, *Viscoelastic Properties of Polymers (third ed.)*: John Wiley and Sons, New York, 1980.

[10] L. E. Nielsen and R. F. Landel, *Mechanical Properties of Polymers and Composites. 2nd ed*: New York: Marcel Dekker Inc, 1994.

[11] T. Instruments, "Determination of the linear viscoelastic region of a polymer using a strain sweep on the DMA 2980", *Thermal Analysis and Rheology*.

[12] G. Erhard, "Structure and Properties," in *Designing with Plastics*, ed Cincinnati: Hanser Gardner, 2006, pp. 31-67.

Chapter 5

Thermo-Mechanical Analysis of Bonded System (Flexible Substrate-Adhesive-Carrier) Using Finite Element Modeling

5.1 Introduction

Adhesives with different mechanical properties were investigated in the context of stress-distortion of bonded system (Flexible substrate-Adhesive-Carrier) as described in the previous chapters. It was found that the rigid adhesive with low loss factor leads to less distortion of the bonded flexible plastic film and enables precise photolithographic alignment, but this adhesive can also lead to large wafer bow depending upon the carrier. Acceptable stress-bow on a 6 inch wafer scale was achieved using a carrier with high modulus and coefficient of thermal expansion that is closely matched to the flexible substrate. Conversely, the more compliant adhesive allows the stress of the bonded system to be relaxed with less bow, but leads to significantly greater flexible substrate distortion. Designing of new adhesive formulations will be required to implement the temporary bond-debond technology successfully for scaling-up and also for different flexible micro-electronics applications to meet the different processing requirements. As advancements in photolithography allow for some distortion compensation and automated handling tools have a limited tolerance for curvature of the wafer, there exists a viable operating window that appropriately trades-off distortion and bonded system bow. However, it is time consuming and expensive to design an adhesive empirically with required rheology to control the trade-off

between bow and distortion. However, theoretical understanding of the interactions among the properties of carrier, adhesive and substrate will help to predict the trend in bow-distortion behavior under thermal cycles. A model will reduce the time and cost needed for the design of new adhesive formulation with required rheology. Therefore, it is important to develop a model of the bonded system under thermal cycles predicting the bow-distortion behavior.

5.2 Theory of viscoelasticity

The study of polymer viscoelasticity treats the interrelationships among elasticity, flow and molecular motion with time and/or temperature [1]. Because of the unique long-chain molecular structure, viscoelastic nature is inherent to polymeric materials [2]. Polymers are broadly classified in two categories: thermoplastics or linear polymers and thermosets or crosslinked polymers [3]. The fundamental physical difference between the two is thermoplastics have only secondary bonds like van der Waals bonds and hydrogen bond between chains, while thermosets also have primary covalent bonds between chains. Unique tests and analysis approaches have been adopted for polymers to determine their viscoelastic nature [2]. One of the fundamental methods used to characterize the viscoelastic time dependent behavior of a polymer is the *relaxation test.* In a relaxation test, a constant strain is applied quasi-statically (i.e. the sudden strain must not induce any dynamic or inertia effects) to a uniaxial tensile (or compression or torsion) bar at zero time. The stress needed to maintain the constant strain will decrease with time for polymers. The initial sudden strain

occurs more rapidly than can be accommodated by the long chain molecular structure of polymer. However with time, there is reversible motion of the physical crosslinks or trapped entanglements as the polymer chains slip past one another, rotate and translate, so less stress is needed to maintain the same strain level [1]. Eventually the stress will go to zero for an ideal thermoplastic polymer, which contains only physical crosslinks. However the stress will decrease to a constant value for a thermoset polymer because of the presence of chemical crosslinks which will not relax with polymer motion. In relaxation as the stress is a function of time [$\sigma(t)$] and the strain is constant [ε_o], the modulus will also vary with time. The modulus so obtained is defined as relaxation modulus of the polymer and is given by,

$$E(t) = \frac{\sigma(t)}{\varepsilon_o} = \text{Relaxation modulus} \tag{5.1}$$

In addition to the relaxation test, another fundamental characterization test for viscoelastic materials is the *creep test* in which a constant stress is applied quasi-statically to a uniaxial tensile (or compression or torsion) bar at zero time. Inverse to relaxation, the strain under the constant load increases with time and the test provides the creep compliance defines as:

$$D(t) = \frac{\varepsilon(t)}{\sigma_o} = \text{Creep compliance} \tag{5.2}$$

Similarly, continuous loading gradually induces strain accumulation in creep as the polymer molecules rotate and translate to accommodate the load. The strain will tend to a constant value after a long time for a thermoset, while the strain will increase without bound for a thermoplastic for similar reasons as described for

relaxation behavior.

It is desirable to represent the viscoelastic nature of the polymers by a model in order to gain greater insight into relaxation and creep behavior and eventually their relationship to polymer structure. The simplest classical mechanical models for describing viscoelastic behavior include two elements: a spring for elastic behavior and a damper (or dashpot) for viscous behavior. Spring and damper elements can be combined in a variety of arrangements to develop mathematically amenable models of viscoelastic behavior. The simplest two such arrangements are the Maxwell model and Kelvin model [1-2, 4]. The Maxwell model consists of spring and dashpot in series as shown in Figure 5.1(a). Both the spring and the dashpot are subjected to the same stress but are permitted independent strains.

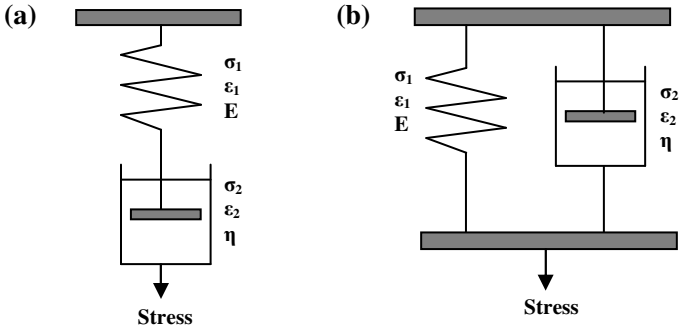

Figure 5.1: Schematic representation of (a) Maxwell model, (b) Kelvin model

The governing equation for the system strain rate according to Maxwell model is:

$$\dot{\varepsilon} = \frac{1}{E}\dot{\sigma} + \frac{1}{\eta}\sigma$$

where $\sigma = \sigma_1 = \sigma_2$ (5.3)

$$\varepsilon = \varepsilon_1 + \varepsilon_2$$

Here σ is the applied stress, ε is the total strain, σ_1 is the stress in the spring, ε_1 is the strain in the spring, σ_2 is the stress in the dashpot and ε_2 is the strain in the dashpot. E is the tensile modulus of the spring and η is the viscosity of the fluid in the dashpot. The Maxwell model is generally acceptable as a first approximation to relaxation behavior of polymer, but is inadequate for description of creep [2]. Using equation 5.3, the resulting stress in relaxation is,

$$\sigma(t) = \varepsilon_o E e^{\frac{-t}{\tau}} \tag{5.4}$$

where $\tau = \frac{\eta}{E}$, is the relaxation time of the polymer.

Again using equation 5.3, the resulting strain in creep is,

$$\varepsilon(t) = \sigma_o \left(\frac{1}{E} + \frac{t}{\eta} \right) \tag{5.5}$$

Therefore, the model predicts that stress decays exponentially with time but postulates that strain will increase linearly with time at constant stress.

The Kelvin model consists of a spring and a dashpot in parallel as shown in Figure 5.1(b). The governing equation for Kelvin model is:

$$\begin{aligned} &\sigma = E\varepsilon + \eta\dot{\varepsilon} \\ \text{where} \quad &\sigma = \sigma_1 + \sigma_2 \\ &\varepsilon = \varepsilon_1 = \varepsilon_2 \end{aligned} \tag{5.1}$$

The variable and parameter definitions are identical to those given above for the Maxwell model. The Kelvin model is generally acceptable as a first approximation to creep behavior, but is inadequate for prediction of relaxation [2]. This model predicts at constant stress, the strain tends to σ/E at long time. While a few problems in viscoelasticity can be solved with the Maxwell or Kelvin elements alone, more often these elements are used together or in other

combinations. For example the combination of Maxwell element and the Kelvin element in series, known as the four-element model, undergoes an elastic deformation, followed by creep on the application of constant stress [1]. More complex arrangements of elements are often used, especially if multiple relaxation or creep events are involved. Typically Maxwell elements in parallel are used for relaxation and Kelvin elements in series are used for creep [2]. In a Generalized Maxwell model where a series of Maxwell elements are connected in parallel, the strain is the same in all of the individual elements and the total stress is the summation of the individual stresses experienced by each element. Therefore the solution for stress relaxation is given by the following equation:

$$\sigma(t) = \varepsilon_o \sum_{i=1}^{n} E_i e^{\frac{-t}{\tau_i}} \tag{5.7}$$

The relaxation modulus is given by,

$$E(t) = \sum_{i=1}^{n} E_i e^{\frac{-t}{\tau_i}} \tag{5.8}$$

This type of exponential expansion representation is referred to as Prony series. However, the generalized model can only be used to represent a thermoplastic if all the τ_i values are nonzero. In order to represent a thermoset, a free spring is included in the generalized model also known as Maxwell-Weichert model. The resulting stress and the relaxation modulus then become,

$$\sigma(t) = \varepsilon_o \left(\sum_{i=1}^{n} E_i e^{\frac{-t}{\tau_i}} + E_\infty \right) \tag{5.9 a}$$

$$E(t) = \sum_{i=1}^{n} E_i e^{\frac{-t}{\tau_i}} + E_\infty \tag{5.9 b}$$

where E_∞ is the equilibrium relaxation modulus. A schematic of generalized Maxwell model with free spring is shown in Figure 5.2.

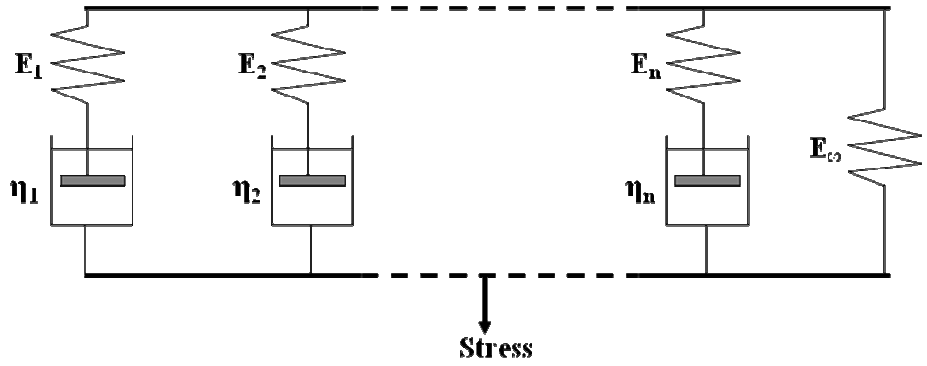

Figure 5.2: Schematic representation of Generalized Maxwell model with free spring

Time-Temperature Superposition:

The viscous property of a polymer is strongly dependent on time and temperature. The relationship between property changes of a polymer with time and property changes of a polymer with temperature is described using the time-temperature-superposition principle (TTSP), which states that the viscous behavior of a polymer at high temperature is identical to that at a low temperature if the time is properly scaled [5-6]. The term thermo-rheological simplicity refers to the key caveat that all the relaxation times (of all prony components) of a polymer must be affected by temperature in the same way. Thus the relaxation times of the bulk polymer at one temperature can be found from those at another temperature by multiplying each relaxation time with the scaling factor known as the shift factor a_T as defined by the following relation:

$$\tau_i(T) = a_T \tau_i(T_o) \tag{5.10}$$

There are two widely used shift factors; Williams-Landel-Ferry (WLF) shift

factor and Tool-Narayanaswamy (TN) shift factor. Williams, Landel and Ferry [7] applied the TTSP to a large number of polymers and found the following empirical expression for the shift factor:

$$\log_{10} a_T = \log_{10} \frac{\tau(T)}{\tau(T_o)} = \frac{-C_1 (T - T_o)}{C_2 + (T - T_o)} \tag{5.11}$$

where C_1 and C_2 are material constants and T_o is the reference temperature. In the WLF equation no particular chemical structure of polymer is assumed other than linear amorphous polymer above glass transition temperature [8]. Tool-Narayanaswamy shift factor is developed using Arrhenius activation energy equation,

$$\tau(T) = A e^{\frac{-E_a}{RT}} \tag{5.12}$$

where τ is the relaxation time, E_a is the activation energy, R is the gas constant and T is the absolute temperature. Rewriting in logarithmic form,

$$\ln \tau(T) = \ln A - \frac{E_a}{RT} \tag{5.13}$$

Taking the ratio at an arbitrary temperature and reference temperature gives,

$$\log_{10} a_T = \log_{10} \frac{\tau(T)}{\tau(T_o)} = -\frac{E_a}{2.303R}\left(\frac{1}{T} - \frac{1}{T_o}\right) \tag{5.14}$$

There is no limitation of using the shift factor developed from the Arrhenius activation energy equation below the glass transition temperature [8].

5.3 Thermo-Mechanical Stress Analysis of Multi-layer Structure

The thermo-mechanical behavior of multilayer structure is a subject of perennial interest [9-13]. Multilayered structures have extensive applications as

microelectronic, optical and structural components [9]. The difference in the CTE between layers leads to residual stresses in multilevel structures subjected to temperature change during its fabrication and applications. It is important to determine these stresses to realize cost-effective and high reliability devices. The temporary bonded system (Flexible substrate-Adhesive-Carrier) is a tri-layer structure of dissimilar material. As the bonded system goes through thermal cycles during TFT processing, its response to thermo-mechanical stress needs to be critically evaluated to make temporary bond-debond process successful. These stresses are relaxed through bowing of the bonded system (substrate-adhesive-carrier), which causes wafer handling problems, and through deformation of flexible plastic substrate, which leads to alignment issues during multiple photolithographic steps. Stoney's formula [10] has long been one of the most important tools for understanding thermo-mechanical stress for bi-layered structures like spin coated or deposited thin film on substrates. The stress in the film, σ_f is related to the radius of curvature, *R* of the system as follows:

$$\sigma_f = \frac{E_s t_s^2}{6 t_f R} \tag{5.15}$$

Here *E* is Young's modulus, *t* is thickness and the subscripts, *s* and *f* refer to substrate and film respectively. However, Stoney's formula applies only for thin film approximation ($t_f \ll t_s$) and equal modulus of the film and substrate ($E_s \approx E_f$). Stoney's equation has been modified to account for the biaxial modulus of film and substrate, thicker film and multilayered structures [11-12, 14-15]. However the materials forming the layers in these models are assumed to

be elastic.

Based on Stoney's equation thermal stress analysis of a bi-layer structure with adhesive bonding has been performed [16]. Different thickness silicon wafers were bonded to glass wafers using polymeric adhesive. The basic structure and variables definition used in the analysis are shown in Figure 5.3.

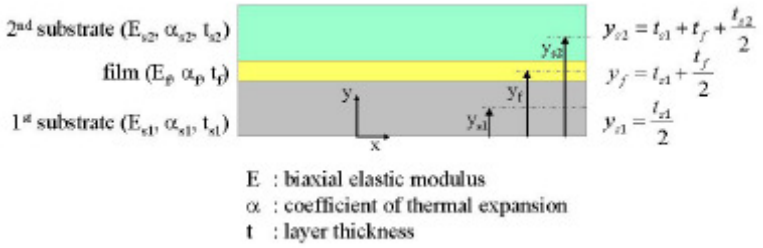

Figure 5.3: Basic structure and variable definition used in the thermal stress analysis of adhesive bonded bilayer structure [16]

The analytical modeling result is summarized in the following equations:

$$B = -\frac{L_s^2}{8(EI)_b}\left[\sigma_f t_f \left(y_f - \delta_b\right)\right] - \frac{L_s^2}{8(EI)_b}\left[E_{s2}t_{s2}\left(\alpha_{s2}-\alpha_{s1}\right)\left(T^*-T_o\right)\left(y_{s2}-\delta_b\right)\right] \quad (5.16)$$

where $\delta_b = \dfrac{E_{s1}t_{s1}y_{s1} + E_{s2}t_{s2}y_{s2}}{E_{s1}t_{s1} + E_{s2}t_{s2}}$ and

$$(EI)_b = E_{s1}t_{s1}\left\{\left[\frac{t_{s1}^2}{12} + \left(y_{s1}-\delta_b\right)^2\right] + \frac{E_{s2}t_{s2}}{E_{s1}t_{s1}}\left[\frac{t_{s2}^2}{12} + \left(y_{s2}-\delta_b\right)^2\right]\right\}$$

Here B is the measured wafer bow at room temperature after cooling, T_o is room temperature and T^* is characteristic temperature at which the bonded 3 layers are free of stress determined from bow vs. temperature data. σ_f is the stress in the adhesive layer determined separately using Stoney's equation by coating the 1st substrate only with adhesive and applying the same thermal load as that applied to

the bilayer system. Good agreement is found between the predicted and measured wafer bow. The model showed the bow is mostly dependent on the thermal mismatch of two wafers-silicon and glass for adhesive bonding.

Models using analytical methods of structural mechanics have been developed [17-21] for bi-layer assemblies bonded using thin, compliant adhesive to predict the interfacial stresses due to thermal expansion mismatch. To account for the thin layer of adhesive, two methods, the trilayer beam model [22] and adhesive joint model are used [21, 23]. The first method treats the thin layer of the adhesive as the same as the other two layers and models the structure as an assembly of three beams. Considering that the adhesive layer is much thinner than the other two layers, the second method follows the formulation of an adhesive joint [24] and models the adhesive layer as a two-parameter elastic foundation with consideration of the interfacial peel and shear stresses [17, 20-21]. Compared to the trilayer method, the adhesive-joint-based method is much simpler and can provide closed-form expressions of thermal stresses [17].

Fewer works have been done to develop analytical stress models for adhesive joints analyzing viscoelastic nature of adhesive layer subjected to thermal loads. Radhakrishnan *et al.* [25-26] used 3-parameter solid model to describe the displacement of fiber-optic assembly due to viscoelastic behavior of the bonding adhesive under thermal load. The standard 3-parameter solid model consists of either the Kelvin model in series with a spring or the Maxwell model in parallel with a spring. A 3-parameter solid model was used in this study since the behavior of epoxy used as bonding adhesive was closer to that of a solid than a

liquid.

The effect of thermal cycling on the state of residual stress was investigated for viscoelastic polymeric materials bonding stiff elastic substrates using numerical techniques, including finite element methods [27-31]. Due to the complexity of developing a closed form solution for a system with time and temperature dependent material properties and time varying temperature and coupled boundary conditions, they used numerical techniques to acquire approximate solutions.

5.4 Modeling Technique

The bonded system is a tri-layer structure where a viscoelastic adhesive is sandwiched between a rigid carrier and flexible substrate. To account for the viscoelastic nature of the adhesive to describe the stress-distortion of the system requires incorporating material nonlinearities in the model. There are a number of variables involved with the carriers; for example, thickness, CTE and modulus need to be considered in the model. From experimental results, it was found that distortion-bowing behavior correlated directly with the relative loss factor of adhesive to that of flexible plastic substrate. Therefore it is important to investigate if the viscoelastic behavior of flexible substrate is needed to be included in the stress-distortion model of the bonded system. Also the model involves coupled thermal-structural analysis computing displacement, stress-strain field due to differential thermal expansion. The analytical solutions have the limitation of applications to complex problems. Therefore, it is desirable to

develop a simple numerical model to simulate the bow-distortion of bonded wafer. In contrast to analytical solutions, which show the exact behavior at any point within the system, numerical solutions approximate exact solutions only at discrete points, called nodes. There are two common classes of numeric methods: 1) finite difference method and 2) finite element method. With finite difference methods, the differential equation is written for each node, and the derivatives are replaced by difference equations resulting in a set of linear equations. Although finite difference methods are easy to understand and employ in simple problems, they become difficult to apply to problems with complex geometries or complex boundary conditions [32]. In contrast, the finite element method uses integral formulations rather than difference equations to create a system of algebraic equations and can be employed for complex geometries. Finite Element Analysis was performed to model the stress-distortion of bonded system using the commercial software ANSYS as described in the following sections.

5.4.1 Finite Element Analysis using ANSYS

The Finite Element Analysis (FEA) is a numerical procedure that can be used to obtain solutions to a large class of engineering problems involving stress analysis, heat transfer, electromagnetism and fluid flow. The basis of FEA relies on the decomposition of the problem domain into a finite number of subdomains (elements) for which the systematic approximate solution is constructed by applying the variational or weighted residual methods [33]. The complete solution is generated by connecting or assembling the individual solutions, allowing for

continuity at the interelemental boundaries. The variational approach relies on the minimum total potential energy principle that states for a stable system the displacement at the equilibrium position occurs such that the value of the system's total potential energy is a minimum. The weighted residual methods are based on assuming an approximate solution for the governing differential equation. Substitution of the solution into the differential equations lead to some residuals or errors which is required to vanish in a weighted average sense over the domain.

The basic steps involved in any FEA consist of the following:

Preprocessing Phase:

1. Discretize the solution domain into finite number of subdomains; i.e. subdivide the problem into elements and nodes. Some of the common elements in FEA are shown in Figure 5.4.

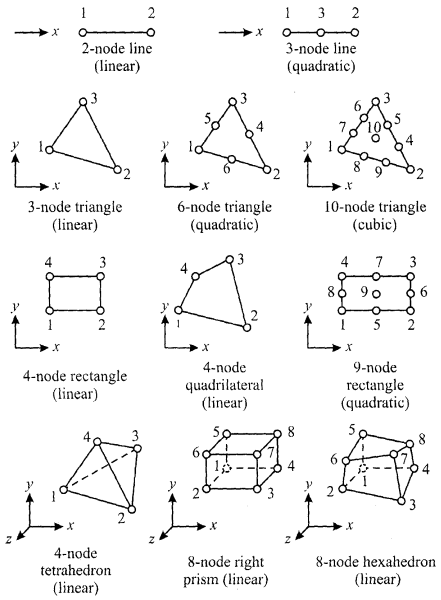

Figure 5.4: Commonly used one-, two-, and three-dimensional finite elements [33].

2. Assume a shape function to represent the physical behavior of an element.

3. Develop equations and the matrix for an element.
4. Assemble the element matrices for each subdomain to obtain the global matrix for the entire domain.
5. Apply boundary conditions, initial conditions and loading.

Solution Phase

6. Solve a set of linear or nonlinear algebraic equations simultaneously to obtain nodal results such as displacement values or temperature values at different nodes.

Postprocessing Phase

7. Obtain additional information for example principal stresses and heat fluxes.

The construction of solution using FEA requires either the development of a computer program based on the FEA formulation or the use of a commercially available FEA program tool such as ANSYS.

ANSYS analysis approach

There are three main steps in a typical ANSYS analysis.

1. Model Generation: This step involves element type specification, material properties definition, creation of the model geometry and making simplifications, idealizations and finally meshing. If the physical system under consideration exhibits symmetry in geometry, material properties and loading, then it is computationally advantageous to model only a representative portion. The dimensionality of a problem can be reduced from three to two through an idealization. There are three distinct two-

dimensional idealizations: 1) plane stress, 2) plane strain, and 3) axisymmetry. A state of plane stress exists for thin components subjected only to in-plane external loading, i.e. no lateral loads. A state of plane strain exists for a long components subjected only to uniform lateral external loading. In a solid of revolution, location of a point in the body can be identified by cylindrical coordinates, r, θ, and z, with z being the axis of rotation. When a solid of revolution is subjected to loading that can also be obtained by revolution about the z-axis, then the results become independent of θ. This is called an Axisymmetric Condition [33]. Reduction of dimensionality of a problem through an idealization can reduce the computational cost significantly. For meshing it is important that the mesh is adequately fine or coarse. One technique to decide on mesh density is to perform the analysis with an initial mesh and then reanalyze by using twice as many elements. If there are substantial differences between the two, the analysis should continue with a more refined mesh and a subsequent comparison until convergence is established.

2. Solution: This step involves analysis type and analysis options definition, specifications of boundary conditions and obtaining the solution. There are wide ranges of analysis disciplines for example, structural analysis computing deformation, stress-strain field, reaction forces in a solid body, thermal analysis computing temperature field and heat flux in a solid body, thermo-mechanical analysis computing displacement, stress-strain

field due to differential thermal expansion [32-33]. Analysis can be done for steady-state or transient condition.

3. Review Results: In this step, the results over the entire or portion of the model are reviewed. This includes plotting of contours, vector displays, deformed shapes and listing of result in tabular format.

5.4.2 Model Generation

Bow and distortion model of a bonded system formed from three layers of dissimilar material is desired. The bottom layer is a carrier which is a circular wafer of 150 mm diameter. The middle layer is a thin adhesive film which is uniformly coated on the wafer. The top layer is a laminated plastic substrate of same diameter as that of wafer. The bonded system is baked to 180^{o}C. The temperature ramps up to 180^{o}C from room temperature in approximately 3 hrs, dwells at 180^{o}C for 1 hr and then ramps down to room temperature in approximately 6 hrs. The bonded system bows as it runs through the thermal cycle predominately through thermal-mechanical property mismatches between the carrier and flexible substrate. After bake the bow was measured at the 120 mm periphery of the 150 mm bonded wafer.

During high temperature processing, deformation or distortion of flexible plastic substrate occurs as the plastic substrates are not dimensionally stable. Following the bake, metal film and silicon stack were deposited and patterned to measure photolithographic registration misalignment which quantifies the distortion of flexible plastic substrate. The bow-distortion measurement method is

described in detail in Chapter 3.

Model Simplification

The dimensionality of the problem is reduced from three to two through axisymmetric idealization. The axisymmetric idealization is verified against experimental data also. Square shape wafers were bonded following the procedure as described in Chapter 2. After final bake the bow is measured for both X and Y direction as shown in Figure 5.5(a). Bow values are similar for X and Y direction as illustrated in Figure 5.5(b) which indicates that bow is independent of θ.

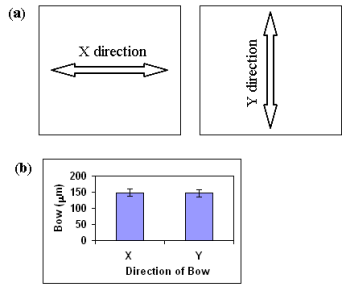

Figure 5.5: Experimental verification of axisymmetric idealization from bow measurement a) direction of bow measurement b) bow in X and Y direction

Also due to symmetry in geometry, material properties and loading, only half portion of bonded system is modeled. The simplifications of the model are illustrated in Figure 5.6.

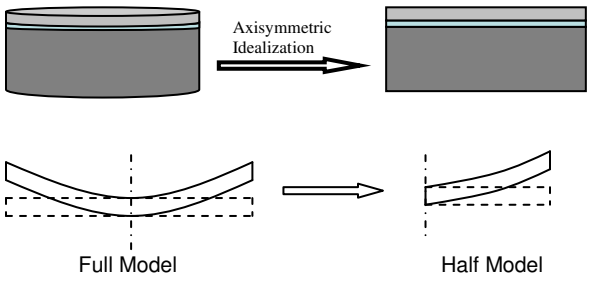

Figure 5.6: Model simplification by a) axisymmetric idealization and b) modeling half portion of actual system

Element Type Specification

For elastic material, 2D structural element PLANE 42 was used. This element is defined by four nodes having two degrees of freedom at each node: translations in the nodal X and Y directions. The element can be used either as a plane element (plane stress or plane strain) or as an axisymmetric element. The axisymmetric option was used in the model. For viscoelastic material, 2D structural element PLANE 182 was used. The element is defined by four nodes having two degrees of freedom at each node: translations in the nodal X and Y directions. The axisymmetric option was used for the element in the model. For this element, the non-linear properties of material are expressed in terms of Prony series using the following kernel functions:

$$G = G_\infty + \sum_{i=1}^{n_G} G_i \exp(-\frac{t}{\tau_i^G}) \qquad (5.17\ a)$$

$$K = K_\infty + \sum_{i=1}^{n_K} K_i \exp(-\frac{t}{\tau_i^K}) \qquad (5.17\ b)$$

where G_∞ and G_i = shear relaxation moduli

K_∞ and K_i = Bulk relaxation moduli

τ_i^G , τ_i^K = relaxation time for each Prony component

Introducing the relative moduli,

$$\alpha_i^G = \frac{G_i}{G_o} \quad \text{and} \quad \alpha_i^K = \frac{K_i}{K_o} \qquad (5.18)$$

where $G_o = G_\infty + \sum_{i=1}^{N_G} G_i$ and $K_o = K_\infty + \sum_{i=1}^{N_K} K_i$

The kernel functions can be equivalently expressed as

$$G = G_o \left[\alpha_\infty^G + \sum_{i=1}^{n_G} \alpha_i^G \exp\left(-\frac{t}{\tau_i^G} \right) \right] \quad (5.19\text{ a})$$

$$K = K_o \left[\alpha_\infty^K + \sum_{i=1}^{n_K} \alpha_i^K \exp\left(-\frac{t}{\tau_i^K} \right) \right] \quad (5.19\text{ b})$$

Prony coefficients (α_∞, α_i and τ_i) are then determined using a nonlinear regression model implemented in the ANSYS code for which curve fitting of the temporal evolutions of shear and /or bulk moduli are needed. The optimization is based on the comparison between the predicted and experimental relaxation behavior.

Material Properties Specification

Material properties are defined using the *material model* option. Three different material property sets need to be specified for the analysis: one for the carrier, one for the adhesive and one for the flexible substrate. Linear material properties can be constant or temperature dependent, isotropic or orthotropic. The thermal expansion coefficient and the elasticity parameters like Young's modulus and Poisson ratio are defined for linear materials.

Properties of Carrier: Different carriers including Silicon wafers, Alumina wafers, and D263T, AF45 and Corning eagle 2000 glass wafers were modeled to investigate the role of thermo-mechanical properties of carrier on bow. The properties of the carriers used in the model are given in Table 5.1.

Table 5.1: Physical properties of carriers

Carrier Type	Young's Modulus E_c (GPa)	Poisson Ratio	CTE, α_c (ppm/^{o}C)	Thickness (μm)
Silicon	130	0.28	2.6	680
Eagle 2000	71	0.23	3.2	700
AF 45 Glass	66	0.23	4.5	700
D263 T Glass	73	0.21	7.2	550-1100
Alumina	390	0.22	8.1	640

Properties of Adhesives: Two different types of adhesive, Elastomer PSA and UV PSA are modeled for which both linear and nonlinear properties need to be specified to define the viscoelastic behavior of the material. Young's modulus for UV PSA is considered constant, whereas a temperature dependent Young's modulus is defined for Elastomer PSA. The modulus values were extracted from temperature ramp experimental data shown in Chapter 4. CTE of adhesive layer does not affect the thermally induced stresses in an assembly as long as thickness and modulus of adhesive are small compared to the thickness and moduli of the bonded materials [20]. Therefore, the CTE values of adhesives were assumed and considered to be similar to acrylic (extruded) material. The linear properties of adhesives used in the model are given in Table 5.2.

Table 5.2 a: Physical properties of adhesives

Adhesive Type	Young's Modulus E_c (MPa)	Poisson Ratio	CTE, α_c (ppm/^{o}C)
UV PSA	3	0.4	234
Elastomer PSA	Table 5.2 b	0.48	234

Table 5.2 b: Temperature dependent Young's Modulus (E_c) for Elastomer PSA

Temperature (^{o}C)	50	75	100	125	150	175	200
Modulus (MPa)	1.012	0.928	0.798	0.637	0.441	0.265	0.145

The nonlinear properties of adhesive are determined using viscoelastic material curve fitting option in ANSYS. Curve fitting determines the material constants by relating the experimental relaxation data to the Prony series

expansion. It requires input the experimental relaxation data as a text file, define the order of Prony series expansion and perform the nonlinear regression. Shift functions can be used to characterize the material's temperature dependency.

The relaxation behaviors of adhesives were characterized using a dynamic mechanical analyzer (DMA, Texas Instruments Q800). The relaxation experiments were performed within linear viscoelastic region as described in Chapter 4. The samples were prepared following the same procedure as described in Chapter 4. The sample was strained at constant 1% and the relaxation modulus was monitored as a function of time. The normalized relaxation modulus data for Elastomer PSA at different temperature sets and also the best fit to data are shown in Figure 5.7. WLF shift function was used to generate the master curve. The relaxation modulus decays to zero with time showing similar trend of thermoplastic polymer.

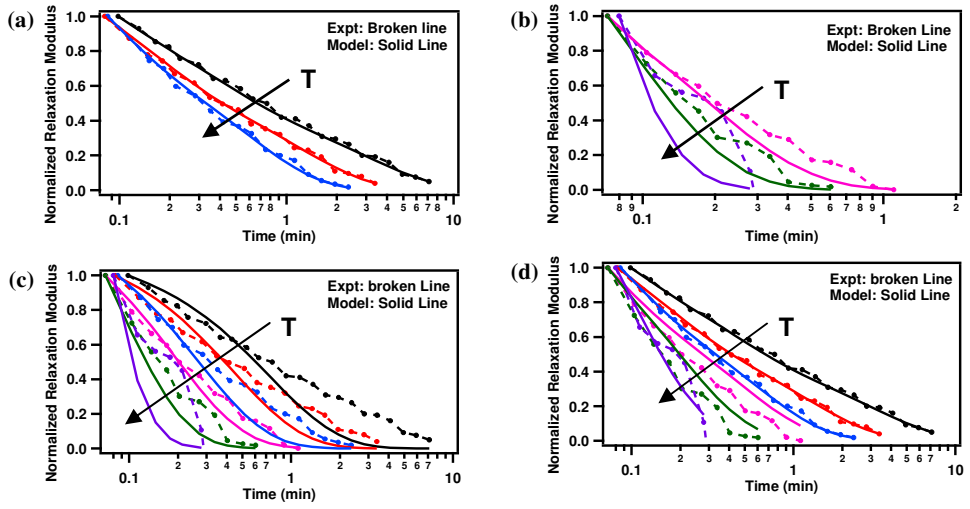

Figure 5.7: Comparison between simulated and experimental relaxation curves for Elastomer PSA fitting a) low temperature data sets b) high temperature data sets and c) both low and high temperature data sets d) low temperature data sets but simulating both low and high temperature data sets. Black: 35^{o}C, Red: 50 ^{o}C, Blue: 65 ^{o}C, Magenta: 75 ^{o}C, Green: 100 ^{o}C and Violet: 125 ^{o}C; broken line: expt. data and solid line: simulated data.

Two factors were considered in determining results acceptability; one is visual fit and the other is residual values. It can be seen in Figure 5.7(a) that for low temperatures (35 ^{o}C, 50 ^{o}C and 65 ^{o}C) the simulated relaxation curves fit well to experimental relaxation curves and the residual was small, 0.275. However at high temperatures (75 ^{o}C, 100 ^{o}C, and 125 ^{o}C) the fitting of the data was difficult as illustrated in Figure 5.7(b) and the residual was high, 7.66. At high temperatures relaxation was very fast; relaxation modulus decayed to zero within a minute at 75 ^{o}C and within 0.2 minute at 125 ^{o}C. Also the simulated relaxation curves considering both low and high temperature data sets do not fit well to experimental relaxation curves as shown in Figure 5.7(c). The residual was high, 22.28. Figure 5.7(d) shows comparison between simulated and experimental relaxation curves for both low and high temperature data sets where the relaxation parameters, determined from fitting only low temperature data sets, were used. Visually the fit looks better in Figure 5.7(d) than that shown in Figure 5.7(c) though in Figure 5.7(c), the relaxation parameters, determined from fitting both low and high temperature data sets, were used. Therefore, the relaxation parameters, determined from fitting only low temperature data sets, were used in further finite element analysis. The determined relaxation parameters and the coefficients of shift function are given in Table 5.3.

Table 5.3: Fitted relaxation parameters and shift function for Elastomer PSA for different temperature sets

Temperature	Relative Moduli			Relaxation Time (min)			Shift Function (WLF)		
	α_1	α_2	α_3	τ_1	τ_2	τ_3	T_o	C1	C2
35C-50C-65C	0.31	0.345	0.34	0.025	0.1424	1.22	50	3.04	129.6
75C-100C-125C	0.919	0.0809		0.006	0.087		100	267	20387
35C-50C-65C-75C-100C-125C	0.888	0.1118		0.0015	0.0809		100	300	20387

Similarly, the relaxation modulus of UV PSA was obtained using DMA. The normalized relaxation modulus data at different temperatures and also the fit to data are shown in Figure 5.8(a) and Figure 5.8(b) respectively. WLF shift function was used to generate the master curve. The relaxation modulus decays to a constant value. UV PSA is crosslinked polymer and hence showing the trend of thermoset or crosslinked polymer

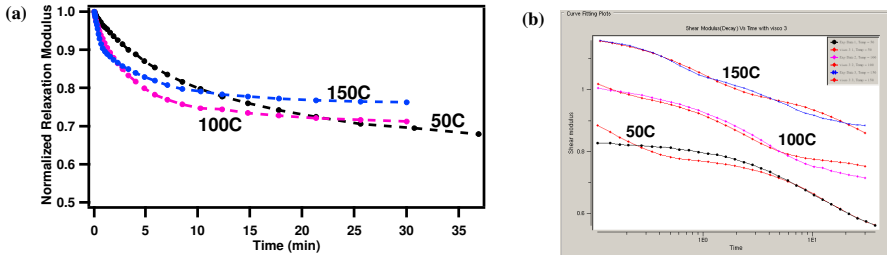

Figure 5.8: Relaxation behavior of UV PSA. a) Normalized relaxation modulus as a function of time b) Comparison between simulated and experimental relaxation curves. Blue: 150 ^{o}C Expt data; Magenta: 100 ^{o}C Expt data; Black: 50 ^{o}C Expt data and Red: Simulated data

From fitting of the three data sets (50 ^{o}C-100 ^{o}C-150 ^{o}C) covering the process temperature range (25 ^{o}C-180 ^{o}C), relaxation parameters and the coefficients of shift function were determined for UV PSA. The residual error of the fit was 0.04. The parameters determined that are used for further finite element analysis are given in Table 5.4.

Table 5.4: Fitted relaxation parameter and shift function for UV PSA

Temperature	Relative Moduli			
	α_1	α_2	α_3	α_∞
50C-100C-150C	0.156	0.179	0.204	0.46
	Relaxation Time (min)			
	τ_1	τ_2	τ_3	
	0.022	0.753	74.8	
	Shift Function (WLF)			
	T_o (^{o}C)	C1	C2	
	80	-69.9	2985	

Properties of Flexible Substrate: Heat stabilized polyethylene-naphthalate (HS-PEN) was modeled as a plastic substrate for which both linear and nonlinear properties need to be specified to define the viscoelastic behavior of the material. A temperature dependent Young's modulus and thermal expansion coefficient were specified for HS-PEN. The modulus values were extracted from temperature ramp experimental data shown in Chapter 4. The CTE data was supplied by the vendor, *DuPont Teijin Films*. A Poisson ratio of 0.35 is used [34]. The modulus and CTE values are given in Table 5.5.

Table 5.5: Temperature dependent physical properties of HS-PEN

Temperature (^{o}C)	25	50	75	100	125	150	175
Modulus (GPa)	3.98	3.8	3.42	2.89	2.6	1.8	0.8
Temperature(^{o}C)	60	100	140	180			
CTE, α_c (ppm/^{o}C)	17	19	36	54			

The rheology data of HS-PEN was studied to choose the temperature range to use for relaxation experiments. The rheology data is shown n Figure 4.6.

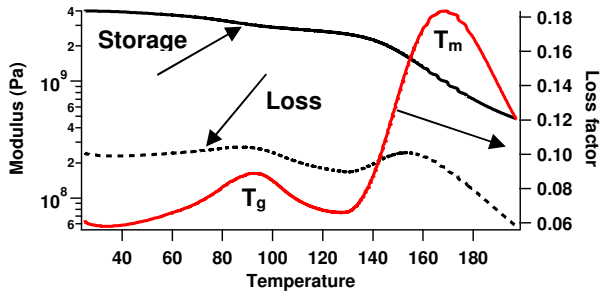

Figure 4.6: Variation of storage and loss modulus and loss factor as a function of temperature for HS PEN

It can be seen from Figure 4.6 that the glass transition temperature of HS PEN is within the relevant process temperature window for the bonded system. Therefore it was difficult to develop a general master curve covering the whole process temperature range. It was assumed that the maximum process temperature

will play the dominant role in controlling the stress-distortion of bonded system. Therefore the relaxation behavior of PEN was determined at 135 ^{o}C-150 ^{o}C-165 ^{o}C covering the upper portion of the process temperature range (25 ^{o}C-180 ^{o}C) and extended for the entire temperature range using shift function. The relaxation behavior of PEN was characterized using the DMA. The normalized relaxation modulus data at different temperatures for PEN are shown in Figure 5.9(a). The relaxation modulus decays to a constant value which is a common trend for thermoset or crosslinked polymer. Though PEN is thermoplastic polymer, it is semicrystalline. The crystalline regions behave as a type of physical cross-link, tying the chains together [8]. As a result of this highly entangled nature of the polymer chains, the movement of the amorphous polymer becomes restricted and the stress cannot be relaxed fully. WLF shift function is usually valid for linear amorphous polymer whereas for TN shift function there is no such limitations [8]. Since PEN is semicrystalline polymer, TN shift function was used to extend the relaxation behavior over the entire temperature range (25 ^{o}C-180 ^{o}C).

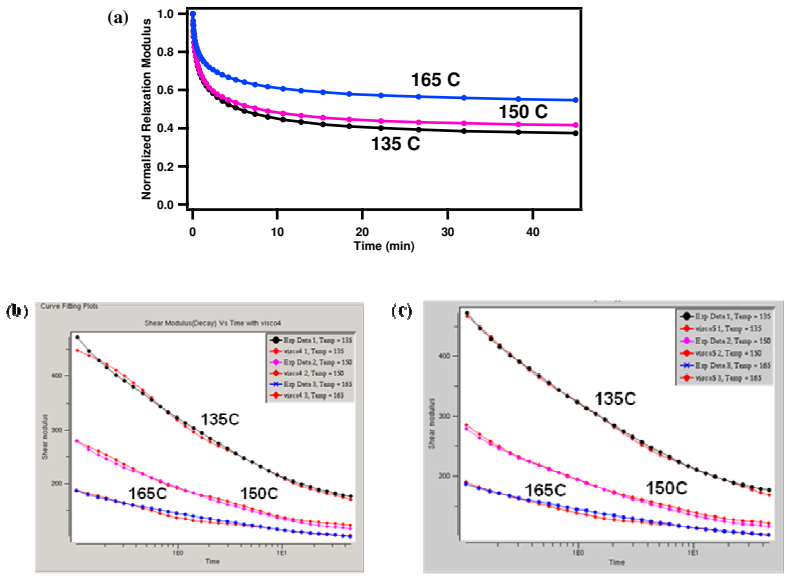

Figure 5.9: a) Relaxation behavior of HS-PEN: Normalized relaxation modulus as a function of time. Comparison between simulated and experimental relaxation curves: b) using four Maxwell elements and c) using five Maxwell elements. Blue: 165 ^{o}C Expt. data; Magenta: 150 ^{o}C Expt. data; Black: 135 ^{o}C Expt. data and Red: Simulated data

From fitting of the three data sets, relaxation parameters and the coefficients of shift function were determined for HS-PEN. Fitting parameters using three, four and five Maxwell elements gave a residual value of 0.11, 0.07 and 0.05 respectively. Visually the fit looked best with five Maxwell elements as shown in Figure 5.9(b) and also residual value was smallest. Therefore the relaxation parameters determined using five Maxwell elements are used for further finite element analysis. The parameters determined are given in Table 5.6.

Table 5.6: Fitted relaxation parameter and shift function for PEN

Temperature	Relative Moduli					
	α_1	α_2	α_3	α_4	α_5	α_∞
135C-150C-165C	0.094	0.127	0.245	0.301	0.049	0.184
	Relaxation Time (min)					
	τ_1	τ_2	τ_3	τ_4	τ_5	
	1.785	0.198	0.024	0.002	34.76	
	Shift Function (TN)					
	T_o (^{o}C)		C1			
	158		3923			

Building Model Geometry

A tri-layer structure was modeled to simulate the bonded system. Due to axisymmetric idealization, three rectangular areas were built to model the round bonded wafers. The rectangles had width of 75 mm since only half of the 150mm diameter wafer was modeled. The height of the bottom rectangle varied from 0.55 mm to 1.1 mm to simulate different thickness carriers. The height of the middle rectangle was 5μm to simulate the adhesive film of thickness 5μm. The height of the top rectangle was 125μm to simulate the 125μm thick plastic substrate HS PEN. The three rectangles were connected together using the *Gluing* operation of the *Boolean* option. Gluing makes sure that the areas share interface entities like nodes and lines.

Meshing

In the model, all three rectangles had large aspect ratios (lateral dimension to thickness). The middle rectangle that simulates the adhesive layer had maximum aspect ratio of 15000:1. The bottom layer had an aspect ratio of 136:1 for a 0.55 mm thick carrier and 68:1 for a 1.1 mm thick carrier. In ANSYS, the suggested maximum aspect ratio for elements is 20:1. Meshing the rectangles maintaining even the suggested maximum aspect ratio will result in a very large number of elements and nodes. Therefore meshing was done starting with coarse mesh size and gradually increasing the mesh density until the subsequent comparison shows no significant difference. The Automatic mesh generation feature of ANSYS was used, which still provides specific preferences for mesh density and shape. The desired mesh density was achieved defining fixed number

of element edges along the lines within the solid model using the *NDIV* option. The meshing was done using *Mapped Meshing* since the geometry of the areas to be meshed were regular and the number of divisions on opposite sides have an equal number of divisions. The attributes of elements e.g. material type, element type, were modified after the mesh is generated. A mesh size of 100x7, 100x2 and 100x3 defining the number of element edges on lines in x and y direction were used for the bottom layer (carrier), the middle layer (adhesive) and the op layer (plastic substrate) respectively for meshing. Further increase in mesh density did not make any significant difference in simulated results. The mesh size is illustrated in Figure 5.10.

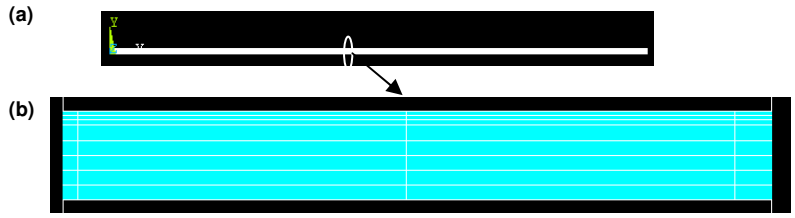

Figure 5.10: 2-D finite element mesh for (a) entire model and (b) zoomed to a small region of the model

5.4.3 Solution

After model generation including meshing, the solution conditions are defined. First the analysis type was specified as transient using the *Solution Controls* option since the thermal loadings change as a function of time. Then the boundary conditions were applied on nodes. Boundary conditions can be specified in three different ways: Type I (specification of primary variable), Type II (specification of derivative of primary variable) and Type III (specification of linear combination of primary variable and its derivative). The displacement

constraint which is a Type I boundary condition was specified along a segment of the boundary as follows and is illustrated in Figure 5.11:

$U_x = 0$ and $U_y = 0$ @ (x,y) = (0,0)

$U_x = 0$ @ x = 0

where U_x and U_y are displacement in X and Y direction respectively.

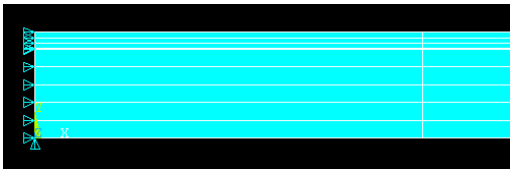

Figure 5.11: Displacement constraints applied as boundary conditions

Thermal load was applied on nodes to simulate the thermal bake cycle. ANSYS accommodates the application of time dependent loads through the use of multiple *Load Steps*. The first step was specified as temperature ramped up to 180^{o}C from 25 ^{o}C in 3hrs. The second step was dwell at 180^{o}C for 1hr. The third and last step was specified as temperature ramped down to 25^{o}C from 180 ^{o}C in 6hrs. The solution was generated for each thermal step.

5.4.4 Review Results

After a solution is obtained, the result can be reviewed in either the *General Postprocessor* or the *Time History Postprocessor*. In the *General Postprocessor* the solution at a specific time was reviewed in graphical displays like deformed shapes and contour plots that provided easy understanding how the model bonded system deforms under different conditions for example varying the properties of carrier, adhesive and/or substrate.

5.5 Results and Discussion

5.5.1 Simulation of bow of bonded system

The model was developed to simulate the stress-bow of bonded system (Plastic Substrate-Adhesive-Carrier) considering three cases:

5.5.1.1 Case I: Fully elastic

The bonded system is fully elastic i.e. all three layers, carrier, adhesive and plastic substrate were considered elastic. Linear properties for all three layers were specified. The properties of 0.9 mm thick D263T glass wafer were used for carrier. After building the model geometry and meshing the three layers, boundary conditions and thermal load steps were applied and obtained the solution. The y direction displacements at three temperature load steps are shown in Table 5.7. Experimental bow values were measured only after the complete thermal cycle i.e. after the temperature ramped down to 25 ^{o}C. Hence the simulated Y displacement after the 3rd thermal step is equivalent to experimentally measured bow value. Since experimental bow value was measured at 120 mm periphery of 150 mm diameter wafer, the simulated Y displacement value was taken for the node located in x direction at 60 mm. The comparison between experimental bow value and simulated Y displacement is also shown in Table 5.7.

Table 5.7: Comparison between experimental bow value and simulated Y displacement considering fully elastic system

Adhesive Type	Model Y Displacement (μm)			Expt. Bow (μm)
	25 ^{o}C-180 ^{o}C (3 hr)	180 ^{o}C (1 hr)	180 ^{o}C-25 ^{o}C (6 hr)	
Elastomer PSA	-179.3	-179.3	0	66 ± 8
UV PSA	-179.9	-179.9	0	144 ± 2

The simulations indicate that both adhesives show similar high bow values after temperature ramped up to 180 ^{o}C from 25 ^{o}C. During dwelling at 180 ^{o}C, the bow remained constant and after temperature ramped down to 25 ^{o}C from 180 ^{o}C, the bow values returned to zero. This behavior is expected for fully elastic system. The simulated bow behavior is completely different from what is observed experimentally. For both adhesives there is a bow after temperature ramp down to 25 ^{o}C from 180 ^{o}C and UV PSA showed higher bow value as compared to that for Elastomer PSA. Therefore the elastic model is not adequate to describe the experimental data as expected.

5.5.1.2 Case II: Viscoelastic adhesive only

In this case, the carrier and plastic substrate were considered elastic, but adhesive was considered to be viscoelastic. Linear properties for all three layers were specified. In addition viscoelastic properties of adhesives were specified. The comparison between experimental bow value and simulated Y displacement is shown in Table 5.8.

Table 5.8: Comparison between experimental bow value and simulated Y displacement considering adhesive as viscoelastic material

Adhesive Type	Model Y Displacement (μm)			Expt. Bow (μm)
	25 ^{o}C-180 ^{o}C (3 hr)	180 ^{o}C (1 hr)	180 ^{o}C-25 ^{o}C (6 hr)	
Elastomer PSA	-95.9	-95.9	+4.47	66 ± 8
UV PSA	-179.8	-179.8	+0.0004	144 ± 2

The simulations indicate that the UV PSA system showed higher bow value as compared to Elastomer PSA after temperature ramp up to 180 ^{o}C from 25 ^{o}C. The respective bows remained unchanged for both adhesives during dwelling

at 180 ^{o}C. The bow value for UV PSA system returned to almost zero whereas Elastomer PSA system showed a small bow value after temperature ramp down to 25 ^{o}C from 180 ^{o}C. UV PSA is more rigid than Elastomer PSA and hence behaves more like an elastic material. Therefore in case of UV PSA, the model behaves more like a fully elastic system and as temperature ramps down to 25 ^{o}C the bow goes to almost zero. Experimentally UV PSA showed higher bow than that for Elastomer PSA. Therefore the model considering only adhesive as viscoelastic material is not adequate to describe the experimental data.

5.5.1.3 Case III: Viscoelastic adhesive and substrate

In this case, the flexible plastic substrate along with adhesive was considered to be viscoelastic. Therefore, nonlinear properties of plastic substrate PEN were specified to define the viscoelasticity. The comparison between experimental bow value and simulated Y displacement is shown in the Table 5.9.

Table 5.9: Comparison between experimental bow value and simulated Y displacement considering both adhesive and plastic substrate as viscoelastic material

Adhesive Type	Model Y Displacement (μm)			Expt. Bow (μm)
	25 ^{o}C-180 ^{o}C (3 hr)	180 ^{o}C (1 hr)	180 ^{o}C-25 ^{o}C (6 hr)	
Elastomer PSA	-34.7	-34.6	+60.5	66 ± 8
UV PSA	-41.2	-41.2	+136	144 ± 2

In simulation, both adhesive systems show moderate bow value after temperature ramp up to 180 ^{o}C from 25^{o}C. The respective bows remained unchanged during dwelling at 180 ^{o}C. However after temperature ramp down to 25 ^{o}C from 180 ^{o}C, the two adhesives behave differently; UV PSA showed much higher bow as compared to that of Elastomer PSA, which follows the trend of the observed experimental bows. Also the simulated bow values quantitatively agree

well with the experimental bow values for both adhesives. Therefore the viscoelasticity of PEN is crucial to consider for simulating the bow of bonded system. The model considering the viscoelasticity of both adhesive and PEN adequately describes the experimental data. This result indicates that beside the viscous flow of adhesive, the viscous flow of PEN also relaxes the stress of bonded system and hence influences the bow of bonded system. In Figure 5.12, the comparison between the initial undeformed and deformed shape after complete thermal cycling of model bonded system is shown. The shape is deformed more for UV PSA as compared to that of Elastomer PSA.

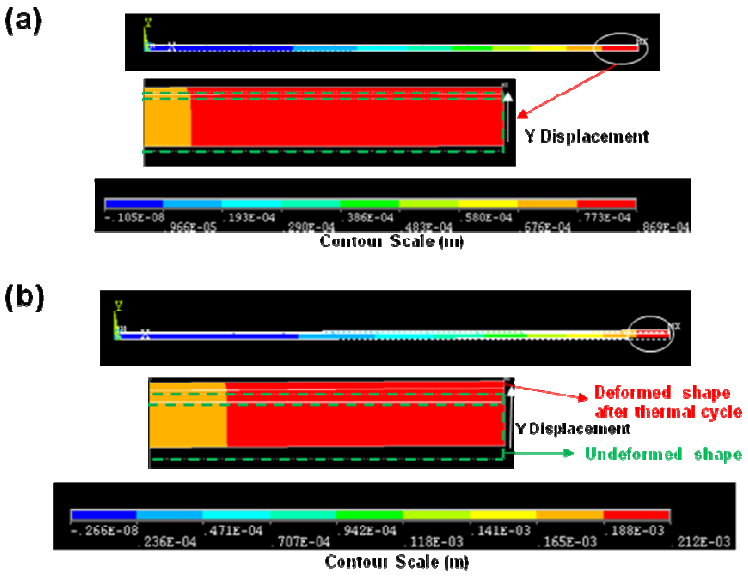

Figure 5.12: Simulated Y displacement for the model considering carrier as elastic material, adhesive and plastic substrate as viscoelastic material (a) for Elastomer PSA and (b) for UV PSA. Dotted areas show undeformed shape and solid areas show deformed shape. The shape is deformed more for UV PSA as compared to that of Elastomer PSA

Next the bows of bonded systems were simulated for different types of carriers and quantitatively compared against the experimental values. The comparison of simulated bow with the experimental bow is shown in Table 5.10.

Table 5.10: Comparison of model predicted bow to observed bow for different types of carriers

Carrier Type	Model Y Displacement (μm)			Expt. Bow (μm)
	25 °C-180 °C (3 hr)	180 °C (1 hr)	180 °C-25 °C (6 hr)	
Silicon	-43.1	-43.0	+153	192 ± 8
0.9mm D263T	-82.4	-81.1	+136	144 ± 2
Eagle 2000	-81.0	-80.8	+267	334 ± 27
AF 45	-78.7	-78.6	+255	292 ± 11
0.7mm D263T	-73.8	-73.7	+229	235 ± 9
0.55mm D263T	-127.6	-127.4	+378	327 ± 10
1.1mm D263T	-25.4	-25.3	+90	96 ± 1
Alumina	-13.3	-13.2	+52.4	56 ± 3

The model predicts the observed bow values reasonably well especially for lower bow values. To judge the adequacy of the model, coefficient of determination (R^2) was determined. R^2 is often referred as the amount of variability in the data explained or accounted for by the model [35]. The calculated R^2 value is 0.87. R^2 is calculated using the following equation:

$$R^2 = \frac{SS_R}{SS_T} = 1 - \frac{SS_E}{SS_T} \tag{5.20}$$

where $SS_E = \sum_{i=1}^{n} \left(y_i - \hat{y}_i \right)^2$ is error sum of squares

$SS_R = \sum_{i=1}^{n} \left(\hat{y}_i - \overline{y} \right)^2$ is regression sum of squares and

$SS_T = \sum_{i=1}^{n} \left(y_i - \overline{y} \right)^2$ is total corrected sum of squares

Here y_i is experimental data, $\hat{y}_i$ is simulated data and $\overline{y}$ is average of experimental data.

The comparison between model predicted bow and observed bow is illustrated in Figure 5.13(a). Also the comparisons between model predicted and experimentally observed trend of bow with carrier CTE and carrier thickness are

shown in Figure 5.13(b) and Figure 5.13(c).

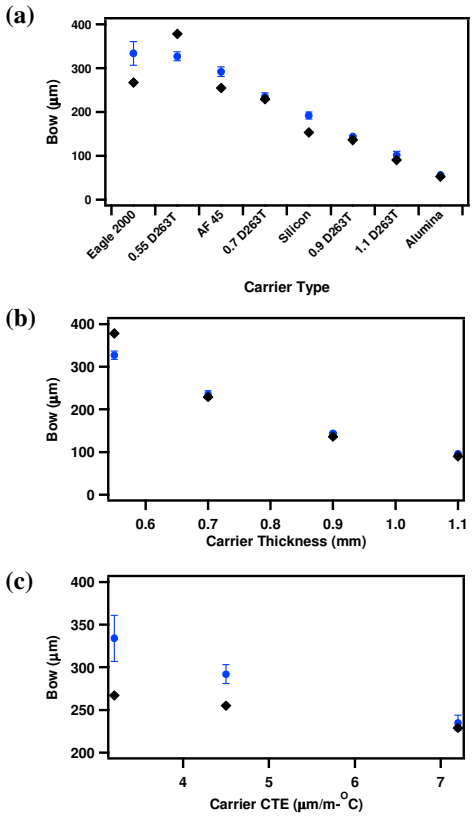

Figure 5.13: Comparison of model predicted bow to observed bow (a) for different carriers (b) for different carrier thickness (c) for different carrier CTE

It can be seen from Figure 5.13 that the model predicts the trend of bow with carrier thickness better (R^2 = 0.91) than that with carrier CTE (R^2 = 0.78). Consider Stoney's equation as given in equation (3.4),

$$B = \frac{3L^2}{4}\left(\frac{E_f t_f (\alpha_f - \alpha_s)\Delta T}{E_s t_s^2}\right) \tag{3.4}$$

From Stoney's equation it can be seen that bow has a direct dependence on carrier thickness. However, bow depends on mismatch in CTE between carrier and flexible substrate. Therefore, if there is error in CTE values of flexible substrate used in the model, then the simulated bow will deviate from experimental bow.

For example, simulation was performed using CTE values of 54 ppm/^{o}C and 17 ppm/^{o}C for the substrate bonded to Eagle 2000 carrier. The simulated bow is found to be 475 μm and 131 μm respectively whereas the simulated bow is 334 μm for the temperature dependant CTE (54-17 ppm/^{o}C) of the substrate used in the model. The CTE of adhesive layer will not affect the bow as the thickness and modulus of adhesive are small compared to the thickness and moduli of the carrier and substrate [20]. Simulation was performed varying the CTE of adhesive by orders of magnitude and no significant variation in bow was found.

5.5.2 Simulation of distortion of bonded system

The model considering the carrier as an elastic material and both adhesive and plastic substrate as viscoelastic materials predicted the experimental bow data well (R^2=0.87) without benefit of any adjustable parameters. We will now investigate if this model can also predict the distortion of the bonded system. The displacement in x direction of the top layer of the model bonded system after complete thermal cycle will be considered as characteristic of the distortion of plastic substrate PEN. The metal layer (1500Å) and silicon stack layer (4800 Å) deposited for distortion measurement were ignored as the layers were very thin compared to the carrier, adhesive and plastic substrate. The total displacement in the x direction over 75mm width is converted to ppm unit for direct comparison with experimental data. The properties of 0.9mm thick D263T glass carrier were used in model to simulate the same carrier properties as used in experiment. The comparison between the experimental and simulated distortion for both Elastomer

PSA and UV PSA are given in Table 5.11.

Table 5.11: Comparison of model predicted distortion to observed distortion

Adhesive Type	Model X Displacement (μm)			Model Distortion (ppm)	Expt. Distortion	
	25 °C-180 °C (3 hr)	180 °C (1 hr)	180 °C-25 °C (6 hr)		X (ppm)	Y (ppm)
Elastomer PSA	+154	+153	-29.8	-496.7	376±137	510±76
UV PSA	+68	+68	-3.2	-35.5	0.3±1.6	-0.2±0.2

The model cannot quantitatively predict the distortion values. The model does qualitatively predict higher distortion for the Elastomer PSA system than that for UV PSA as observed experimentally. The model predicted that contraction of PEN during cooling is higher than expansion of PEN during heating, resulting in net contraction after the complete thermal cycle for both adhesives. However expansion of PEN was observed experimentally after complete thermal cycle for Elastomer PSA; there was insignificant expansion or contraction for UV PSA. This behavior indicates that PEN behaved more rigid like during cooling than that during heating. Within process temperature range (25 °C -180 °C), PEN passes through its glass transition temperature. In the glassy region, molecular motions are largely restricted to vibrations and short range rotational motions [8]. In the rubbery region, the molecular motions involved are long and short range translational and configurational changes due to rotation around bond angles and as the temperature is increased polymer chains may able to slide past one another. Therefore during heating as PEN goes from glassy region to rubbery region, it flows and expands. However during cooling as PEN passes through glassy region, due to reduced molecular mobility there will be less deformation. In viscoelastic model of PEN, only the rubbery region was

considered and the master curve was generated to extend the data for complete process temperature range. The glassy region was not modeled separately to take into account the different viscoelastic nature in that region. Also PEN is semicrystalline material. There will be change in degree of crystallinity with temperature [36]. This obviously complicates the time-temperature behavior considerably and does not allow broad generalization. Therefore the viscoelastic model of PEN needs to be modified to better predict the distortion.

5.5.3 Design of Adhesive

The model quantitatively simulates the bow of bonded systems for both Elastomer PSA and UV PSA well and also predicts the qualitative trends for distortion. The model shows that the viscoelastic properties of adhesive are critical in controlling the bow and distortion of bonded system during thermal processing as observed experimentally also. Therefore the model can in principle be used to design an adhesive system with optimum viscoelastic properties to minimize bow and distortion. Since model could quantitatively predict bow of bonded system for different carriers and adhesive, we will use the model to investigate how the viscoelastic properties of adhesive can be tuned to control bow of the bonded system.

Intuitively, the modulus of adhesive will impact the deformation behavior of bonded system. So it will be interesting to investigate the effect of initial modulus (E_o) of adhesive on stress-bow of bonded system. The E_o values were tuned keeping relaxation behavior constant similar to Elastomer PSA and UV

PSA. The simulated bow as a function of initial modulus (E_o) for relaxation behavior similar to Elastomer PSA and UV PSA is shown in Figure 5.14.

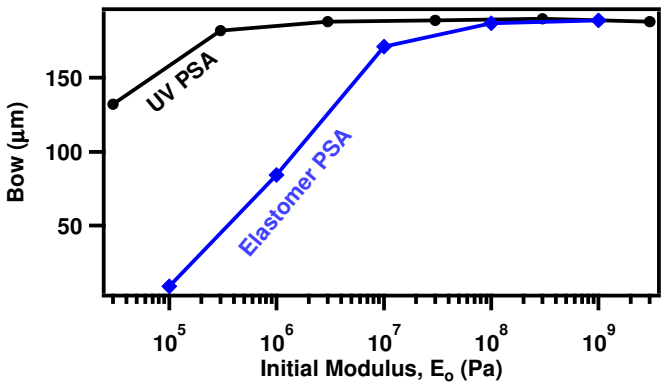

Figure 5.14: Simulated bow as a function of initial modulus (E_o)

It can be seen from Figure 5.14 that bow values for both relaxation behavior similar to Elastomer PSA and UV PSA plateau to the same value around 190 µm for the system investigated (0.9mm D263T Glass-HS PEN) at higher E_o. However for relaxation behavior similar to Elastomer PSA the bow decreases to almost zero values with decreasing E_o. For relaxation behavior similar to UV PSA the bow decreases from its plateau to a moderate value of 132 µm with four order of magnitude variation in E_o. Therefore for intermediate and low values of E_o, relaxation behavior shows a dominant effect on bow. For high values of E_o, irrespective of relaxation behavior, the bow is high around 190 µm. However for polymeric adhesive, value of E_o lies within low to intermediate region ($<10^7$ Pa), UV PSA and Elastomer PSA have E_o values of $3x10^6$ Pa and $0.1\text{-}1x10^6$ Pa respectively in 25 ^oC-180 ^oC temperature range. Therefore for polymeric adhesive, bow will depend on both initial modulus and relaxation modulus.

We found empirically that the viscoelastic properties of adhesive are critical to control the bow-distortion of bonded system. In model, the viscoelastic properties of adhesive were characterized from relaxation behavior. The relaxation behavior was modeled using two parameters: relaxation time (τ) and relative relaxation modulus (α). Therefore these two relaxation parameters of adhesives were tuned to investigate the effect of viscoelasticity of adhesive on bow and distortion. Taking relaxation parameters of Elastomer PSA as base, the parameters were tuned by order of magnitudes. The tuned relaxation time and corresponding simulated bow values are given in Table 5.12 where the relative relaxation modulus used was same as that for Elastomer PSA.

Table 5.12: Simulated bow tuning relaxation time

Model	Relaxation Time (min)			Simulated Bow (μm)
	τ_1	τ_2	τ_3	
1	0.0025	0.1424	1.22	87
Elastomer PSA	0.025	0.1424	1.22	87
2	0.25	0.1424	1.22	87
3	2.5	0.1424	1.22	94
4	25	0.1424	1.22	133
5	250	0.1424	1.22	212
6	2500	0.1424	1.22	210
7	25000	0.1424	1.22	209

The simulated bow as a function of relaxation time for different models and the corresponding simulated relaxation behavior tuning the relaxation time are shown in Figure 5.15(a) and Figure 5.15(b) respectively. The relaxation behavior is shown for reference temperature of Elastomer PSA which is 50^{o}C. The relaxation modulus is normalized against the modulus at time zero (E_0). The relaxation behavior of PEN at 50^{o}C is also shown for comparison with relaxation behavior of adhesives modeled.

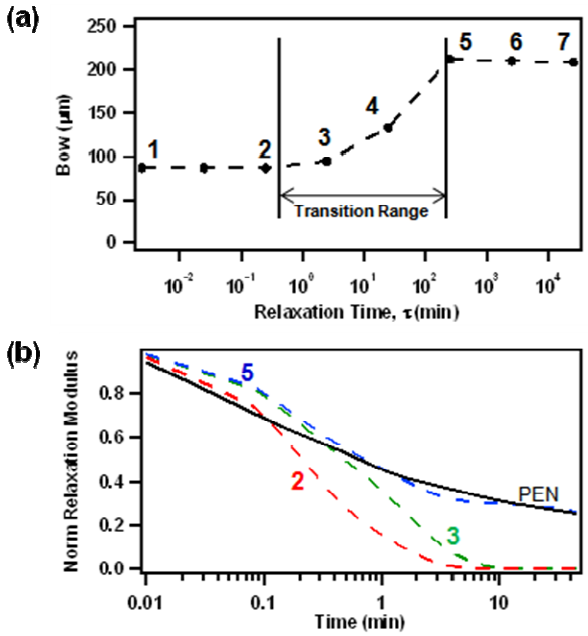

Figure 5.15: (a) Simulated bow as function of relaxation time for different models (1-7) as described in Table 5.12; (b) Simulated relaxation behavior as a function of time for different models (2, 3 and 5) and for PEN.

From Figure 5.15(a) it can be seen there is a transition range for bow with relaxation time. As relaxation time decreases to a certain value, simulation shows it does not matter how fast the adhesive relaxes the stress and bow remains the same. Similarly as relaxation time increases to a certain value, the adhesive relaxes the stress slow enough that any further increase in relaxation time does not have any effect on bow. Only within transition range, bow increases with increasing relaxation time. To understand the cause of this transition range we compared the relaxation behavior of different models with that of PEN as illustrated in Figure 5.15(b). No direct correlation is observed between the relaxation behavior of different models and PEN. For the specific case studied, the transition range of the relaxation time is 1 min to 250 min and bow varies

from 87 μm to 210 μm. In this case the applied thermal load is ramping up the temperature to 180 ^{o}C in 180 min and then dwelling for 60 min at 180 ^{o}C and after total 240 min ramping down the temperature to 25 ^{o}C. The simulated higher end of transition range of relaxation time indicates that if the relaxation time scale is higher than the total heating time, then the stress cannot relax before the cooling cycle starts and hence further increase in relaxation time does not make any effect. The lower end of transition range of relaxation time may indicate that within 1 min the stress is relaxed fully and further decrease in relaxation time does not make any effect. Therefore for different process temperature ranges and ramping rates, the rheology of adhesive will need to be designed within different range of relaxation time to control bow.

The other parameter used in the model to characterize the rheology of adhesive was relative relaxation modulus. Therefore the relative relaxation modulus was tuned to change the rheology of adhesive and to investigate the effect of adhesive rheology on bow. The relative relaxation modulus and corresponding simulated bow values are given in Table 5.13 where relaxation time used was same as that for Elastomer PSA. The simulated distortion values are also shown in Table 5.13.

Table 5.13: Simulated bow and distortion tuning relative relaxation modulus

Model	Relative Relaxation Modulus				Simulated Bow (μm)	Simulated Distortion (μm)
	α_1	α_2	α_3	α_∞		
I	0.11	0.145	0.14	0.605	211	-7.4
II	0.11	0.145	0.24	0.505	210	-7.7
III	0.21	0.245	0.24	0.305	209	-8.8
IV	0.23	0.295	0.26	0.215	207	-9.72
V	0.27	0.305	0.3	0.125	203	-11.5
VI	0.28	0.325	0.32	0.075	197	-13.7
VII	0.3	0.345	0.33	0.025	170	-20.4
Elastomer PSA	0.31	0.345	0.34	0.005	87	-31.5
VIII	0.31	0.345	0.344	0.001	26.2	-21.8

The infinite relative relaxation modulus (α_∞) is defined as:

$$\alpha_\infty = \frac{E_\infty}{E_0} = 1 - \sum_{i=1}^{3} \alpha_i$$

where E_∞ is equilibrium relaxation modulus and E_0 is modulus at time zero.

The simulated bow and distortion as a function of infinite relative relaxation modulus (α_∞) for different models and the corresponding simulated relaxation behavior tuning α_∞ are shown in Figure 5.16 (a) and Figure 5.16(b).

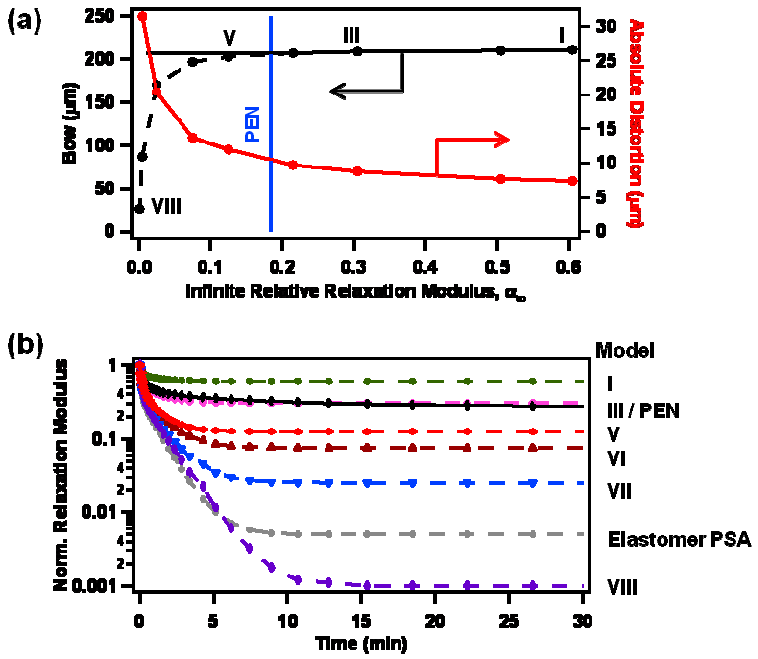

Figure 5.16: (a) Simulated bow and distortion as function of infinite relative relaxation modulus (b) Simulated relaxation behavior as a function of time for different models (I, III, V, VI, VII, VIII and Elastomer PSA) as described in Table 5.13 and for PEN.

From Figure 5.16(a) it can be seen that as α_∞ increases, bow increases and then reaches a plateau. Distortion shows a decreasing trend with increasing α_∞. To elucidate why bow becomes independent of α_∞ after certain value, the relaxation behavior of PEN is considered. As illustrated in Figure 5.16(b), α_∞

for Model I and III are higher than that of PEN whereas α_∞ for Model V, VI, VII, Elastomer PSA and Model VIII are lower than that of PEN. For Model I and III the bows are similar, for Model V bow starts to decrease and as the α_∞ decreases for Model VI, VII, Elastomer PSA and Model VIII, bow decreases. Also illustrated in Figure 5.16(a), the α_∞ of PEN which is indicated by the straight line, the bow for the adhesives with α_∞ less than that of PEN has a decreasing trend and greater than that of PEN remains same. Bow and distortion have opposite trend with α_∞, so for designing of an adhesive that minimizes both bow and distortion, requires a trade-off between the distortion and bow of the bonded system. We observed experimentally also, as described in Chapter 4, that the relative viscoelastic flow properties of the bonding adhesive to that of the bonded flexible substrate is directly correlated to bow and distortion. Intuitively, the viscoelastic flow properties of material should be related to the relaxation parameters, the material with high viscoelastic flow will relax faster and will also relax to a low equilibrium modulus as compared to that of a material with less viscoelastic flow. This phenomenon of bow and distortion having opposite trend with relaxation parameters leaves a narrow range of window of relaxation parameters to design an adhesive minimizing both bow and distortion.

5.6 Conclusion

Understanding the stress response (rheology) of the adhesive can provide an important tool for making improvements in the bond-debond processes, and in particular to obtain bonded wafers with minimum bow and distortion. A Finite

Element Model using ANSYS tool was developed to simulate the stress-bow of bonded system. Two adhesives, Elastomer PSA and UV PSA having significantly different viscoelastic properties, were modeled using Prony series to characterize their relaxation behavior. The model was verified against the experimental bow data of bonded systems that used different carriers varying the thermo-mechanical properties like thickness, modulus and CTE. It was found that it is critical to consider the viscoelastic property of flexible plastic substrate PEN to predict the trend in bow with viscoelastic property of adhesive quantitatively. The model, considering carrier as elastic material and both PEN and adhesive as viscoelastic material, match the bow data well. It was found experimentally that the more compliant adhesive, Elastomer PSA, allows the stress of the bonded system to be relaxed with less bow and the more rigid adhesive, UV PSA, leads to large wafer bow. The model also simulated less bow for Elastomer PSA that relaxes stress faster and to almost zero stress than that for UV PSA that relaxes stress slowly and also stress does not decay completely. The model was also used to simulate the distortion of bonded system. The model could predict the trend in distortion with viscoelastic property of adhesive qualitatively. As experimentally observed, the model simulated greater distortion for Elastomer PSA than that for UV PSA. However, expansion of plastic substrate PEN was observed experimentally after complete thermal cycle but model simulated contraction of PEN. The discrepancy was attributed to the fact that PEN passes through glassy region during thermal cycle which was not modeled in characterizing the viscoelastic properties of PEN. Finally the model was suggested to use for designing of adhesive formulations

tuning the viscoelastic properties to control the stress-distortion of bonded system. By tuning the relaxation time, it was found the bow can be controlled with in a range. Also equilibrium relaxation modulus of adhesive relative to PEN was found to be important parameter to control stress-distortion.

5.7 References

[1] L.H.Sperling, "Polymer viscoelasticity and rheology," in *Introduction to Physical Polymer Science*, ed: John Wiley & Sons Inc., 1992, pp. 458-502.

[2] H. F. Brinson and L. C. Brinson, "Characteristics, applications and properties of polymers," in *Polymer Engineering Science and Viscoelasticity: An Introduction*, ed: Springer, 2008, pp. 75-95.

[3] H. F. Brinson and L. C. Brinson, "Polymerization and classification," in *Polymer Engineering Science and Viscoelasticity: An Introduction*, ed: Springer, 2008, pp. 99-121.

[4] M. T. Shaw and W. J. MacKnight, "Viscoelastic models," in *Introduction to Polymer Viscoelasticity*, ed New Jersy: Wiley Interscience, 2005, pp. 51-69.

[5] M. T. Shaw and W. J. MacKnight, "Time-Temperature correspondence," in *Introduction to Polymer Viscoelasticity*, ed New Jersy: Wiley Interscience, 2005, pp. 107-125.

[6] H. F. Brinson and L. C. Brinson, "Time and temperature behavior of polymers," in *Polymer Engineering Science and Viscoelasticity*, ed New York: Springer, 2008, pp. 221-235.

[7] M. L. Williams*, et al.*, "The temperature dependence of relaxation mechanisms in arorphous polymers and other glass-forming liquids," *Journal of the American Chemical Society,* vol. 77, pp. 3701-3706, 1955.

[8] L. H. Sperling, "Glass-Rubber Transition Behavior," in *Introduction to Physical Polymer Science*, ed New York: Wiley Interscience, 1992, pp. 334-351.

[9] C. H. Hsueh, "Modeling of elastic deformation of multilayers due to residual stresses and external bending," *Journal of Applied Physics,* vol. 91, pp. 9652-9656, 2002.

[10] G. G. Stoney, "The tension of metallic films deposited by electrolysis," *Proceedings of the Royal Society of London. Series A,* vol. 82, pp. 172-175, 1909.

[11] P. Townsend*, et al.*, "Elastic relationships in layered composite media with approximation for the ease of thin films on a thick substrate," *Journal of Applied Physics,* vol. 62, pp. 4438-4444, 1987.

[12] J. S. Kim and K. W. Palik, "The multilayer-modified Stoney's formula for laminated polymer composites on a silicon substrate," *Journal of Applied Physics,* vol. 86, pp. 5474-5479, 1999.

[13] K.-S. Chen and K.-S. Ou, "Modification of curvature-based thin-film residual stress measurement for MEMS applications," *Journal of Micromechanics and Microengineering,* vol. 12, pp. 917-924, 2002.

[14] M. Benabdi and A.A.Roche, "Mechanical properties of thin and thick coatings applied to various substrates," *Journal of Adhesion Science and Technology,* vol. 11, pp. 281-299, 1997.

[15] A. Atkinson, "Residual stress and fracture of laminated ceramic membranes," *British Ceramic Proceedings,* vol. 54, 1995.

[16] J.-H. Lim*, et al.*, "Warpage modeling and characterization to simulate the fabrication process of wafer-level adhesive bonding," *IEEE Int'l Electronics Manufacturing Technology Symposium,* 2007.

[17] J. Wang and S. Zeng, "Thermal stresses analysis in adhesive/solder bonded bimaterial assemblies," *Journal of Applied Physics,* vol. 104, p. 113508, 2008.

[18] S. Guo*, et al.*, "Effect of residual stress on the energy release rate of wedge and DCB test specimens," *International Journal of Adhesion & Adhesives,* vol. 26, pp. 285-294, 2006.

[19] S. Amijima and T. Fujii, "A microcomputer program for stress analysis of adhesive-bonded joints," *International Journal of Adhesion & Adhesives,* vol. 7, pp. 199-204, 1987.

[20] E. Suhir, "Calculated thermal induced stresses in adhesively bonded and soldered assemblies. ," in *Proc ISHM Int Symp Microelectron*, Atlanta, Georgia 1986, pp. 383–92.

[21] Z. Q. Jiang, *et al.*, "Thermal stresses in layered electronic assemblies," *Journal of Electronic Packaging,* vol. 119, pp. 127-132, 1997.

[22] H. R. Ghorbani and J. K. Spelt, "Interfacial thermal stresses in trilayer assemblies," *Journal of Electronic Packaging,* vol. 127, pp. 314-323, 2005.

[23] E. Suhir, "Stresses in adhesively bonded bi-material assemblies used in electronic packaging," *Materials Research Society Symposium Proceedings,* vol. 72, pp. 133-138, 1986.

[24] M. Goland and E. Reissner, "The stresses in cemented joints," *Journal of Applied Mechanics,* vol. 11, p. 17, 1944.

[25] S. Radhakrishnan, *et al.*, "Material behavior uncertainty in the design of bonded systems – Part I: Shear displacement and stress prediction," *Materials and Design* vol. 28, pp. 2706-2711, 2007.

[26] S. Radhakrishnan, *et al.*, "Material behavior uncertainty in the design of bonded systems – Part II: Exhaustive materials characterization and design guidelines," *Materials and Design,* vol. 28, pp. 2712-2718, 2007.

[27] G. R. Humfeld and D. A. Dillard, "Residual stress development in adhesive joints subjected to thermal cycling," *Journal of Adhesion* vol. 65, pp. 277-3.6, 1998.

[28] S. Yadagiri, *et al.*, "Viscoelastic analysis of adhesively bonded joints," *Computers and Structures,* vol. 27, pp. 445-454, 1987.

[29] E. Deier and J. Wilde, "Thermo-mechanical behavior of the die attachment adhesive of a MEMS pressure sensor," *14th European Microelectronics and Packaging Conference & Exhibition*, Friedrichshafen, Germany, 2003.

[30] S. Amijima and T. Fujii, "Extension of a one-dimensional finite element model program for analysing elastic-plastic stresses and progressive failure of adhesive bonded joints," *International Journal of Adhesion & Adhesives,* vol. 9, pp. 243-250, 1989.

[31] I. Sadaba, *et al.*, "A study of residual stress effects due to adhesive bonding of MEMS components," *Applied Mechanics and Materials,* vol. 5-6, pp. 493-500, 2006.

[32] S. Moaveni, *Finite Element Analysis: Theory and Application with ANSYS*. New Jersey: Pearson Education Inc., 2003.

[33] E. Madenci and I. Guven, *The Finite Element Method and Applications in Engineering using ANSYS*. New York: Springer, 2006.

[34] W. A. Macdonald, "Advanced flexible polymeric substrates," in *Organic Electronics: Materials, Manufacturing and Applications* H. Klauk, Ed., ed Weinheim: Wiley VCH, 2006, p. 172.

[35] D. C. Montgomery and G. C. Runger, "Multiple linear regression," in *Applied Statistics and Probability for Engineers*, 3rd ed: John Wiley & Sons, 2003, pp. 410-467.

[36] P. C. Painter and M. M. Coleman, "Mechanical and rheological properties," in *Essentials of Polymer Science and Engineering*, ed Lancaster: DEStech Publications Inc., 2009, pp. 445-469.

Chapter 6

Conclusions and Recommendations

Electronic circuits on flexible substrate represent a paradigm shift from traditional rigid substrate based microelectronics. Flexible electronics offer the opportunity to create energy-efficient products that are lightweight, ultrathin, and rugged along with the potential for very large area electronics with the ability to flex, curve, conform and roll [1]. Though 'roll-to-roll processing (R2R)' of flexible substrates allows for continuous production, significant increase in throughput and reduction in device cost; the entry cost into R2R electronics manufacturing from new process development, tool set design and installation will limit the applications of flexible electronics in near future [2]. Therefore, it is important to develop a viable interim manufacturing option that will allow flexible electronics to enter the market in volume much sooner than possible using true R2R processing. In this dissertation, a temporary bond-debond method was developed that enables direct fabrication of high performance electronic devices on flexible plastic substrates and facilitates processing of flexible substrates using automated standard semiconductor and flat-panel tool sets without tool modification. In this method, the flexible substrate is temporarily adhered to rigid carrier using polymeric adhesive. The carrier suppresses the bending and warping of the flexible structure during processing; provides requisite planarity, dimensional stability, and lithographic registration during device fabrication. Once device fabrication is complete, the flexible substrate is debonded from the

carrier and the substrate regains its flexibility. We have demonstrated that after debonding of the flexible TFT backplane from the rigid carrier, this backplane can be integrated with flexible frontplane electronics to create a functional electrophoretic display [3].

However, electronic displays have an increasing demand for scaling up the size [4-6]. The leading display companies like Samsung, LG Display and Sony are working on Gen 8 size (2200 mm x 2500 mm) display glass substrates [6]. Flexible displays also need increasing the dimensions to be competitive with rigid displays. In addition large-area wall-sized flexible displays offer the advantage of rolled away when not in use. Therefore, it will be attractive to investigate in improving the temporary bond-debond technology for scaling-up on a next generation size of Gen II panel (370 mm x 470 mm) from the developed 150mm size wafer. The scale-up of temporary bond-debond technique to GEN II size panel will require a number of areas to be studied in future. For example, new coating technique for adhesive will be required to develop, as spin coating used to coat 150 mm round wafer will not be suitable for large rectangular size panels. With spin coating it is difficult to coat the corners of the panels. The uniformity of the coated adhesive is important since any uncoated area and air bubble trapped within the adhesive will result in blistering of the adhesive [7]. Alternately, the adhesive coating can be done using screen printer and spray coater as these methods instead of spinning, move the panels in X and Y direction and can coat the corners without any difficulty. Using these methods, also there will be less utilization of adhesive as compared to that using spin coating method. Another

aspect that will need attention in future for scaling–up of temporary bond-debond technology will be the control of stress that develops during the thermal processing cycles.

We have found that the fundamental challenge for the temporary bond-debond technique is the control of stress that develops during the processing steps predominately through thermo-mechanical property mismatches between the carrier and flexible substrate. The stress is relaxed through bowing of the bonded system, which leads to wafer handling issues and through deformation of flexible plastic substrate which leads to alignment issues during multiple photolithographic steps. We have showed that for a given adhesive / flexible substrate system, the physical properties of the carrier on bow of the bonded system scale according to the well established Stoney's equation [8]. Minimization of the bow requires maximizing the modulus and thickness of the carrier and minimizing the mismatch in CTE between carrier and flexible substrate. Moreover we have found the more compliant adhesive with high viscoelastic loss factor allows the stress of the bonded system to be relaxed with less bow. Conversely the more rigid adhesive with low viscoelastic loss factor leads to large wafer bow.

The GEN II size panel is rectangular, different than the round 150 mm wafer, which was used in this study. Some initial study has been performed to examine if the shape of the substrate has any effect on the stress. Preliminary experiments were done with rectangular, square and round wafers of size 150 mm x 118 mm, 150 mm x 150 mm and 150 mm diameter respectively. Interestingly,

we have found that all wafers have similar bow for same circular scan size; x and y direction bow measurement for square wafers have similar bow. These initial experimental results indicate that the shape of wafers does not alter the mechanism associated with stress of bonded system. The bow will scale proportionally with the size of the panels. However the automated handling tools have limited tolerance limit (< 80 μm) for bow. Therefore, the increased bow with increased size of panel will require further investigation with the selection of carriers and adhesives to minimize the stress-bow of bonded HS-PEN. As mentioned earlier, the thermo-mechanical properties such as thickness, modulus and CTE of the carrier and the viscoelastic properties such as loss factor of the adhesive are the critical parameters that control the stress of the bonded system.

We also addressed the unique challenge involved in fabrication of flexible electronics is that the flexible plastic substrates are not dimensionally stable like traditional glass or silicon substrates. Deformation of the substrate occurs as the substrate passes through the processing thermal cycles. This deformation of the substrate imposes difficulties in ensuring the registration of layers during multiple photolithographic steps to create an active device. We have demonstrated a route to minimize the flexible substrate distortion (1.2 ± 2 ppm) using temporary bond-debond process. We have showed that the viscoelastic loss factor of adhesive correlates strongly with the registration of layers. Low viscoelastic loss factor of adhesive leads to insignificant distortion of the flexible plastic substrate HS-PEN. Therefore, distortion is expected not to be an issue for scaling-up temporary bond-debond method using an adhesive with low viscoelastic loss factor. However we

have found that low viscoelastic loss factor of adhesive also leads to large wafer bow. Therefore the balance between bow and distortion needs to be controlled tuning the viscoelasticity of adhesive to obtain bonded system with minimum bow and distortion. By blending two adhesives, Elastomer PSA with high viscoelastic loss factor and UV PSA with low viscoelastic loss factor, we have found that a narrow window in loss factor controls distortion and bow of the bonded wafer. More significantly we have found that the relative loss factor of the adhesive to the flexible plastic substrate correlate directly with the distortion-bowing behavior. Higher loss factor of adhesive compared to that of substrate allows the stress to be relaxed with less bow, but leads to significantly greater dimensional distortion. Conversely, lower loss factor of adhesive compared to that of substrate allows less distortion but leads to larger wafer bow. These results provide insight into the critical material properties to be considered for the design of adhesive formulations to be utilized with bonding-debonding for the fabrication of flexible electronics.

We have performed the bond-debond experiment using only one flexible plastic substrate HS-PEN. To demonstrate the general applicability of considering the relative loss factor of the adhesive to that of the flexible plastic substrate to control the bow-distortion of bonded system, it will be interesting to determine bow-distortion behavior of bonded system using different types of plastic substrates. The plastic substrates can be either semicrystalline or amorphous thermoplastic polymers [9-10]. The group of thermoplastic semicrystalline polymers includes polyethylene terephthalate (PET), e.g. Teijin Melinex with a T_g

of 80 ^{o}C; and polyetheretherketone, e.g. Victrex PEEK with a T_g of 140 ^{o}C along with polyethylene naphthalate (PEN). The group of thermoplastic amorphous polymers includes polycarbonate (PC), e.g. Teijin PURE-ACE with a T_g of 150 ^{o}C and polyethersulphone (PES), e.g. Sumitomo Bakelite with a T_g of 220 ^{o}C. The third category is high T_g materials that includes aromatic fluorene-containing polyarylates (PAR), e.g. Ferranias Arylite with a T_g of 340 ^{o}C and polyimide (PI), e.g. DuPont Kapton with a T_g of 360 ^{o}C. These plastic substrates have a wide range of T_g (80 ^{o}C - 360 ^{o}C) that provides a wide variation in loss factors within process temperature range (25 ^{o}C - 180 ^{o}C). The PES, PAR and PI plastic substrates are in glassy region whereas PET, PEEK and PC plastic substrates pass through transition from glassy to rubbery region within process temperature range. In glassy region the molecular motions are largely restricted to vibrations and short range rotational motions [11] and hence there is less viscous flow. Therefore, in glassy region, the deformation of plastic substrate should be low. However, along with Tg, other properties like CTE, optical clarity, water absorption and modulus need to considered for plastic substrates to be used for flexible electronics [10]. The basic properties of these plastic substrates are shown in Table 6.1 [10].

Table 6.1: Basic properties of plastic substrates potential to be used for flexible electronics

Properties	PET	PC	PES	PAR	PI
T_g, ^{o}C	80	150	220	340	360
CTE, ppm/^{o}C (-55 to 85 ^{o}C)	15	60-70	54	53	17
Transmission, % (400-700nm)	>85	>90	90	90	yellow
Water absorption, %	0.14	0.2-0.4	1.4	0.4	1.8
Young's modulus, GPa	5.3	1.7	2.2	2.9	2.5

From Table 6.1, it can be seen that though PC, PES and PAR have high T_g, these plastic substrates also have high CTE. During thermal processing, stress is predominately evolves through CTE mismatch between carrier and substrate. High CTE of substrate will cause high mismatch in CTE, result in high stress which is not desirable. The plastic substrate PI is yellow and hence will not be suitable for bottom emissive displays. However, PI has low CTE along with high T_g and these properties in principal should result in low stress and deformation. Therefore, PI will be a good candidate to investigate further as a substrate for flexible microelectronics applications which will not require light emission through substrate.

A valid physically-based model of the bonded system considering the thermo-mechanical properties of carrier and viscoelastic properties of both adhesive and flexible substrate could provide the fundamental understanding of bow-distortion behavior with the properties of carrier, adhesive and substrate. The theoretical understanding gained could then in principle be used to enable rational design of a bonded system with optimum properties of carrier, adhesive and substrate. Thus the model will help to implement temporay bond-debond technology successfully for scaling-up with less time and cost than possible empirically. We have developed a finite element model using ANSYS tool for simulating the stress-bow of bonded system. We have found that the model fails to predict the trend in bow with properties of carrier and adhesive if the viscoelasticity of PEN is not considered. The bow simulated, considering carrier as elastic material and both PEN and adhesive as viscoelastic material, agree well

with the bow experimentally observed. The model was also used to simulate the distortion of bonded system. The model predicted higher distortion for more compliant adhesive as found experimentally. However the model predicted PEN will contract after thermal cycle whereas expansion of PEN was observed experimentally. The discrepancy was attributed to the fact that PEN passes through glassy region during process thermal cycles which was not considered in the developed viscoelastic model of PEN. We used shift function to generate master curve from only a portion of process temperature region. The viscoelastic model of PEN requires further investigation to better predict the distortion of bonded system. In the future model, instead of using shift function, the relaxation behavior of PEN should be determined experimentally for each region e.g. glassy region, transition region and rubbery region and model the viscoelasticity of PEN for each region separately. It is expected using the viscoelastic model of PEN at each region in the corresponding temperature region will simulate the bow-distortion of bonded system with better agreement.

We have proposed that the developed model can be used for design of adhesive formulations with required rheology to control the stress-distortion of bonded system. The simulation indicates that for a specified carrier-flexible substrate, there is a limited range for relaxation parameters of the adhesive e.g. relaxation time (τ) and relative relaxation modulus (α) within which the stress-distortion can be controlled. For very fast (τ<1 min) or slow relaxation (τ>250 min) the stress-bow becomes independent of relaxation time for the specific case studied. Also equilibrium relaxation modulus i.e. relaxation modulus at infinite

time, of adhesive compared to PEN is found to be important parameter to be considered to control stress-distortion of bonded system.

The narrow range of the relaxation parameters i.e. loss factor of adhesive for a specified carrier-flexible plastic substrate system indicates that tuning the rheology of adhesive alone will not be sufficient to implement temporary bond-debond technology with acceptable stress-distortion for GEN II size substrates. The properties of carrier and substrate also need to be considered along with the properties of adhesive to minimize the deformation of bonded system. A carrier with higher modulus and CTE than those of alumina carrier or thicker alumina carrier (> 0.7 mm) in principal should reduce the deformation. A substrate with low loss factor is expected to provide less distortion but also relax less stress through viscous flow. However, an adhesive with loss factor higher than that of substrate will relax some stress. Therefore it will require to balance between the loss factor of substrate and adhesive that will provide the acceptable bow-distortion of bonded system for GEN II size substrates.

In summary, we developed a novel technology based upon temporary bond–debond to enable the fabrication of thin-film devices directly on flexible substrates. Tuning of viscoelastic properties of adhesive as well as thermo-mechanical properties of carrier was required for proper alignment of lithographic layers and low bow to enable automated handling. By careful choice of adhesive and carrier, TFT arrays for display backplanes were successfully produced on flexible substrates.

References

[1] H.-L. Chen*, et al.*, "Guest Editorial," *Journal of Display Technology,* vol. 5, pp. 169-171, 2009.

[2] B. Jorgensen, "Not quite ready to roll; Despite advancements, roll-to-roll processing faces hurdles.," in *IPC Association Connecting Electronics Industries* June 15 ed, 2009.

[3] J. Haq*, et al.*, "Temporary bond-debond process for manufacture of flexible electronics: Impact of adhesive and carrier properties on performance," *Journal of Applied Physics,* vol. 108, pp. 1-7, 2010.

[4] H. B. Chen*, et al.* (Nov 2007) Roundtable: Display vendors augment Gen 7 and 7.5 fabs. *Electronic Design, Strategy News*.

[5] Y. S. Jsyang, "LG Display plans a 8 gen OLED-TV production fab for 55 inch size in 2011," in *Etnews*, ed, 2011.

[6] C. Camaroto, Gen 8 Now the Most Important Fab for LCD TV Panel Production, *Quarterly Large-Area Production Strategy Report,* 2010.

[7] J. Haq*, et al.*, "Temporary bond-debond technology for high performance transistors on flexible substrates," *Journal of the Society for Information Display* vol. 18, pp. 884-891, 2010.

[8] G. G. Stoney, "The tension of metallic films deposited by electrolysis," Proceedings of the Royal Society of London. Series A, vol. 82, pp. 172-175, 1909.

[9] W. A. MacDonald, et al., "New developments in polyester films for flexible electronics.," Materials Research Society Symposium Proceedings vol. 769, pp. 283–290, 2003.

[10] W. A. MacDonald, et al., "Engineered films for display technologies," in Flexible Flat Panel Displays, G. P. Crawford, Ed., ed, 2005, pp. 11-33.

[11] L. H. Sperling, "Glass-Rubber transition behavior," in *Introduction to Physical Polymer Science,* ed New York: Wiley Interscience, 1992, pp. 334-351.

Bibliography

[1] Abbie Gregg*, et al.*, "Roll-to-Roll manufacturing of flexible displays," in *Flexible Flat Panel Displays*, ed, 2005, pp. 409-445.

[2] A. Abouraddy and Y. Fink, "Multimaterial photosensitive fiber constructs enable large-area optical sensing and imaging," in *Proceedings of SPIE*, Orlando, 2009, pp. H1-H10.

[3] K. J. Allen, "Reel to real: prospects for flexible displays," *Proceedings of the IEEE,* vol. 93, pp. 1394-1399, 2008.

[4] S. Amijima and T. Fujii, "A microcomputer program for stress analysis of adhesive-bonded joints," *International Journal of Adhesion & Adhesives,* vol. 7, pp. 199-204, 1987.

[5] S. Amijima and T. Fujii, "Extension of a one-dimensional finite element model program for analysing elastic-plastic stresses and progressive failure of adhesive bonded joints," *International Journal of Adhesion & Adhesives,* vol. 9, pp. 243-250, 1989.

[6] E. H. Andrews and A. J. Kinloch, "Mechanics of adhesive failure," *Proceedings of the Royal Society London A,* vol. 322, pp. 385-399, 1973.

[7] G. Arjavalingam*, et al.*, "Multi-layer thin film structure and parallel processing method for fabricating same ", *US Patent* 5258236, 1993.

[8] A. Atkinson, "Residual stress and fracture of laminated ceramic membranes," *British Ceramic Proceedings,* vol. 54, 1995.

[9] M. Benabdi and A.A.Roche, "Mechanical properties of thin and thick coatings applied to various substrates," *Journal of Adhesion Science and Technology,* vol. 11, pp. 281-299, 1997.

[10] E. Bonderover and S. Wagner, "A woven inverter circuit for e-textile applications," *IEEE Electron Device Letters,* vol. 25, pp. 295-297, 2004.

[11] P. C. T. Bouten, "Failure test for brittle conductive layers on flexible display substrates," *22nd International Display Research Conference, Conference Proceedings,* pp. 313–316, 2002.

[12] E. Brandon*, et al.*, "Flexible electronics for space applications," *Materials Research Society Symposia Proceedings,* vol. 814, pp. I9.7.1-I9.7.12, 2004.

[13] H. F. Brinson and L. C. Brinson, "Characteristics, applications and properties of polymers," in *Polymer Engineering Science and Viscoelasticity: An Introduction*, ed: Springer, 2008, pp. 75-95.

[14] H. F. Brinson and L. C. Brinson, "Polymerization and classification," in *Polymer Engineering Science and Viscoelasticity: An Introduction*, ed: Springer, 2008, pp. 99-121.

[15] H. F. Brinson and L. C. Brinson, "Time and temperature behavior of polymers," in *Polymer Engineering Science and Viscoelasticity*, ed New York: Springer, 2008, pp. 221-235.

[16] H. F. Brinson and L. C. Brinson, "Diferential constitutive equations," in *Polymer Engineering Science and Viscoelasticity*, ed: Springer, 2008, pp. 196-197.

[17] C.Creton and P.Fabre, "Tack," *Comprehesive Adhesion Science,* vol. 2, pp. 1-24, 2001.

[18] C. Camaroto, Gen 8 Now the Most Important Fab for LCD TV Panel Production. *Quarterly Large-Area Production Strategy Report,* 2010.

[19] S. Carson, "Flexible electronic structures show potential for artificial muscles or biological tissues," *Argonne,* vol. I11, pp. 28-30, 2007.

[20] R. P. Chartoff*, et al.*, "Dynamic Mechanical Analysis (DMA)," in *Thermal Analysis of Polymers, Fundamentals and Applications*, J. D. Menczel and R. B. Prime, Eds., ed: John Wiley & Sons, Inc., 2008.

[21] H. B. Chen*, et al.* (Nov 2007) Roundtable: Display vendors augment Gen 7 and 7.5 fabs. *Electronic Design, Strategy News*.

[22] H.-L. Chen*, et al.*, "Guest Editorial," *Journal of Display Technology,* vol. 5, pp. 169-171, 2009.

[23] K.-S. Chen and K.-S. Ou, "Modification of curvature-based thin-film residual stress measurement for MEMS applications," *Journal of Micromechanics and Microengineering,* vol. 12, pp. 917-924, 2002.

[24] I.-C. Cheng and S. Wagner, "Overview of flexible electronics technology," in *Flexible Electronics : Materials and Applications* W. S. Wong and A. Salleo, Eds., ed: Springer, 2009, pp. 1-20.

[25] K. H. Cherenack*, et al.*, "Amorphous-silicon thin-film transistors fabricated at 300 °C on a free-standing foil substrate of clear plastic," *IEEE Electron Device Letters* vol. 28, pp. 1004-1006, 2007.

[26] J.-H. Choi*, et al.*, "A linear viscoelastic model of matrix/core–shell modifier polymer blends," *Journal of Polymer Science: Part B: Polymer Physics,* vol. 38, pp. 942-953, 2000.

[27] M.-C. Choia, *et al.*, "Polymers for flexible displays: From material selection to device applications," *Progress in Polymer Science* vol. 33, pp. 581-630, 2008.

[28] S. G. Chu, in *Handbook Of Pressure Sensitive Adhesive Technology, 2nd Ed*, D. Satas, Ed., ed New York: Springer, 1989, p. 179.

[29] A. B. Chwang, *et al.*, "Thin film encapsulated flexible organic electroluminescent displays," *Applied Physics Letter,* vol. 83, pp. 413-415, 2003.

[30] G. P. Collins, "Next strech for plastic electronics," *Scientific American,* vol. 291, pp. 76-81, 2004.

[31] G. P. Crawford, "Flexible flat panel display technology," in *Flexible Flat Panel Displays*, G. P. Crawford, Ed., ed: Wiley-SID, 2005, pp. 1-9.

[32] E. Deier and J. Wilde, "Thermo-mechanical behavior of the die attachment adhesive of a MEMS pressure sensor," 14th European Microelectronics and Packaging Conference & Exhibition, Friedrichshafen, Germany, 2003.

[33] R. Dekker, *et al.*, "A 10 mm thick RF-ID tag for chip-in-paper applications," *Proceedings of IEEE Bipolar/BiCMOS Circuits and Technology Meet. (BCTM),* pp. 18-21, 2005.

[34] F. E. Doany and C. Narayan, "Laser release process to obtain freestanding multilayer metal polyimide circuits," *IBM Journal of Research and Development* vol. 41, pp. 151-155, 1997.

[35] V. Dragoi, *et al.*, "Reversible wafer bonding for reliable compound semiconductor processing," *Proceedings of IEEE Semiconductor Processing,* pp. 331-334, 2002.

[36] G. Erhard, "Structure and Properties," in *Designing with Plastics*, ed Cincinnati: Hanser Gardner, 2006, pp. 31-67.

[37] J. D. Ferry, *Viscoelastic Properties of Polymers (third ed.)*: John Wiley and Sons, New York, 1980.

[38] A. H. Firester, "Macroelectronics: large area flexible electronics for sensors, displays, and other applications," in *Proceedings of SPIE*, Bellingham, WA, 2004, pp. 29-37.

[39] I. French, "Thin plastic electrophoretic display fabricated by a novel process," *Proceedings of the SID symposium and exhibition,* pp. 1634-1637, 2005.

[40] I. French and D. McCulloch, "Active matrix displays and other electronic devices having plastic substrates," *International Patent* WO2005/050754 A1, 2005.

[41] G.Fourche, "An overview of the basic aspects of polymer adhesion," *Polymer Engineering and Science,* vol. 35, pp. 957-967, 1995

[42] D. Gamota, "Near-term opportunities for large-area flexible electronics: photovoltaics, displays and sensors could lead an industry revolution," *Printed Circuit Design & Fab,* 2009.

[43] S. Gardner, "Precision photolithography on flexible substrates," ed:Azores, 2006, pp. 1-5.

[44] A. N. Gent and A.J.Kinloch, "Adhesion of viscoelastic materials to rigid substrates: Energy criterion for failure," *Journal of Polymer Sciience PartA,* vol. 9, pp. 659-668, 1971.

[45] H. R. Ghorbani and J. K. Spelt, "Interfacial thermal stresses in trilayer assemblies," *Journal of Electronic Packaging,* vol. 127, pp. 314-323, 2005.

[46] A. P. Ghosh*, et al.*, "Thin-film encapsulation of organic light-emitting devices," *Applied Physics Letter,* vol. 86, p. 223503, 2005.

[47] H. Gleskova*, et al.*, "Mechanics of thin-film transistors and solar cells on flexible substrates," *Solar Energy,* vol. 80, pp. 687-693, 2006.

[48] H. Gleskova*, et al.*, "a-Si:H TFTs made on polyimide foil by PECVD at 150^{o}C," *Proceedings of the Materials Research Society,* vol. 508, pp. 73-78, 1998.

[49] M. Goland and E. Reissner, "The stresses in cemented joints," *Journal of Applied Mechanics,* vol. 11, p. 17, 1944.

[50] S. D. R. Gorkhali*, et al.*, "Reliability of transparent conducting substrates for rollable displays: a cyclic loading inverstigation.," *Society for Information Display, Digest of Technical Papers,* pp. 1332–1335, 2003.

[51] D. Graebling*, et al.*, "Linear viscoelastic behavior of some incompatible polymer blends in the melt: Interpretation of data with a model of emulsion of viscoelastic liquids," *Macromolecules,* vol. 26, pp. 320-329, 1993.

[52] S. Guo*, et al.*, "Effect of residual stress on the energy release rate of wedge and DCB test specimens," *International Journal of Adhesion & Adhesives,* vol. 26, pp. 285-294, 2006.

[53] J.-M. Han*, et al.*, "Novel encapsulation method for flexible organic light-emitting diodes using poly(dimethylsiloxane)," *Japanese Journal of Applied Physics,* vol. 47, pp. 8986-8988, 2008.

[54] T. Hashimoto*, et al.*, "Device manufacturing method " *US Patent,* vol. 7029960, 2006.

[55] P. K. W. Herh*, et al.*, "Rheological properties of structural and pressure-sensitive adhesives and their impact on product performance," *Adhesives & Sealants Industry,* pp. 28-33, 2005.

[56] C. H. Hsueh, "Modeling of elastic deformation of multilayers due to residual stresses and external bending," *Journal of Applied Physics,* vol. 91, pp. 9652-9656, 2002.

[57] J. Huang, "The development of inflatable array antennas," *IEEE Antennas and Propagation Magazine,* vol. 43, pp. 44-50, 2001.

[58] G. R. Humfeld and D. A. Dillard, "Residual stress development in adhesive joints subjected to thermal cycling," *Journal of Adhesion* vol. 65, pp. 277-3.6, 1998.

[59] I-Chun Cheng*, et al.*, "Stress control for overlay registration in a-Si : H TFTs on flexible organic-polymer-foil substrates " *Journal of the Society for Information Display,* vol. 13, pp. 563-568, 2005.

[60] S. Inoue*, et al.*, "Surface-Free Technology by Laser Annealing (SUFTLA) and its application to poly-Si TFT-LCDs on plastic film with integrated drivers," *IEEE Transactions on Electron Devices,* vol. 49, pp. 1353-1360, 2002.

[61] T. Instruments. Determination of the linear viscoelastic region of a polymer using a strain sweep on the DMA 2980. *Thermal Analysis and Rheology*.

[62] Z. Q. Jiang*, et al.*, "Thermal stresses in layered electronic assemblies," *Journal of Electronic Packaging,* vol. 119, pp. 127-132, 1997.

[63] B. Jorgensen, "Not quite ready to roll; Despite advancements, roll-to-roll processing faces hurdles.," in *IPC Association Connecting Electronics Industries* June 15 ed, 2009.

[64] Y. S. Jsyang, "LG Display plans a 8 gen OLED-TV production fab for 55 inch size in 2011," in *Etnews*, ed, 2011.

[65] Kanti Jain*, et al.*, "Flexible electronics and displays," *Proceedings of the IEEE,* vol. 93, pp. 1500-1510, 2005.

[66] B. Kelley, Flexible electronics developing for diverse applications *SPIE Newsroom*, 21 August, 2009

[67] J. S. Kim and K. W. Palik, "The multilayer-modified Stoney's formula for laminated polymer composites on a silicon substrate," *Journal of Applied Physics,* vol. 86, pp. 5474-5479, 1999.

[68] K. R. Kim and K. Y. Baek, "A laser selective etching process for next-generation flexible display," in *Proceedings of the Laser Microfabrication Conference*, Phoenix, USA, 2006, pp. 198-202.

[69] S. P. Lacour*, et al.*, "Mechatronic system of dielectric elastomer actuators addressed by thin film photoconductors on plastic," *Sensors and Actuators A: Physical,* vol. 111, pp. 288-292, 2004.

[70] Y. Lee, *et al.*, "High-Performance Poly-Si TFTs on Plastic Substrates Using a Nano-Structured Separation Layer Approach," *IEEE Electron Device Letters,* vol. 24, pp. 19-21, 2003.

[71] F. Lemmi, *et al.*, "High-performance TFTs fabricated on plastic substrates," *IEEE Electron Device Letters,* vol. 25, pp. 486-488, 2004.

[72] F. Lemmi, *et al.*, "Poly-Si TFTs from glass to plastic substrates: process and manufacturing challanges," *Materials Research Society Symposium Proceedings,* vol. 814, pp. I1.6.1-I1.6.11, 2004.

[73] Y. C. Leong, *et al.*, "The viscoelastic properties of natural rubber pressure-sensitive adhesive using acrylic resin as a tackifier," *Journal of Applied Polymer Science,* vol. 88, pp. 2118-2123, 2003.

[74] H. Lifka, *et al.*, "Ultra-thin flexible OLED device," *Society of Information Display Symposium, Digest Technical Papers,* vol. 38, pp. 1599-1602, 2007.

[75] J.-H. Lim, *et al.*, "Warpage modeling and characterization to simulate the fabrication process of wafer-level adhesive bonding," *IEEE Int'l Electronics Manufacturing Technology Symposium,* 2007.

[76] F. Lorussi, *et al.*, "Strain sensing fabric for hand posture and gesture monitoring," *IEEE Transactions on Information Technology in Biomedicine,* vol. 9, pp. 372-381, 2005.

[77] V. Loryuenyong, *et al.*, "Photo-polymer wafer bonding for double layer transfer," *Materials Research Society Symposium Proceedings,* vol. 768, pp. G5.6.1-G5.6.6, 2003.

[78] W. A. MacDonald, "Advanced flexible polymeric substrates," in *Organic Electronics: Materials, Manufacturing and Applications* H. Klauk, Ed., ed Weinheim: Wiley VCH, 2006, p. 172.

[79] W. A. MacDonald, *et al.*, "Latest advances in substrates for flexible electronics," *Journal of the Society for Information Display* vol. 15, pp. 1075-1083, 2007.

[80] W. A. MacDonald, *et al.*, "New developments in polyester films for flexible electronics.," *Materials Research Society Symposium Proceedings* vol. 769, pp. 283–290, 2003.

[81] W. A. MacDonald, *et al.*, "Enginnered films for display technologies," in *Flexible Flat Panel Displays*, G. P. Crawford, Ed., ed, 2005, pp. 11-33.

[82] E. Madenci and I. Guven, *The Finite Element Method and Applications in Engineering using ANSYS*. New York: Springer, 2006.

[83] N. G. McCrum, *et al.*, *Anelastic and Dielectric Effects in Polymeric Solids*: New York: Wiley, 1967.

[84] M. Miyasaka, "Flexible microelectronics becoming a reality with SUFTLA transfer technology,," *Journal of the Society for Information Display* vol. 15, pp. 479-484, 2007.

[85] S. Moaveni, *Finite Element Analysis: Theory and Application with ANSYS*. New Jersey: Pearson Education Inc., 2003.

[86] D. C. Montgomery and G. C. Runger, "Multiple linear regression," in *Applied Statistics and Probability for Engineers*, 3rd ed: John Wiley & Sons, 2003, pp. 410-467.

[87] L. E. Nielsen and R. F. Landel, *Mechanical properties of polymers and composites. 2nd ed*: New York: Marcel Dekker Inc, 1994.

[88] G. Nisato, "Flexible Devices," WO/2005/048669.

[89] S. M. O'Rourke*, et al.*, "Direct fabrication of a-Si:H thin film transistor arrays on plastic and metal foils for flexible displays," in *Proc. 26th Army Science Conference*, Orlando, FL, 2008.

[90] P. Townsend*, et al.*, "Elastic relationships in layered composite media with approximation for the ease of thin films on a thick substrate," *Journal of Applied Physics,* vol. 62, pp. 4438-4444, 1987.

[91] P. C. Painter and M. M. Coleman, "Mechanical and rheological properties," in *Essentials of Polymer Science and Engineering*, ed Lancaster: DEStech Publications Inc., 2009, pp. 445-469.

[92] I. K. Partridge, in *Multicomponent Polymer Systems*, I. S. Miles and S. Rostami, Eds., ed London: Longman Scientific and Technical, 1992, pp. 149-186.

[93] J. Perrenoud*, et al.*, "Flexible CdTe solar cells and modules: challenges and prospects," in *Proceedings of SPIE* San Diego, 2009, pp. L1-L5.

[94] J. Perrin, "Reactor design for a-Si:H deposition," in *Plasma Deposition of Amorphous-Based Materials*, C. P. Bruno G, Madan A, Ed., ed San Diego, CA,: Academic Press, 1995, pp. 177-241.

[95] R. Puligadda*, et al.*, "High performance temporary adhesives for wafer bonding applications," *Matererials Research Society Symposium Proceedings.,* vol. 970, pp. 239-249, 2007.

[96] S. Radhakrishnan*, et al.*, "Material behavior uncertainty in the design of bonded systems – Part I: Shear displacement and stress prediction," *Materials and Design* vol. 28, pp. 2706-2711, 2007.

[97] S. Radhakrishnan*, et al.*, "Material behavior uncertainty in the design of bonded systems – Part II: Exhaustive materials characterization and design guidelines," *Materials and Design,* vol. 28, pp. 2712-2718, 2007.

[98] G. B. Raupp*, et al.*, "Low-temperature amorphous-silicon backplane technology development for flexible displays in a manufacturing pilot-line environment," *Journal of the Society for Information Display,* vol. 15, pp. 445-454, 2007.

[99] J. Robertson, "Deposition mechanism of hydrogenated amorphous silicon," *Journal of Applied Physics,* vol. 87, pp. 2608-2617, 2000.

[100] A. Romeo*, et al.*, "High-efficiency flexible CdTe solar cells on polymer substrates," *Solar Energy Materials & Solar Cells,* vol. 90, pp. 3407-3415, 2006.

[101] T. P. Russell and H. C. Kim, "Tack--a sticky subject," *Science,* vol. 285, pp. 1219-1220, 1999.

[102] B. F. Ryan*, et al.*, *MINITAB Handbook: Updated for Release 14*. Belmont, CA: Brooks/Cole Thomson Learning, 2005.

[103] I. Sadaba*, et al.*, "A study of residual stress effcts due to adhesive bonding of MEMS components," *Applied Mechanics and Materials,* vol. 5-6, pp. 493-500, 2006.

[104] K. R. Sarma, "a- Si TFT OLED fabricated on low-temperature flexible plastic substrate," *Materials Research Society Symposium Proceedings,* vol. 814, pp. 1-12, 2004.

[105] A. Sazonov*, et al.*, "Low-temperature amorphous and nanocrystalline silicon materials and thin-film transistors," in *Flexible Electronics: Materials and Applications*, W. S. Wong and A. Salleo, Eds., ed: Springer, 2009.

[106] M. T. Shaw and W. J. MacKnight, "Viscoelastic models," in *Introduction to Polymer Viscoelasticity*, ed New Jersy: Wiley Interscience, 2005, pp. 51-69.

[107] M. T. Shaw and W. J. MacKnight, "Time-Temperature correspondence," in *Introduction to Polymer Viscoelasticity*, ed New Jersy: Wiley Interscience, 2005, pp. 107-125.

[108] T. Shimoda and S. lnoue, "Surface Free Technology by Laser Annealing (SUFTLA)," *IEDM Technical Digest. International,* vol. 99, pp. 289-292, 1999.

[109] H. Sirringhaus and S. Burns, "Alignment tolerant patterning on flexible substrates," WO/2006/059162, 2006.

[110] T. Someya and T. Sakurai, "Integration of organic field effect transistors and rubbery pressure sensors for artificial skin applications," *IEEE International Electron Devices Meeting,* vol. 8.4, pp. 203-206, 2003.

[111] T. Someya*, et al.*, " A large area flexible pressure sensor matrix with organic field effect transistors for artificial skin applications," *Proceedings of the National Academy of Sciences* vol. 101, pp. 9966-9970, 2004.

[112] J. H. Souk and W. Lee, "A practical approach to processing flexible displays," *Journal of the Society for Information Display,* vol. 18, pp. 258-265, 2010.

[113] L. H. Sperling, "Polymer viscoelasticity and rheology," in *Introduction to Physical Polymer Science*, ed: John Wiley & Sons Inc., 1992, pp. 458-502.

[114] L. H. Sperling, "Glass-Rubber transition behavior," in *Introduction to Physical Polymer Science*, ed New York: Wiley Interscience, 1992, pp. 334-351.

[115] R. Srinivasan and V. Mayne-Banton, "Self-developing photoetching of Polyethylene terephthalate films by far-ultraviolet excimer laser radiation," *Applied Physics Letter,* vol. 41, pp. 575-578, 1982.

[116] G. G. Stoney, "The tension of metallic films deposited by electrolysis," *Proceedings of the Royal Society of London. Series A,* vol. 82, pp. 172-175, 1909.

[117] E. Suhir, "Stresses in adhesively bonded bi-material assemblies used in electronic packaging," *Materials Research Society Symposium Proceedings,* vol. 72, pp. 133-138, 1986.

[118] E. Suhir, "Calculated thermal induced stresses in adhesively bonded and soldered assemblies," in *Proc ISHM Int Symp Microelectron*, Atlanta, Georgia 1986, pp. 383–92.

[119] E. Suhir, "An approximate analysis of stresses in multilayered elastic thin films," *Journal of Applied Mechanics* vol. 55, pp. 143-148, 1988.

[120] Y. Sun and J. A. Rogers, "Inorganic semiconductor for flexible electronics," *Advanced Materials,* vol. 19, pp. 1897-1916, 2007.

[121] M. F. Tse, "Studies of triblock copolymer-tackifying resin interactions by viscoelasticity and adhesive performance " *Journal of Adhesion Science and Technology,* vol. 3, pp. 551-570, 1989.

[122] J. Vilms and D. Kerps, *Journal of Applied Physics,* vol. 53, p. 1536, 1982.

[123] J. Wang and S. Zeng, "Thermal stresses analysis in adhesive/solder bonded bimaterial assemblies," *Journal of Applied Physics,* vol. 104, p. 113508, 2008.

[124] T. Wang*, et al.*, "RFICs on polydimethylsiloxane for flexible electronics applications," *Electronic Letters,* vol. 43, 2007.

[125] M. L. Williams, *et al.*, "The temperature dependence of relaxation mechanisms in arorphous polymers and other glass-forming liquids," *Journal of the American Chemical Society,* vol. 77, pp. 3701-3706, 1955.

[126] W. S. Wong, *et al.*, " Digital lithographic processing for large-area electronics," *Journal of the Society for Information Display,* vol. 15, pp. 463-470, 2007.

[127] W. S. Wong, *et al.*, "Digital lithography for large-area electronics on flexible substrates," *Journal of Non-Crystalline Solids* vol. 352, pp. 1981–1985, 2006.

[128] X.C.Zhang, *et al.*, "Error analyses on some typically approximate solutions of residual stress within a thin film on a substrate," *Journal of Applied Physics,* vol. 98, p. 053516, 2005.

[129] Y. Xu, *et al.*, "IC-integrated flexible shear stress sensor skin," *Journal of Microelectromechanical Systems,* vol. 12, pp. 740-747, 2002.

[130] S. Yadagiri, *et al.*, "Viscoelastic analysis of adhesively bonded joints," *Computers and Structures,* vol. 27, pp. 445-454, 1987.

[131] H. W. H. Yang, "Water-based polymers as pressure sensititive adhesives-viscoelastic guidelines," *Journal of Applied Polymer Science,* vol. 55, pp. 645-652, 1995.

[132] V. Zardetto, *et al.*, "Substrates for flexible electronics: A practical investigation on the electrical, film flexibility, optical, temperature, and solvent resistance properties," *Journal of Polymer Science Part B: Polymer Physics,* vol. 49, pp. 638-648, 2011.

[133] A. Zosel, "Effect of crosslinking on tack and peel strength of polymers," *Journal of Adhesion,* vol. 34, pp. 201-209, 1991.